Copy
RM L54D19

NACA

RESEARCH MEMORANDUM

AERODYNAMIC CHARACTERISTICS OF SEVERAL FLAP-TYPE TRAILING-EDGE CONTROLS ON A TRAPEZOIDAL WING AT MACH NUMBERS OF 1.61 AND 2.01

By Douglas R. Lord and K. R. Czarnecki

Langley Aeronautical Laboratory
Langley Field, Va.

NATIONAL ADVISORY COMMITTEE
FOR AERONAUTICS

WASHINGTON

June 14, 1954

NATIONAL ADVISORY COMMITTEE FOR AERONAUTICS

RESEARCH MEMORANDUM

AERODYNAMIC CHARACTERISTICS OF SEVERAL FLAP-TYPE TRAILING-EDGE CONTROLS ON A TRAPEZOIDAL WING AT MACH NUMBERS OF 1.61 AND 2.01

By Douglas R. Lord and K. R. Czarnecki

SUMMARY

An investigation has been made at Mach numbers of 1.61 and 2.01 for a range of Reynolds number from 1.7×10^6 to 5.6×10^6 to determine the control effectiveness and hinge-moment characteristics for a series of 25.4-percent-chord trailing-edge controls on a trapezoidal wing having a 23° sweptback leading edge, aspect ratio of 3.1, and taper ratio of 0.4. Pressure-distribution and hinge-moment measurements were made at angles of attack from 0° to 15° for control deflections from -30° to 30°.

Integrated pressure-distribution results and hinge-moment results show that the linear theory overestimated the effect of control deflection. The linear theory predicted well the effect of wing angle of attack on the wing characteristics, but overestimated the effect on the control hinge moments. Modifying the linear-theory method to account for the wing thickness improved the theoretical predictions. The effect of Reynolds number on the control effectiveness and hinge-moment parameters was small for the range tested and the changes with Mach number were the same or somewhat less than predicted theoretically. Increasing the hinge-line gap caused numerical increases in all parameters measured, as did increasing the control trailing-edge thickness on the full-span control.

Correlations were obtained, both theoretically and experimentally, showing the wing lift, root bending-moment, and pitching-moment effectiveness to be functions primarily of control area, control-area moment about the wing root, and control-area moment about the pitch center, respectively.

INTRODUCTION

As part of a general program of research on controls an investigation is under way in the Langley 4- by 4-foot supersonic pressure tunnel to determine the important parameters in the design of controls for use on various types of wings at supersonic speeds and to evaluate various theoretical methods of predicting control characteristics. The first results of the tests were obtained on a delta wing at a Mach number of 1.61 and have been reported in references 1 to 3. The results reported to date have been primarily control hinge-moment characteristics; however, some preliminary pressure distributions and integrated effectiveness characteristics were presented in reference 3.

The second wing being investigated in the control program is a trapezoidal wing of aspect ratio 3.1, taper ratio of 0.4, and having 23° of sweep of the leading edge. This wing was equipped with various 25.4-percent-chord partial and full-span plain flap-type controls, each of which was located at the wing trailing edge, having an unswept hinge line. The control hinge moments, measured directly, and the control effectiveness characteristics, determined from pressure-distribution measurements, are presented in this paper for the trapezoidal-wing tests, and are compared with theoretical predictions.

The wing angle-of-attack range was from 0° to 12° or 15° and the control-deflection range, relative to the wing, was from -30° to 30°. The tests were conducted at Mach numbers of 1.61 and 2.01 for a Reynolds number range of 1.7×10^6 to 5.6×10^6, based on the wing mean aerodynamic chord of 11.72 inches.

SYMBOLS

M	stream Mach number
R	Reynolds number (based on $\bar{c}$)
q	stream dynamic pressure
α	wing angle of attack
δ	control deflection relative to wing (positive when control trailing edge is deflected down)
x	distance from wing apex in chordwise direction
y	distance from wing apex in spanwise direction

$\bar{c}$ wing mean aerodynamic chord

c_R wing root chord

$b/2$ wing semispan

t ratio of control trailing-edge thickness to hinge-line thickness

S semispan-wing area

S_c control area

S_w semispan-wing area, exclusive of control area, $S - S_c$

Q moment of S_c about control hinge line

M_B moment of S_c about wing root

M_A moment of S_c about line through apex perpendicular to the wing root chord

L semispan-wing lift, $q \cos \alpha \left(\int^{S_w} P \, dS_w + \cos \delta \int^{S_c} P \, dS_c \right)$

B semispan-wing root bending moment, $q \left(\int^{S_w} Py \, dS_w + \cos \delta \int^{S_c} Py \, dS_c \right)$

M' semispan-wing pitching moment about 50 percent station of wing mean aerodynamic chord,

$$q \left[\int^{S_w} P(0.564c_R - x) dS_w + \int^{S_c} P(0.746c_R - x) dS_c - 0.182c_R \cos \delta \int^{S_c} P \, dS_c \right]$$

M'' semispan-wing pitching moment about line through apex perpendicular to the wing root chord

H control hinge moment about hinge line, $q \left[\int^{S_c} P(0.746c_R - x) \, dS_c \right]$

C_L lift coefficient, $\frac{L}{qS}$

C_b root bending-moment coefficient, $\frac{B}{2Sbq}$

C_m pitching-moment coefficient, $\frac{M'}{qS\bar{c}}$

$C_{m'}$ pitching-moment coefficient, $\frac{M''}{qS\bar{c}}$

C_h control hinge-moment coefficient, $\frac{H}{2Qq}$

C_{L_δ} $\frac{\partial C_L}{\partial \delta}$

C_{b_δ} $\frac{\partial C_b}{\partial \delta}$

C_{m_δ} $\frac{\partial C_m}{\partial \delta}$

$C_{m'_\delta}$ $\frac{\partial C_{m'}}{\partial \delta}$

C_{h_δ} $\frac{\partial C_h}{\partial \delta}$

C_{h_α} $\frac{\partial C_h}{\partial \alpha}$

All slopes were obtained at $\alpha = 0^\circ$ and $\delta = 0^\circ$.

APPARATUS

Wind Tunnel

This investigation was conducted in the Langley 4- by 4-foot supersonic pressure tunnel, which is a rectangular, closed-throat, single-return type of wind tunnel with provisions for the control of the pressure, temperature, and humidity of the enclosed air. Flexible nozzle walls were adjusted to give the desired test-section Mach numbers of 1.61 and 2.01. During the tests, the dewpoint was kept below -20° F so that the effects of water condensation in the supersonic nozzle were negligible.

Model and Model Mounting

The model used in this investigation consisted of a trapezoidal wing having six interchangeable trailing-edge controls and various associated control adapters (or replacement sections) required to fit the controls to the basic wing. A sketch of the six model configurations is shown in figure 1(a) with the shaded areas denoting the moveable controls. A photograph of the disassembled model is shown in figure 2.

The basic wing had a 23° sweptback leading edge, a root chord of 15.88 inches, a tip chord of 6.17 inches, and a semispan of 17.02 inches. The wing section was a modified hexagon having a ratio of thickness to chord of 4.5 percent based on the local chord. The flat midsection extended from 30 percent chord to 70 percent chord and the corners joining the flat midsection to the leading- and trailing-edge wedges were rounded. The unswept hinge lines were located at the 74.6-percent-chord line for all control configurations. As shown in figure 1(a) control configurations 4, 5, and 6 had identical plan forms, but varying amounts of trailing-edge thickness, $t = 0$, 0.5, and 1.0, respectively. The hinge-line gap was maintained at 0.01 inch (0.08 percent $\bar{c}$) for all configurations except for one series of tests with configuration 4 in which the gap was increased to 0.20 inch (1.71 percent $\bar{c}$) by moving the control and hinge line rearward.

The model was constructed of steel, with the pressure-tube installations made in grooves in the surface which were faired over with a transparent plastic material. The 144 to 169 pressure orifices were located at 5 spanwise stations on the main wing ahead of the control hinge line and at 5 to 8 spanwise stations behind the hinge line, depending on the configuration being tested. The chordwise locations of the pressure orifices are listed in table I and the spanwise locations of the orifice stations are shown in figure 1(b). All screw holes, pits, and mating lines were filled with dental plaster and faired smooth.

The semispan wing was mounted horizontally in the tunnel from a turntable in a steel boundary-layer bypass plate which was located vertically in the test section about 10 inches from the side wall as shown in figure 3. Photographs of three of the model configurations mounted for testing are shown in figure 4. Although the clearness of the plastic material over the tubing installations makes it appear that the wing surface is quite rough, in reality the finish was very smooth.

TESTS

The model angle of attack was changed by rotating the turntable in the bypass plate on which the wing was mounted (see fig. 3). The angle

of attack was measured by a vernier on the outside of the tunnel, inasmuch as the angular deflection of the wing under load was negligible. Control deflection was changed by a gear mechanism mounted on the pressure box which rotated the strain-gage balance, the torque tube, and the control as a unit. The control angles were set with the aid of an electrical control-position indicator mounted inside the wing at the hinge line and were checked with a cathetometer mounted outside the tunnel.

Control hinge moments were determined by means of an electrical strain-gage balance located in the pressure box (fig. 3) which measured the torque on the tube actuating the control surface. The pressure distributions were determined from photographs of the multiple-tube manometer boards to which the pressure leads from the model orifices were connected. The wing lift, pitching-moment, and bending-moment coefficients were determined from integrations of the pressure distributions. As a check on the control hinge-moment coefficients measured directly, values were also determined from the integrated pressure distributions.

Some of the controls were equipped with orifices on one surface only, because structural limitations made it impossible to get the necessary pressure tubes through the torque tube to instrument both surfaces. For these models, the tests were run at positive and negative angles of attack over the control-deflection range and the necessary summations of the forces on the individual surfaces were made at reversed angular conditions. All data are presented as if the tests were made at positive angles of attack only. The majority of the test configurations had a control deflection range from -30° to 30° for angles of attack of 0°, 6°, and 12° and an angle-of-attack range from 0° to 15° for 0° control deflection. Hinge-moment measurements were made at control-deflection intervals of 5° and pressure-distribution measurements were made at control-deflection intervals of 10° and at the end points of curves.

Most of the tests were made at tunnel stagnation pressures of 13.0 and 15.1 pounds per square inch at Mach numbers of 1.61 and 2.01, respectively, corresponding to a Reynolds number based on the wing mean aerodynamic chord of 3.6×10^6. Additional tests were made with configuration 4 in which the tunnel stagnation pressure was varied to give Reynolds numbers of 1.7×10^6 and 5.6×10^6 at $M = 1.61$ and Reynolds numbers of 1.7×10^6 and 4.5×10^6 at $M = 2.01$. In order to insure a turbulent boundary layer over the model during the tests, 3/16-inch-wide strips of No. 60 carborundum were attached to the wing upper and lower surfaces at a distance of 1/4 inch from the leading edge. These strips completely spanned the model except within 1/4 inch of the orifice stations.

PRECISION OF DATA

The mean Mach numbers in the region occupied by the model are estimated from calibrations to be 1.61 and 2.01 with local variations being smaller than ±0.02. There is no evidence of any significant flow angularities. The overall accuracies of the integrated coefficients are not known; however, if the pressure-distribution fairings are assumed to be correct, the repeatability of the integrated coefficients and the estimated accuracies of other pertinent quantities are:

α, deg	±0.05
δ, deg	±0.1
C_L (from integrations)	±0.01
C_b (from integrations)	±0.002
C_m (from integrations)	±0.002
C_h (from direct measurements)	±0.005

The base pressures on the two configurations having trailing-edge thickness were neglected in determining the integrated coefficients. Analysis indicated this effect would be negligible.

THEORY

The linear theory method of reference 4 was used to estimate the control hinge-moment and effectiveness parameters for model configurations 1 to 4. In determining the hinge-moment and effectiveness parameters due to control deflection for configuration 4, the equations of reference 4 were modified to take into account the existence of the bypass plate, which acted as a reflection plane.

The theoretical basic wing lift, bending-moment, and pitching-moment coefficients due to wing angle of attack were determined by summing the integrated pressure distributions in the two-dimensional and conical flow regions on the wing. These pressure distributions were obtained from reference 5.

In order to get an approximation of the effect of wing thickness, theoretical characteristics with thickness were obtained by correcting the linear-theory values by the ratios of the two-dimensional characteristics obtained with thickness to the two-dimensional flat-plate characteristics. The correction method used herein is similar to those used in references 4 and 6. In determining the two-dimensional characteristics with thickness, the equations and charts of reference 7, which employ the shock-expansion technique, were used. Theoretical corrections

for the effect of base pressure on configurations 5 and 6 were neglected since analysis indicated that they would be small.

RESULTS AND DISCUSSION

Effect of Control Deflection

The basic data for each of the 14 test conditions are presented in figures 5 to 18 in the form of variations of wing lift, bending-moment, and pitching-moment coefficients with control deflection and variations of control hinge-moment coefficient with control deflection. The results for the six basic model configurations as well as model configuration 4 with the increased hinge-line gap are presented at $M = 1.61$ for $R = 3.6 \times 10^6$. In addition, results for configuration 4 are presented at $R = 1.7 \times 10^6$ and 5.6×10^6 for $M = 1.61$. At $M = 2.01$, test results for basic configurations 2, 3, and 4 are presented at $R = 3.6 \times 10^6$ and for configuration 4 at $R = 1.7 \times 10^6$ and 4.5×10^6. In all cases the point symbols refer to the integrated pressure-distribution results. The solid lines on the plots of lift, bending-moment, and pitching-moment coefficient are curves faired through the points. The lines on the hinge-moment-coefficient plots are the curves determined from the strain-gage balance measurements, which were obtained at 5° intervals, and indicate the reliability of the integrated pressure-distribution results.

In general, the variations of lift and bending-moment coefficients with control deflection are fairly linear over the range of control deflections for all configurations tested; however, there is an increased slope of the curves at the higher angles of attack and control deflections. The variations of pitching-moment and hinge-moment coefficients with control deflection are also quite linear over the range of control deflections from -20° to 20°. At control deflections exceeding these values, a sudden decrease in slope occurs for many of the test configurations, similar to that observed in reference 3, and which is caused by a forward shift in the center of pressure due to separation of the flow ahead of the high pressure side of the control at large deflections.

Effect of Wing Angle of Attack

The variations of wing lift, bending-moment, and pitching-moment coefficients with angle of attack for the basic wing having a sharp trailing edge are presented in figure 19 for the two test Mach numbers at a Reynolds number of 3.6×10^6. These variations were obtained from the tests of configurations 1, 2, 3, and 4 at zero control deflection,

the variations at other control deflections being parallel although displaced according to the effectiveness of the particular control. The experimental curves of figure 19 are compared with the predictions of the linear theory and the linear theory corrected for thickness.

The curves of figure 19 are all linear over the angle-of-attack range, and lift- and bending-moment-coefficient slopes obtained experimentally are in excellent agreement with both theoretical predictions. The linear-theory prediction of pitching-moment coefficient due to angle of attack appears to be poor; however, it is magnified considerably by the choice of pitching-moment center at the midchord of the mean aerodynamic chord and in reality is a good prediction since the error in center-of-pressure location is only about 5 percent of the mean aerodynamic chord. When the effect of wing thickness is included, the theoretical prediction of pitching-moment coefficient is improved.

Illustrative curves showing the control hinge-moment-coefficient variation with angle of attack for basic model configuration 4 are presented in figure 20 for the two test Mach numbers. In order to prevent needless duplication, the hinge-moment curves for the other test configurations are omitted since the character of the variations are similar and the data are available in figures 5 to 18. The curves of figure 20 are linear over the angle-of-attack range and generally parallel over the range of control deflection, as were the curves for the other configurations.

Effect of Reynolds Number

Comparisons of the variations of wing lift, bending-moment, pitching-moment, and control hinge-moment coefficients with control deflection for model configuration 4 at $M = 1.61$ for the three test Reynolds numbers are presented in figure 21. The changes in variation of lift and bending-moment coefficient with control deflection due to changing the Reynolds number from 1.7×10^6 to 5.6×10^6 are small and inconsistent. The changes in pitching-moment and hinge-moment variations are within the accuracy of the tests. The results at $M = 2.01$ of varying the Reynolds numbers from 1.7×10^6 to 4.5×10^6 (not shown here) are also small and inconsistent. It appears, therefore, that the Reynolds number change had little effect on the characteristics of the model tested.

Effect of Trailing-Edge Thickness

The variations of wing lift, bending-moment, pitching-moment, and control hinge-moment coefficients with control deflections for configurations 4, 5, and 6, for which $t = 0$, 0.5, and 1.0, respectively, are shown

in figure 22. In almost all cases changing from a sharp trailing-edge ($t = 0$) to a half-blunt trailing edge ($t = 0.5$) caused an appreciable increase in the slopes of the curves. Further increasing the thickness to a blunt trailing edge ($t = 1.0$) caused no appreciable change in the curves. This effect can be seen more clearly in the plots of figure 23 showing the control effectiveness and hinge-moment parameters as functions of the ratio of trailing-edge thickness to hinge-line thickness. An increase in slopes due to increasing the trailing-edge thickness is predicted by the thickness-corrected theoretical curves; however, the magnitude and the exact variation with t of the increases in experimental parameters are not predicted. For purposes of comparison, experimental points and theoretical curves are also shown in figure 23 for similar tests (ref. 6) of thickened trailing-edge effect on a partial span control on a swept wing of a complete aircraft configuration. In the tests of reference 6, the increase in slopes from $t = 0$ to $t = 0.5$ was appreciably greater than that from $t = 0.5$ to $t = 1.0$, except for the lift effectiveness. In general, an increase in slope parameters with increasing trailing-edge thickness is in harmony with other supersonic test results on two-dimensional and three-dimensional wings such as references 8 and 9.

Effect of Hinge-Line Gap

The variations of wing lift, bending-moment, pitching-moment, and control hinge-moment coefficient with control deflection are shown in figure 24 for model configuration 4 with hinge-line gaps of 0.01 inch and 0.20 inch. In general, the effect of increasing the hinge-line gap by 1.6 percent of the mean aerodynamic chord was to increase the slopes of the curves, especially at small control deflections. At $\alpha = 0^\circ$, $\delta = 0^\circ$, the increases in slopes varied from 6 percent for the hinge-moment slope parameter to 20 percent for the pitching-moment slope parameter, the latter being the one coefficient that benefited both from the aerodynamic effect and from the geometric effect of moving the hinge line rearward.

Effect of Mach Number

The theoretical and experimental control effectiveness and hinge-moment parameters are plotted as functions of Mach number in figure 25 for the basic configurations having sharp trailing edges. Note that the axes have been shifted and that all parameters have been plotted numerically upward to prevent confusion of the curves and points. The linear theory overestimates the experimental parameters for all model configurations at both test Mach numbers; however, when the effect of wing thickness is included, the theoretical predictions are considerably improved. In general, the experimental change in control effectiveness

and hinge-moment parameters with Mach number is the same or somewhat less than is predicted theoretically.

Effect of Control Size and Location

Correlations of the experimental and theoretical wing lift, bending-moment, and pitching-moment slope parameters with control-area ratio, control-area-moment ratio about the root chord, and control-area-moment ratio about the wing apex, respectively, are presented in figure 26 for the basic configurations having sharp trailing edges. Both the theoretical and experimental points correlate in approximately straight lines, the slopes of the experimental correlations being about 70 percent of those of the linear theory correlations. Inclusion of the wing thickness effect in the theoretical predictions eliminated approximately half of the discrepancy between the experimental and linear theory correlations. The experimental correlations at $M = 1.61$ presented herein were presented in preliminary form in reference 10. Correlations were also shown in reference 10 for various controls on a delta wing, and it was pointed out that similar correlations were obtained on swept and unswept wings from other sources.

CONCLUSIONS

An investigation has been made at Mach numbers of 1.61 and 2.01 to determine the control effectiveness and hinge-moment characteristics for a series of 25.4-percent-chord trailing-edge controls on a trapezoidal wing having a 23° sweptback leading edge, aspect ratio of 3.1, and taper ratio of 0.4. Tests were made at angles of attack from 0° to 15° for control deflections from -33° to 30° and the results indicate the following conclusions:

1. Linear theory overestimated the effectiveness and hinge-moment characteristics due to control deflection and the hinge-moment characteristics due to wing angle of attack, but predicted the basic wing characteristics due to angle of attack very well. Modifying the linear-theory method to account for the wing thickness improved the theoretical predictions.

2. Varying the Reynolds number from 1.7×10^6 to 5.6×10^6 caused little change in the effectiveness and hinge-moment characteristics for the full-span control having a sharp trailing edge.

3. Increasing the trailing-edge thickness of the full-span control from zero thickness to half the hinge-line thickness caused a numerical increase in the control effectiveness and hinge-moment parameters. Further increasing the trailing-edge thickness caused little change in slopes.

4. Within the range of gaps tested, increasing the hinge-line gap on the full-span control having a sharp trailing edge increased numerically the control effectiveness and hinge-moment parameters.

5. The experimental changes of the control effectiveness and hinge-moment parameters with Mach number were the same or somewhat less than predicted theoretically.

6. Correlations were obtained both theoretically and experimentally, showing the wing lift, root bending moment, and pitching-moment effectiveness to be functions primarily of control area, control-area moment about the wing root, and control-area moment about the pitch center, respectively.

Langley Aeronautical Laboratory,
National Advisory Committee for Aeronautics,
Langley Field, Va., April 5, 1954.

REFERENCES

1. Czarnecki, K. R., and Lord, Douglas R.: Hinge-Moment Characteristics for Several Tip Controls on a 60° Sweptback Delta Wing at Mach Number 1.61. NACA RM L52K28, 1953.

2. Czarnecki, K. R., and Lord, Douglas R.: Preliminary Investigation of the Effect of Fences and Balancing Tabs on the Hinge-Moment Characteristics of a Tip Control on a 60° Delta Wing at Mach Number 1.61. NACA RM L53D14, 1953.

3. Lord, Douglas R., and Czarnecki, K. R.: Aerodynamic Characteristics of a Full-Span Trailing-Edge Control on a 60° Delta Wing With and Without a Spoiler at a Mach Number of 1.61. NACA RM L53L17, 1954.

4. Goin, Kennith L.: Equations and Charts for the Rapid Estimation of Hinge-Moment and Effectiveness Parameters for Trailing-Edge Controls Having Leading and Trailing Edges Swept Ahead of the Mach Lines. NACA Rep. 1041, 1951. (Supersedes NACA TN 2221.)

5. Harmon, Sidney M., and Jeffreys, Isabella: Theoretical Lift and Damping in Roll of Thin Wings With Arbitrary Sweep and Taper at Supersonic Speeds - Supersonic Leading and Trailing Edges. NACA TN 2114, 1950.

6. Spearman, M. Leroy, and Webster, Robert A.: An Investigation at Mach Numbers of 1.40 and 1.59 of the Effects of Aileron Profile on the Aerodynamic Characteristics of a Complete Model of a Supersonic Aircraft Configuration. NACA RM L50J31, 1951.

7. Ivey, H. Reese, Stickle, George W., and Schuettler, Alberta: Charts for Determining the Characteristics of Sharp-Nose Airfoils in Two-Dimensional Flow at Supersonic Speeds. NACA TN 1143, 1947.

8. Chapman, Dean R., and Kester, Robert H.: Effect of Trailing-Edge Thickness on Lift at Supersonic Velocities. NACA RM A52D17, 1952.

9. Goin, Kennith L., and Westrick, Gertrude C.: Effects of Trailing-Edge Bluntness on the Lift, Drag, and Pitching-Moment Characteristics of Unswept, 45° Swept, and 45° Delta Wings at Mach Numbers of 1.41, 1.62, and 1.96. NACA RM L53D13, 1953.

10. Lord, Douglas R., and Czarnecki, K. R.: Recent Information on Flap and Tip Controls. NACA RM L53I17a, 1953.

TABLE I

CHORDWISE LOCATIONS OF ORIFICES

[Station spanwise locations shown in figure 1(b)]

Orifices ahead of hinge line:
(orifice locations identical on upper and lower surfaces).

Stations	1	3	4	7	8
$\frac{x}{c_R}$	0.034	0.157	0.275	0.394	0.469
	.093	.203	.308	.414	.482
	.162	.260	.354	.449	.509
	.260	.342	.420	.499	.549
	.358	.423	.485	.548	.588
	.456	.505	.551	.598	.628
	.554	.586	.617	.648	.667
	.603	.627	.650	.673	.687
	.652	.667	.682	.697	.707
	.701	.708	.715	.722	.727
	.737	.737	.737	.737	.737

Orifices behind hinge lines:
(orifices located on upper surface only for configurations 1, 2, 3, and 4; orifice locations identical on upper and lower surfaces for configurations 5 and 6).

Stations	1	2	3	4	5	6	7	8
$\frac{x}{c_R}$	0.757	0.751	0.751	0.750	0.749	0.749	0.748	0.747
	.774	.770	.769	.764	.762	.762	.760	.756
	.838	.825	.822	.807	.798	.798	.792	.782
	.902	.879	.875	.850	.835	.835	.824	.808
	.976	.940	.934	.893	.870	.870	.852	.826

Additional orifices located: On wing inside hinge-line gap at stations 1, 3, 4, 7, and 8 and on control leading edge at stations 3, 4, 5, 7, 8 where applicable.

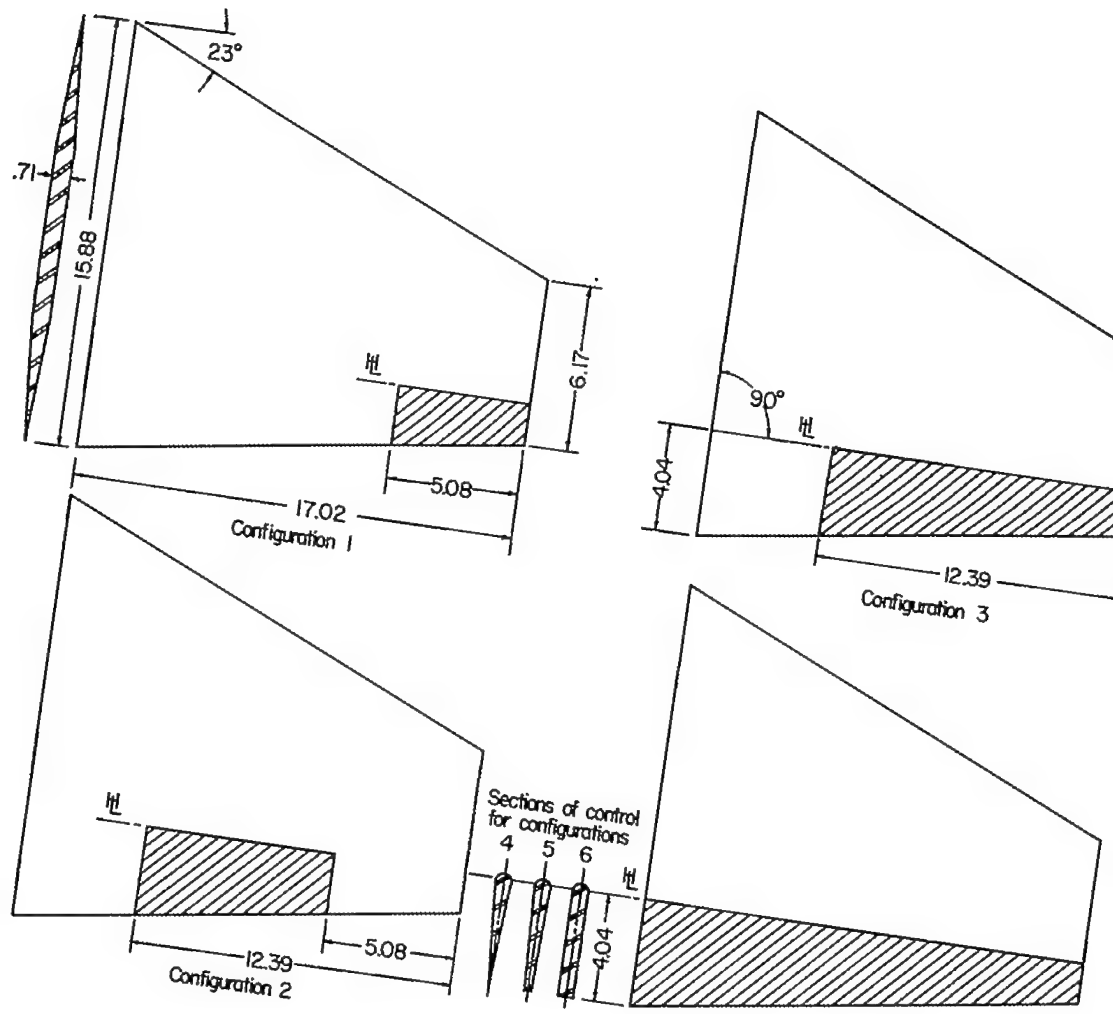

(a) Wing and control plan forms and sections.

Figure 1.- Sketches of model configurations tested. All dimensions are in inches.

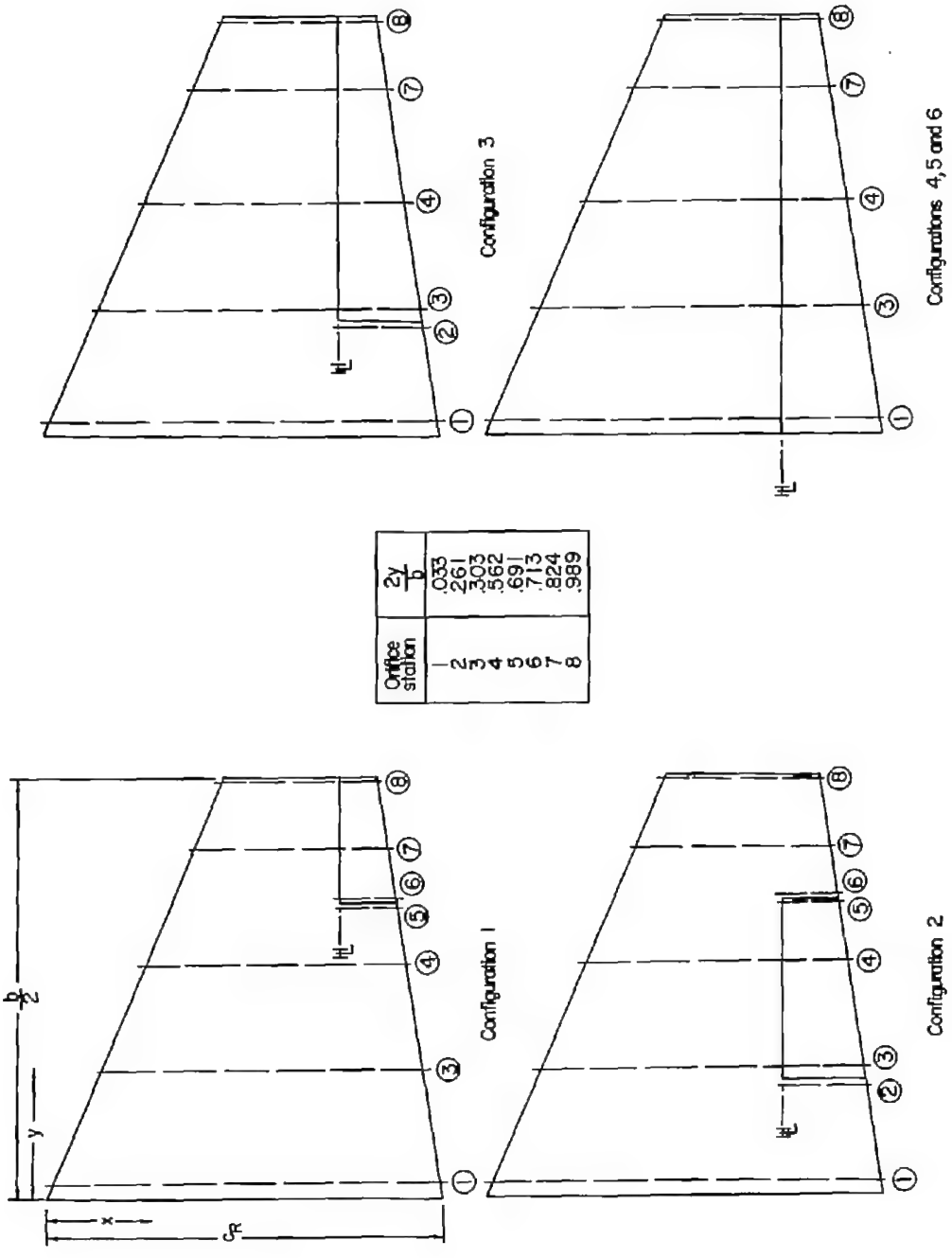

Orifice station	2y/b
2	.033
3	.261
4	.303
5	.562
6	.691
7	.713
8	.824
	.989

(b) Spanwise location of orifice stations.

Figure 1.- Concluded.

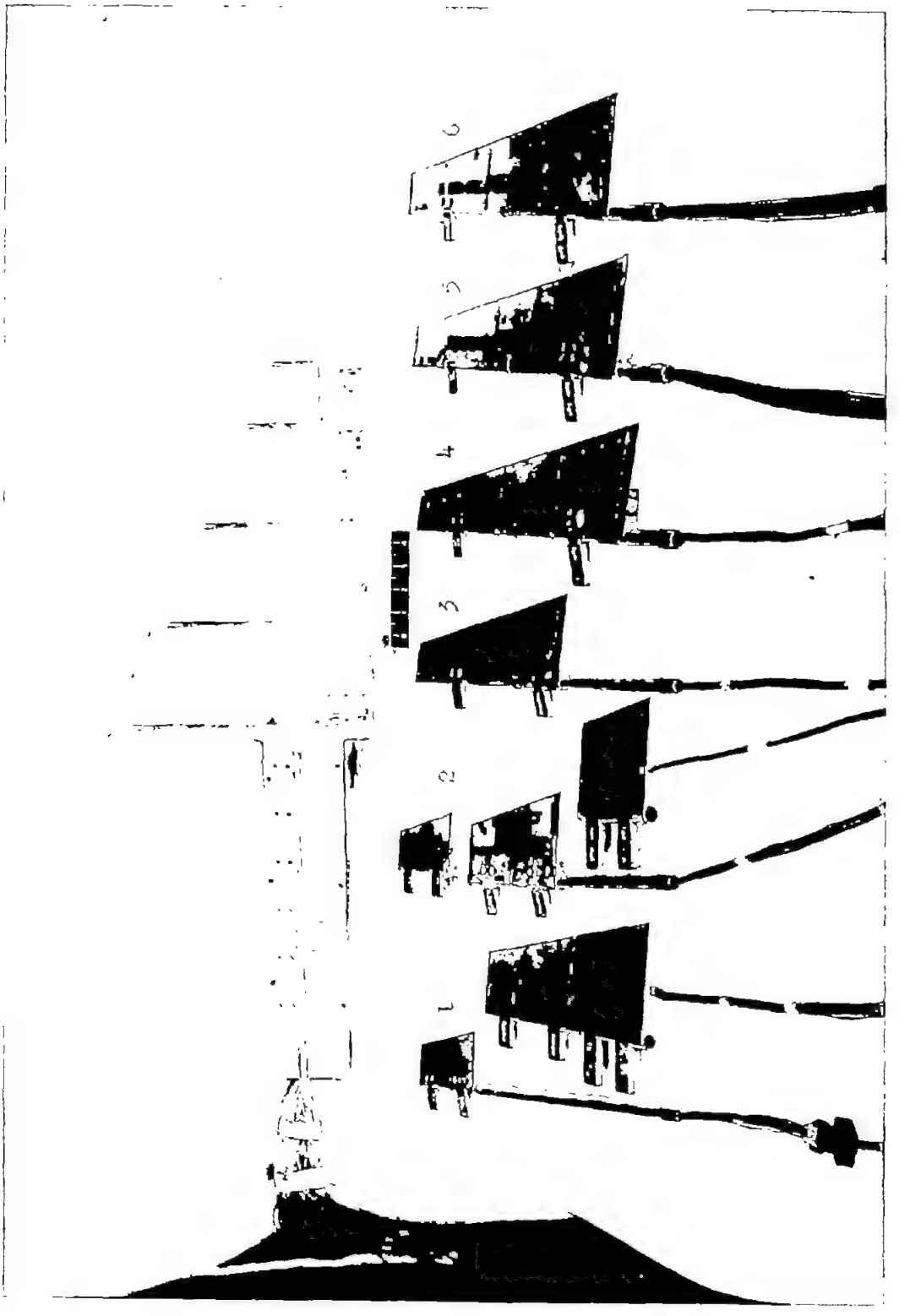

L-79386.1

Figure 2.- Photograph of disassembled model.

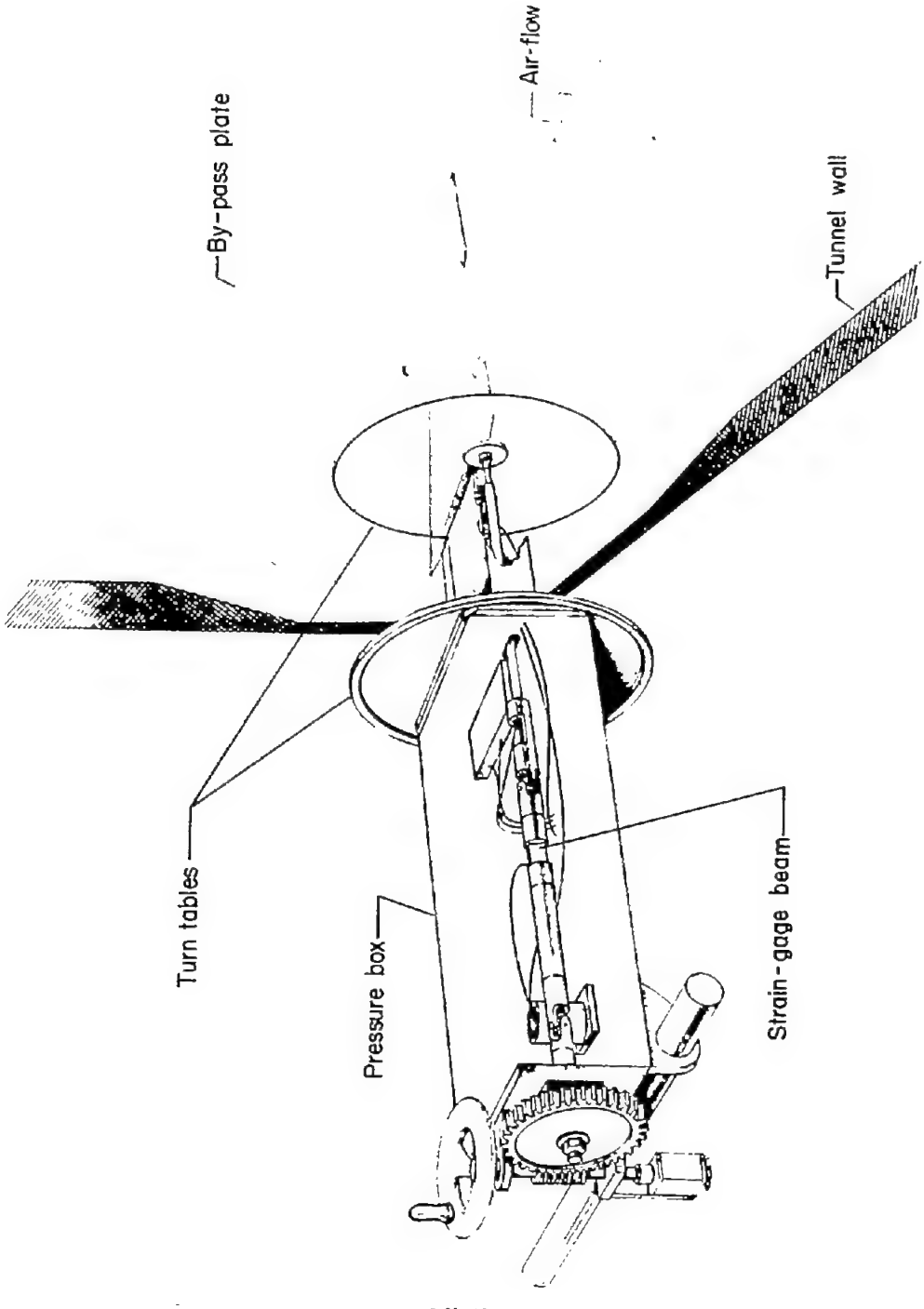

L-83645

Figure 3.- Sketch of test setup.

L-79385

(a) Configuration 1.

Figure 4.- Photographs of three of the model configurations mounted on the bypass plate.

L-79384

(b) Configuration 2.

Figure 4.- Continued.

L-79383

(c) Configuration 4.

Figure 4.- Concluded.

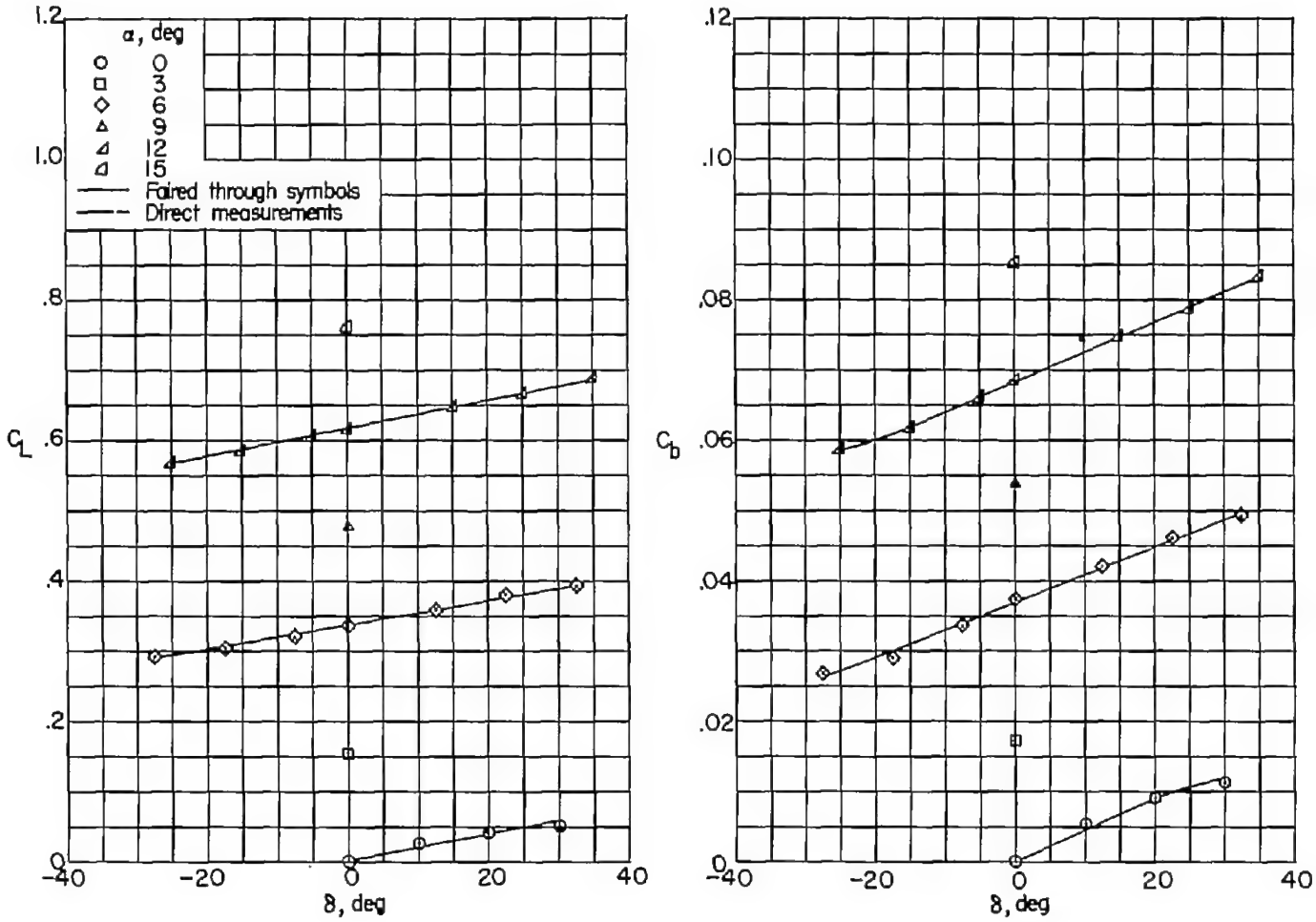

(a) C_L.

(b) C_b.

Figure 5.- Variation of basic coefficients with control deflection for configuration 1. M = 1.61; R = 3.6×10^6.

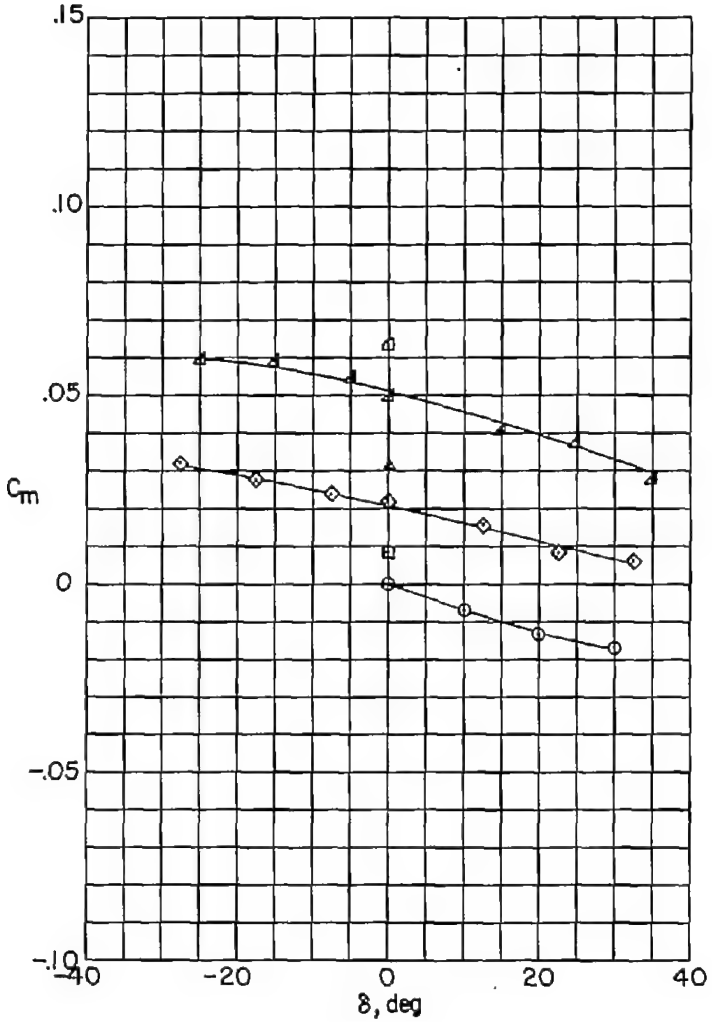

(c) C_m.

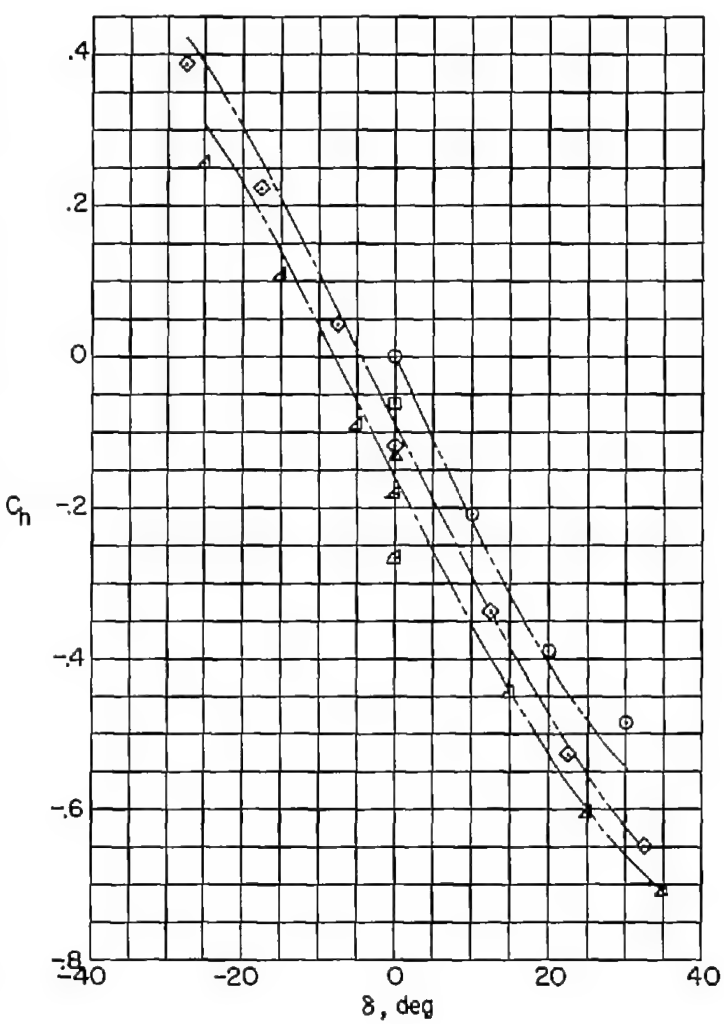

(d) C_h.

Figure 5.- Concluded.

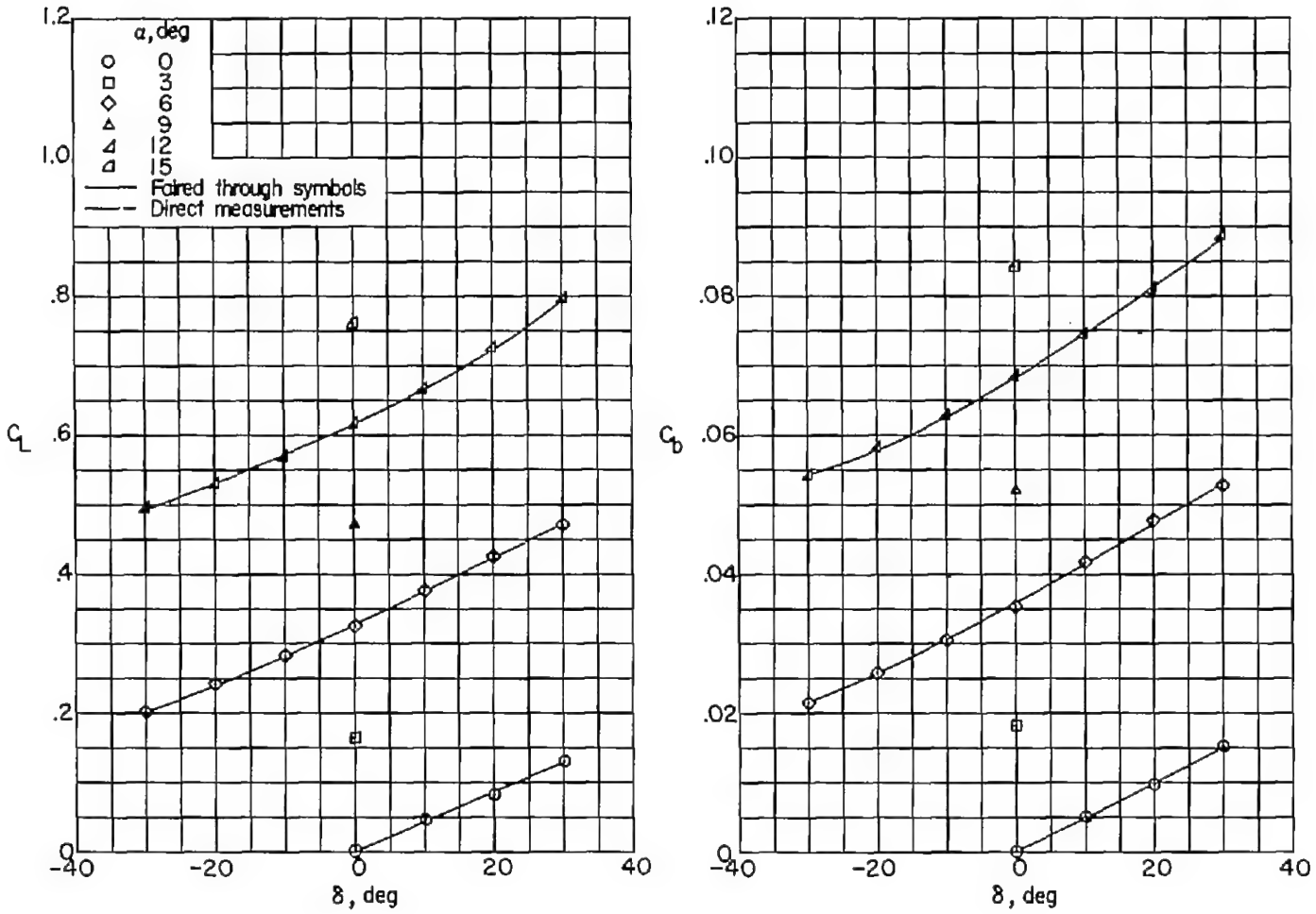

(a) C_L.

(b) C_b.

Figure 6.- Variation of basic coefficients with control deflection for configuration 2. M = 1.61; R = 3.6×10^6.

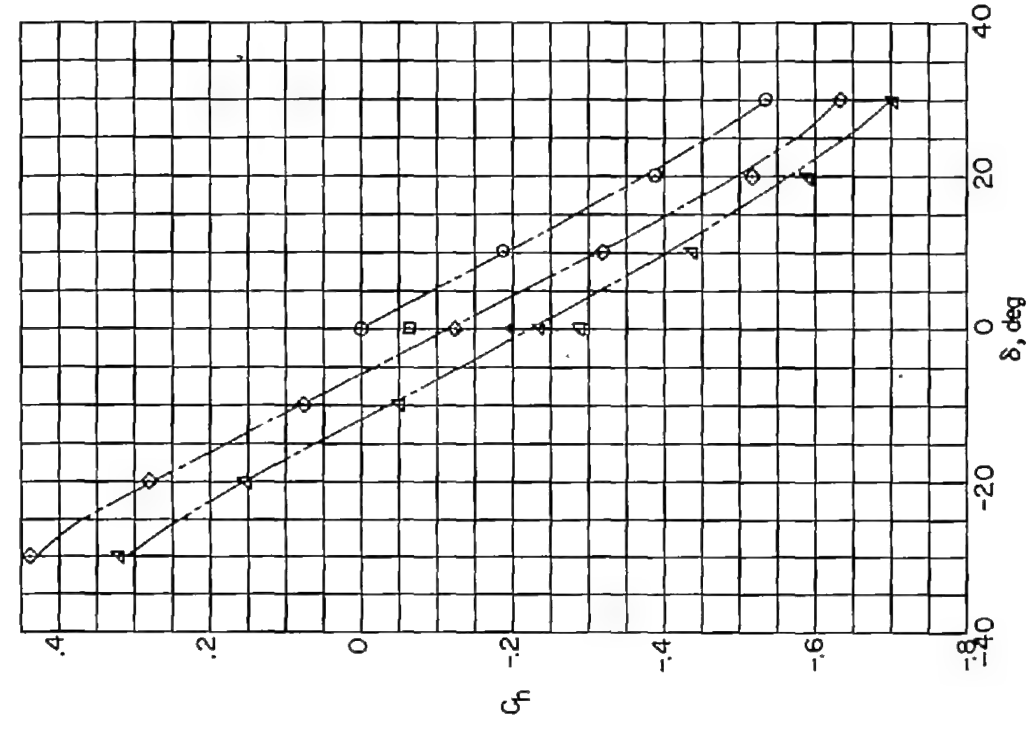

(a) C_h.

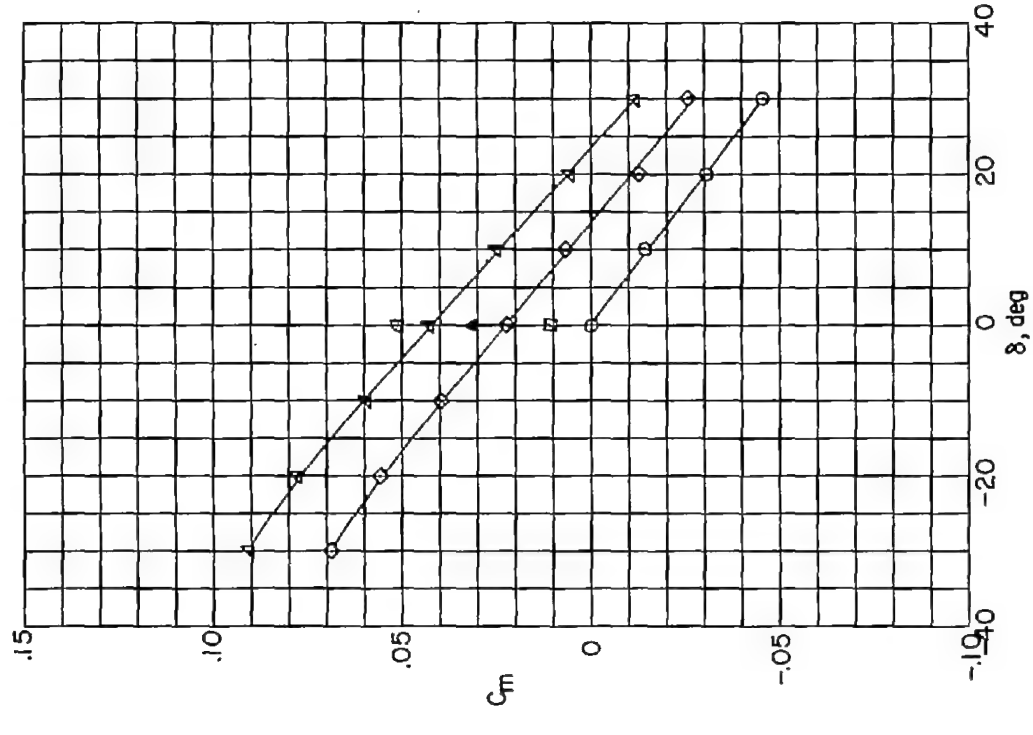

(c) C_m.

Figure 6.- Concluded.

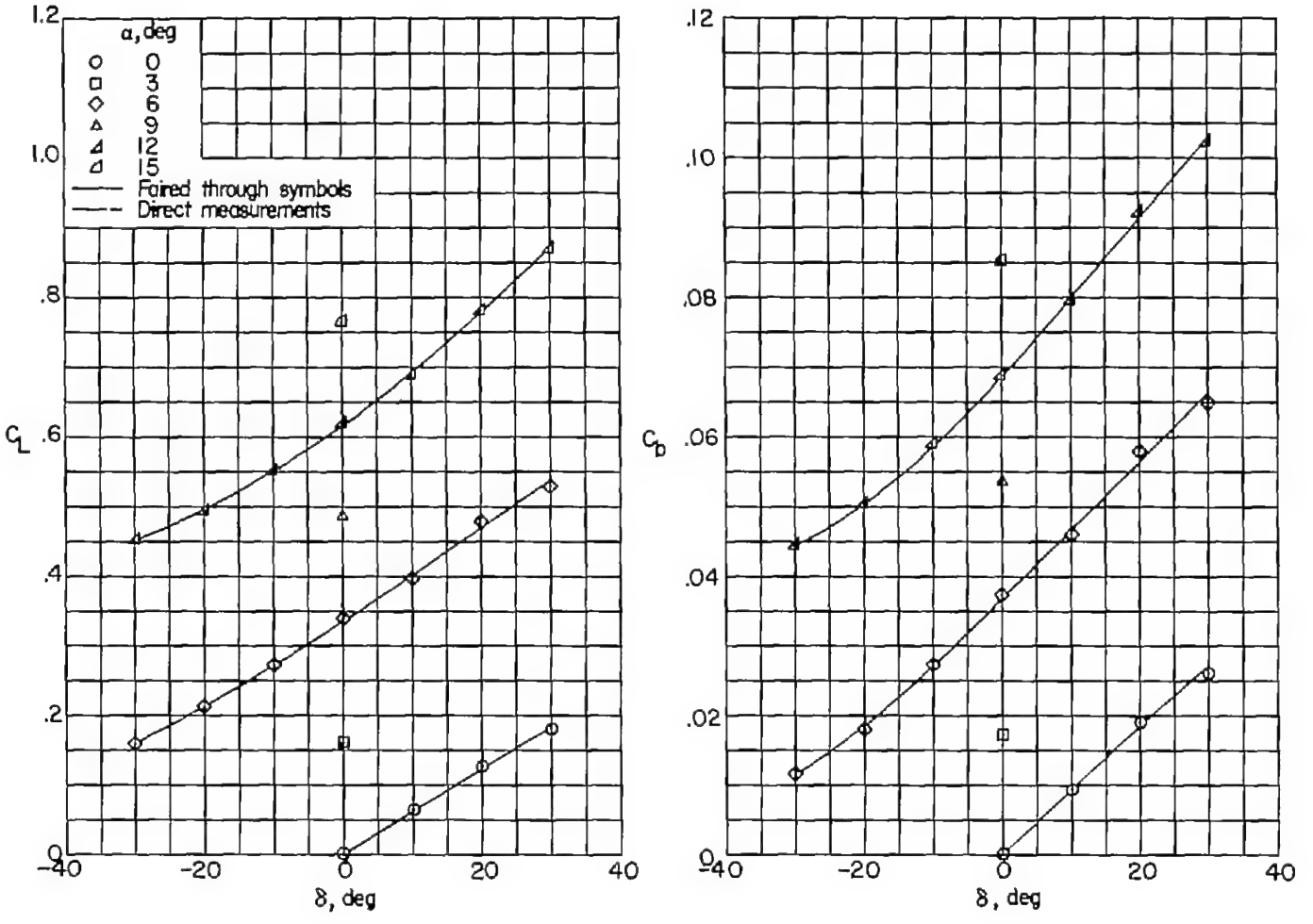

(a) C_L.

(b) C_D.

Figure 7.- Variation of basic coefficients with control deflection for configuration 3. M = 1.61; R = 3.6×10^6.

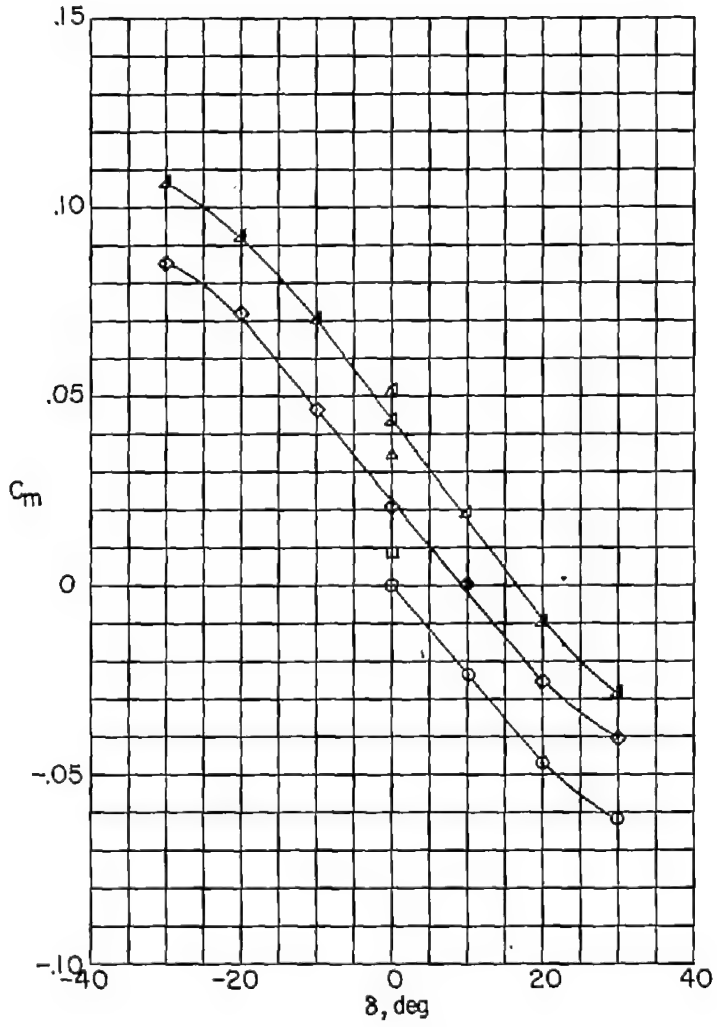

(c) C_m.

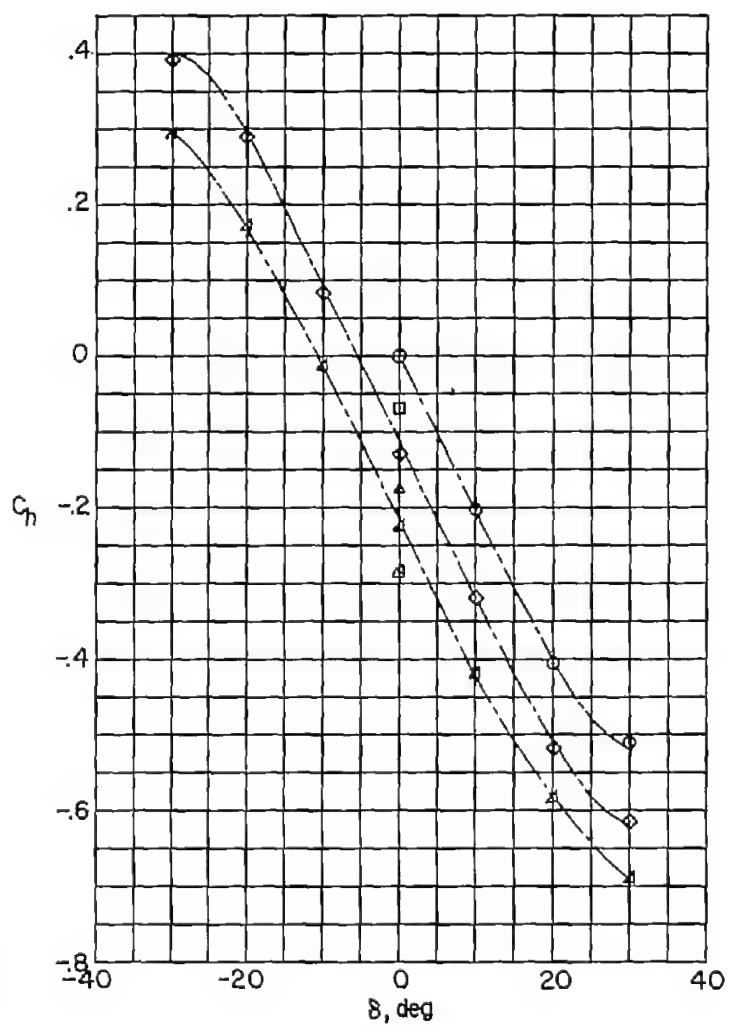

(d) C_h.

Figure 7.- Concluded.

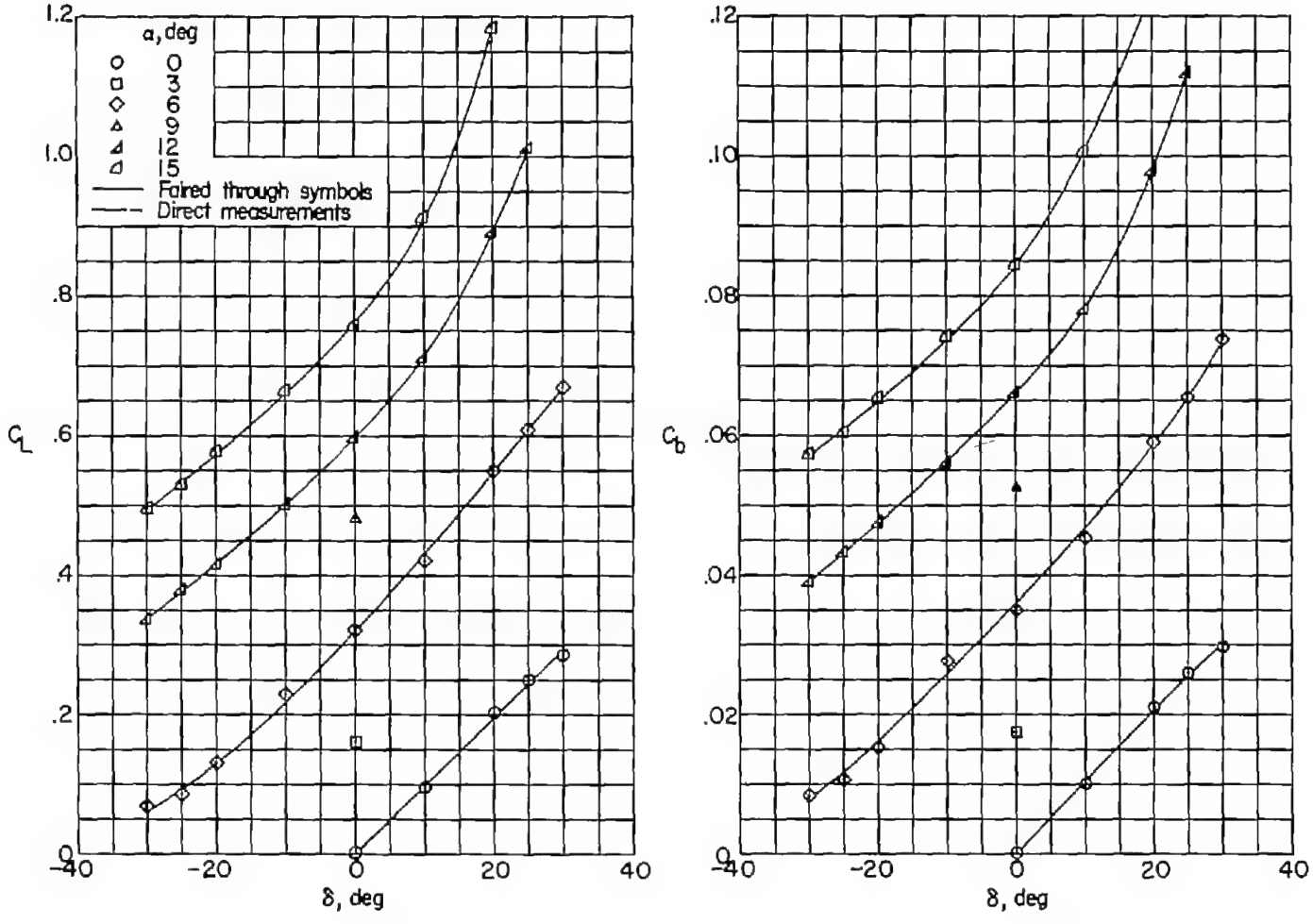

(a) C_L.

(b) C_b.

Figure 8.- Variation of basic coefficients with control deflection for configuration 4. M = 1.61; R = 3.6×10^6.

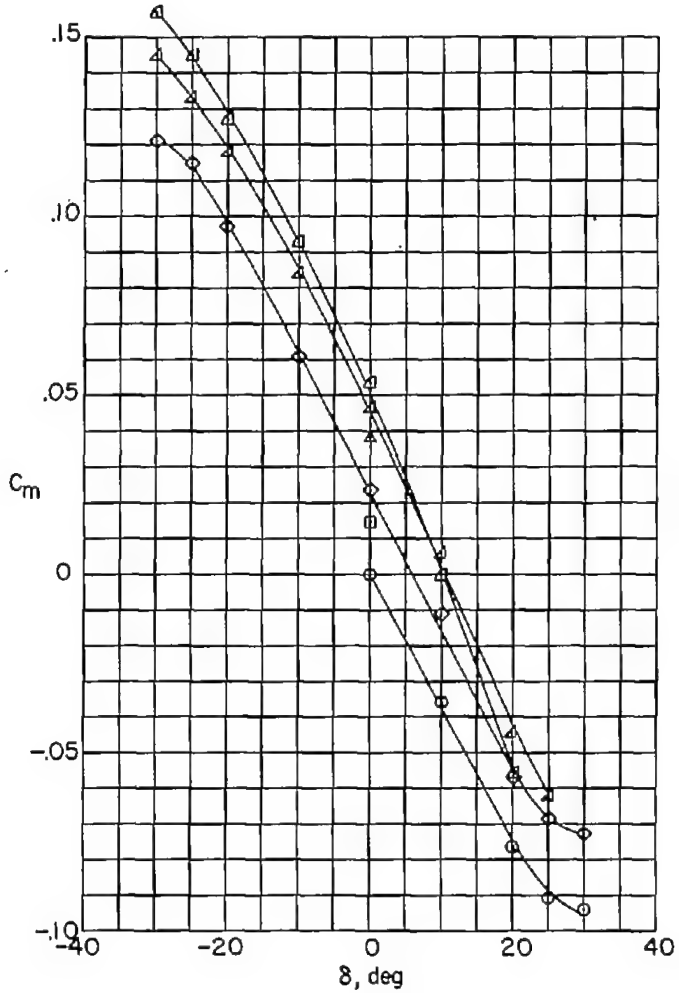

(c) C_m.

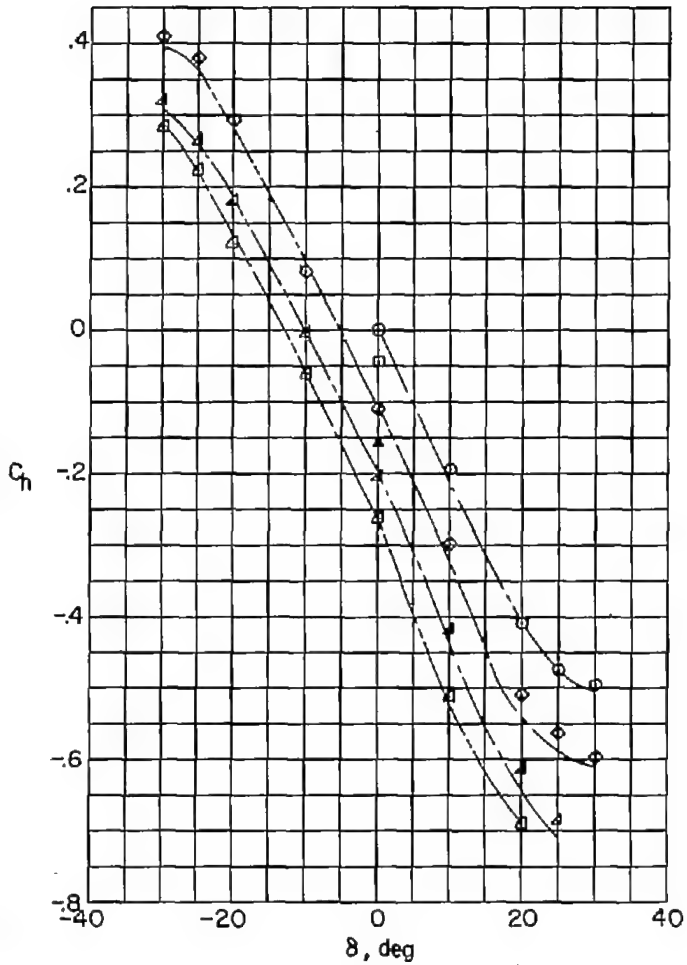

(d) C_h.

Figure 8.- Concluded.

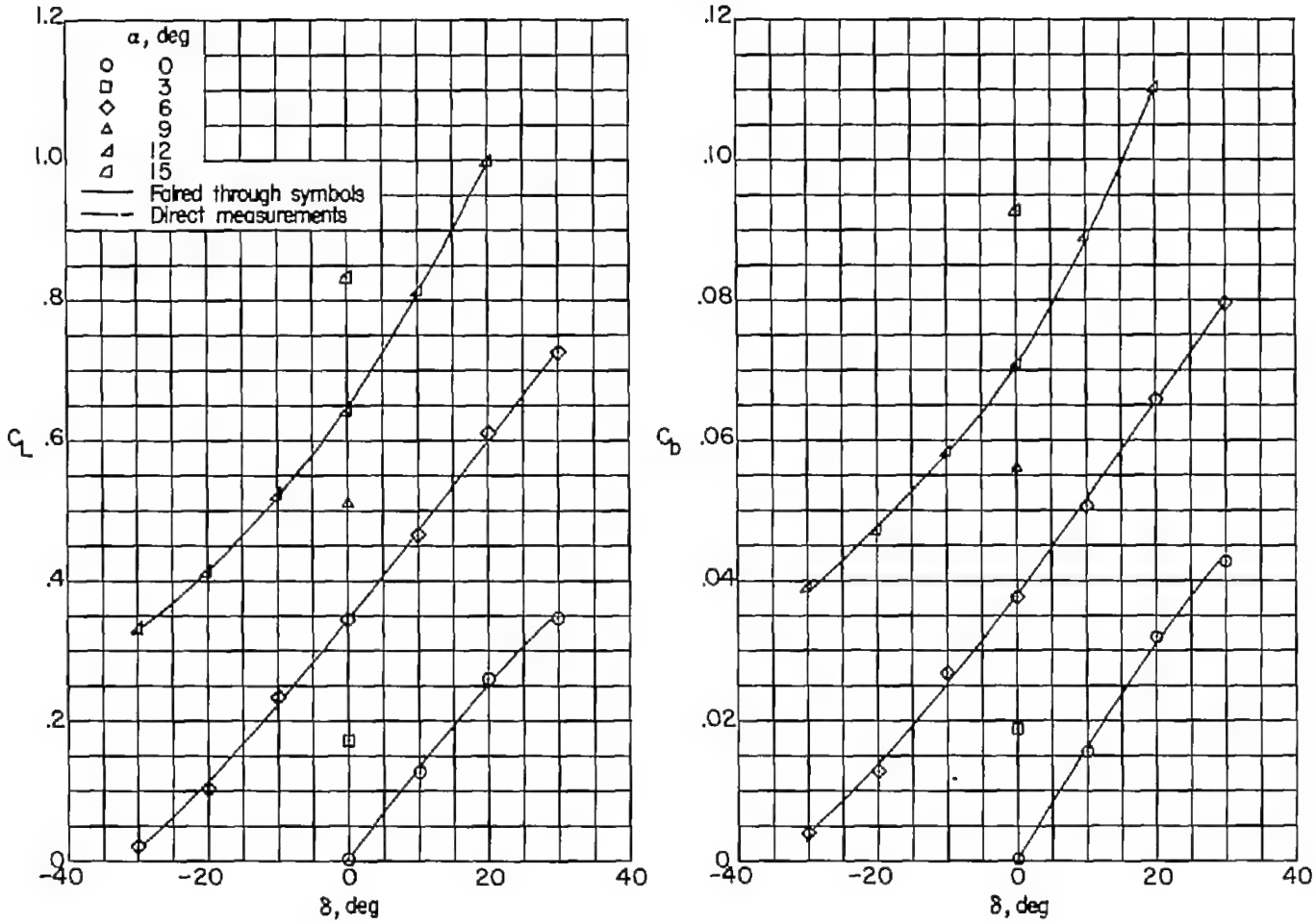

(a) C_L.

(b) C_b.

Figure 9.- Variation of basic coefficients with control deflection for configuration 5. M = 1.61; R = 3.6×10^6.

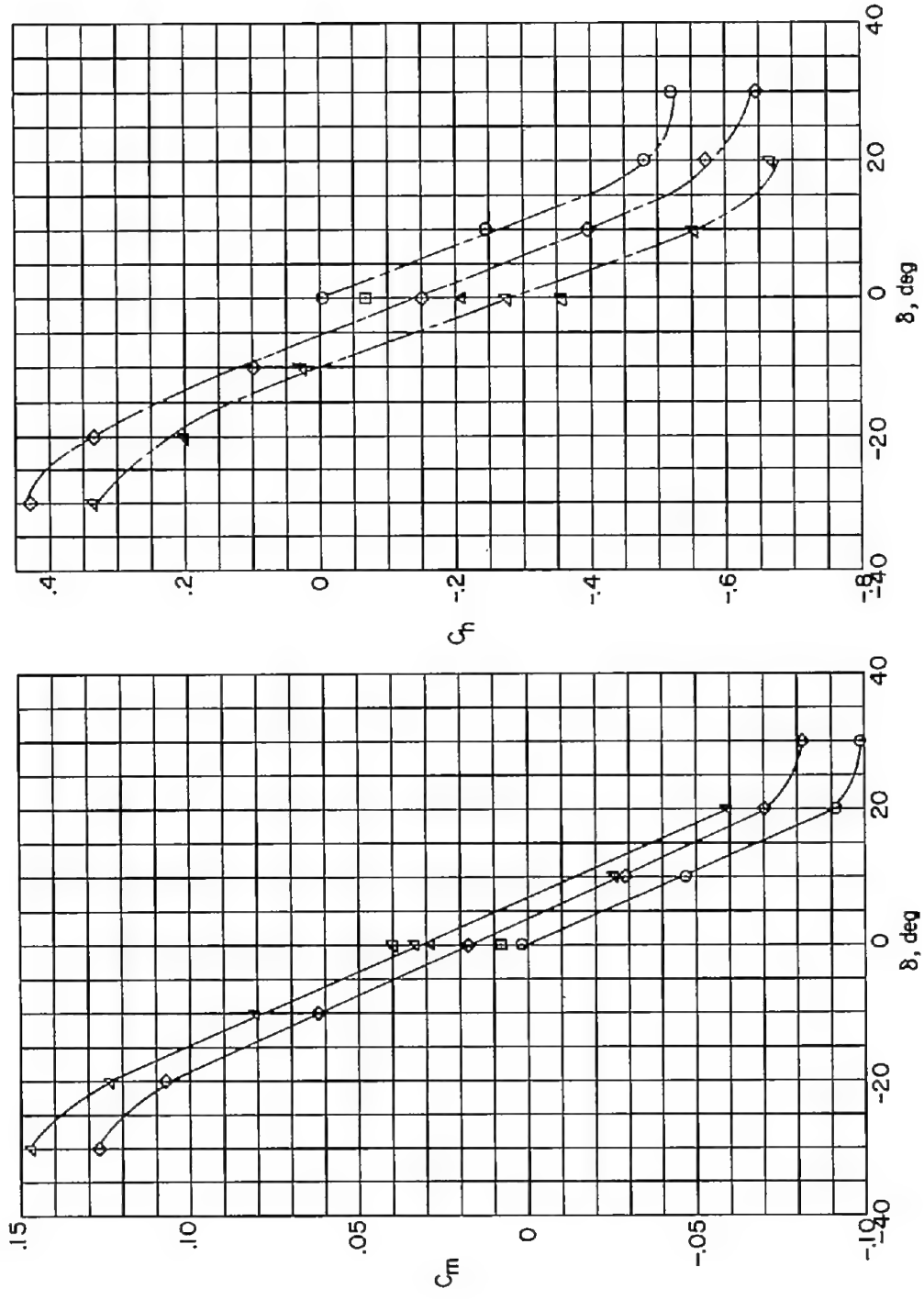

(c) C_m.

(d) C_n.

Figure 9.- Concluded.

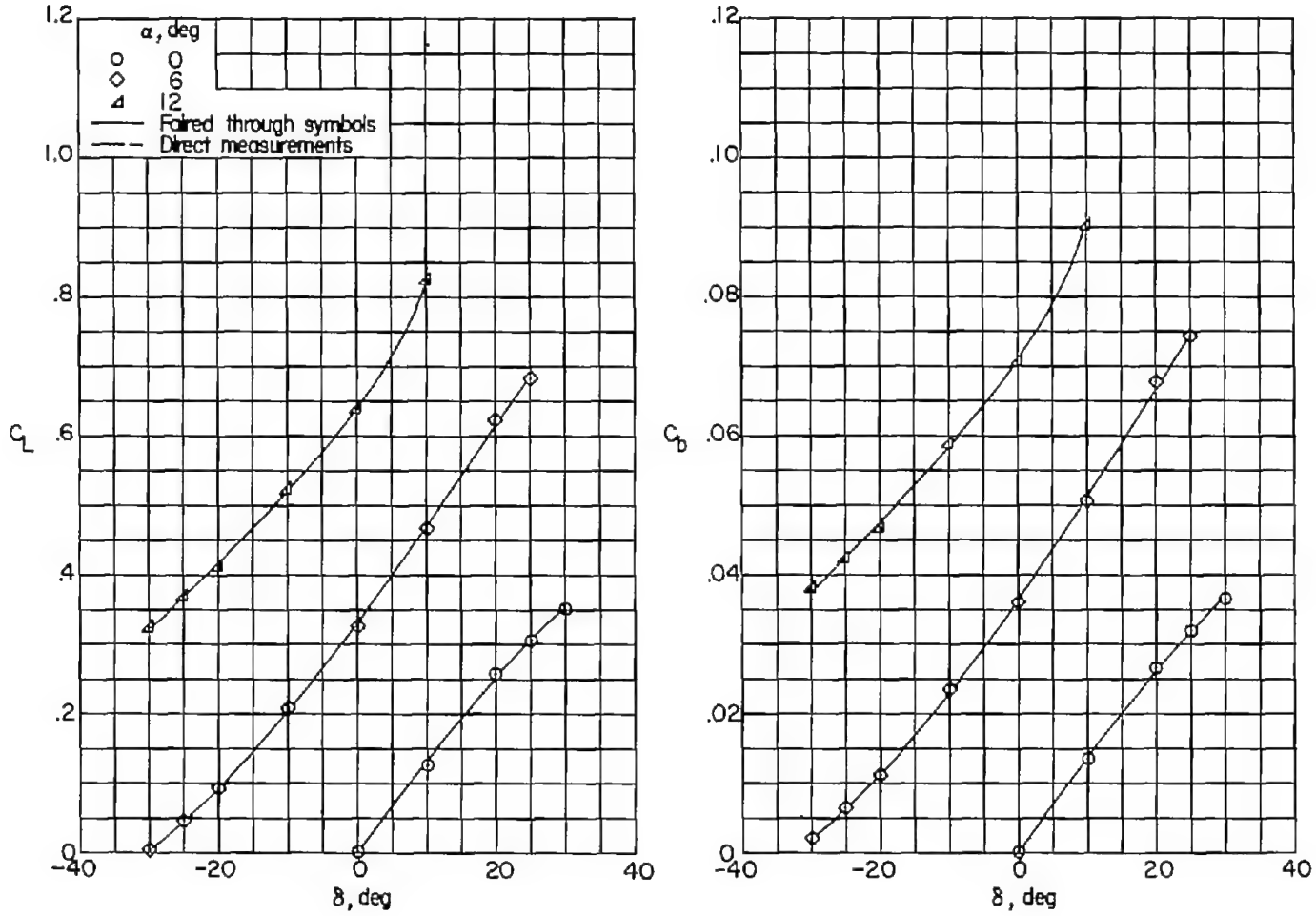

(a) C_L.

(b) C_b.

Figure 10.- Variation of basic coefficients with control deflection for configuration 6. M = 1.61; R = 3.6×10^6.

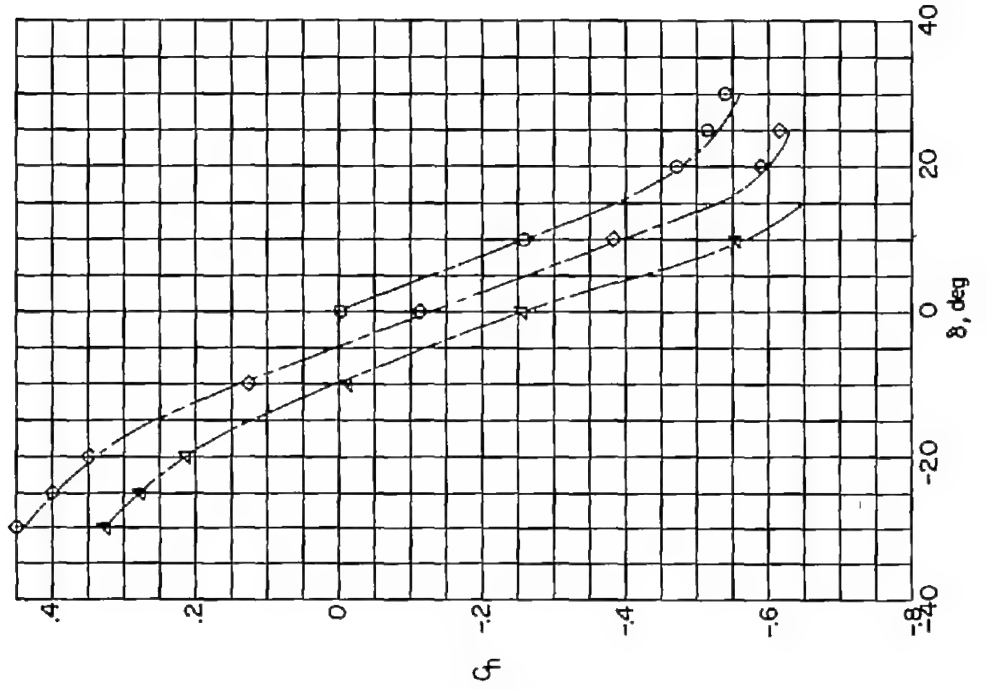

(d) C_n.

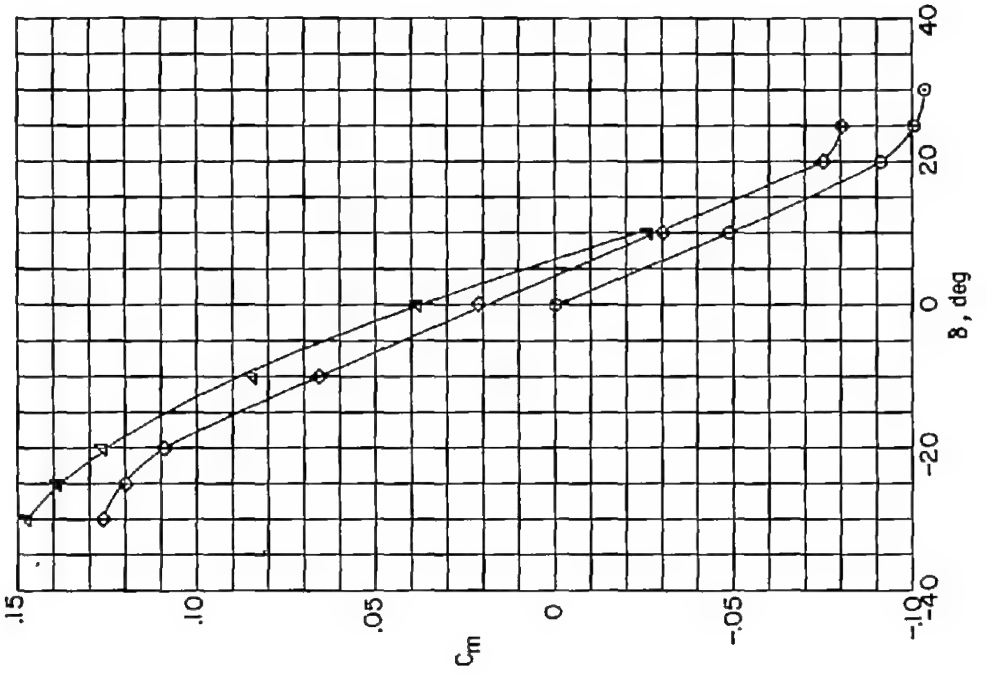

(c) C_m.

Figure 10.- Concluded.

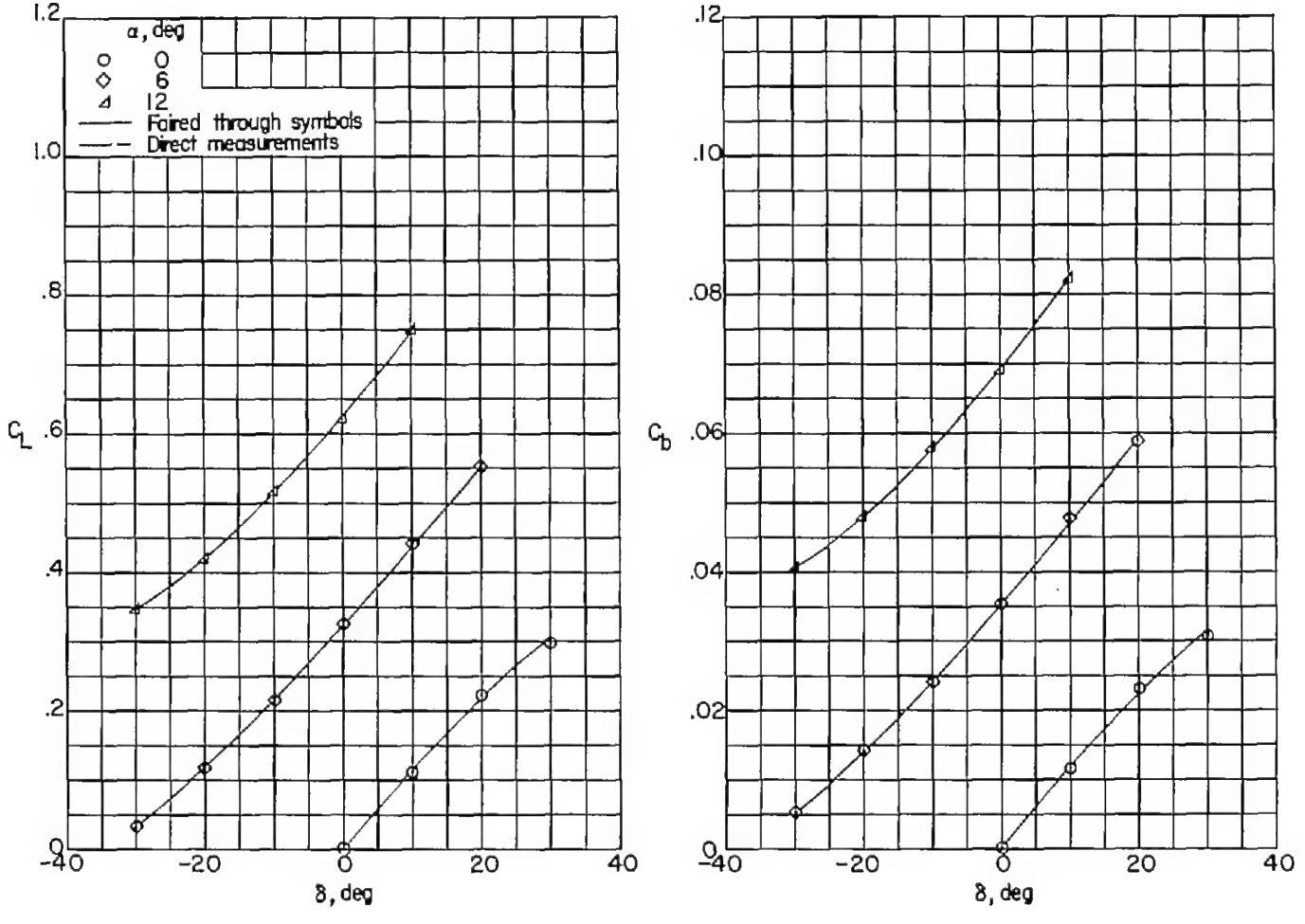

(a) C_L.

(b) C_b.

Figure 11.- Variation of basic coefficients with control deflection for configuration 4 with 0.20 inch hinge-line gap. M = 1.61; R = 3.6×10^6.

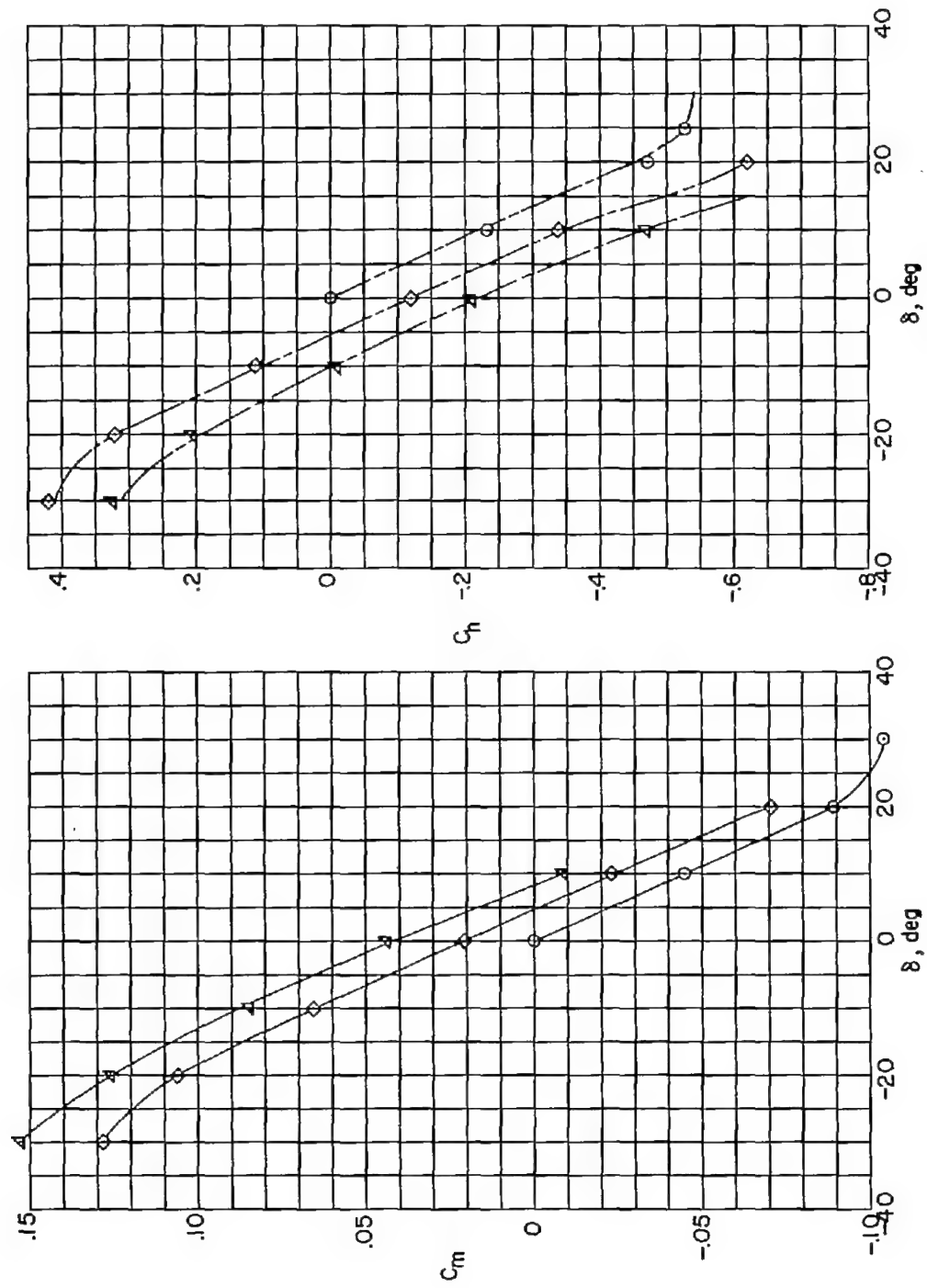

(d) C_h.

(c) C_m.

Figure 11.- Concluded.

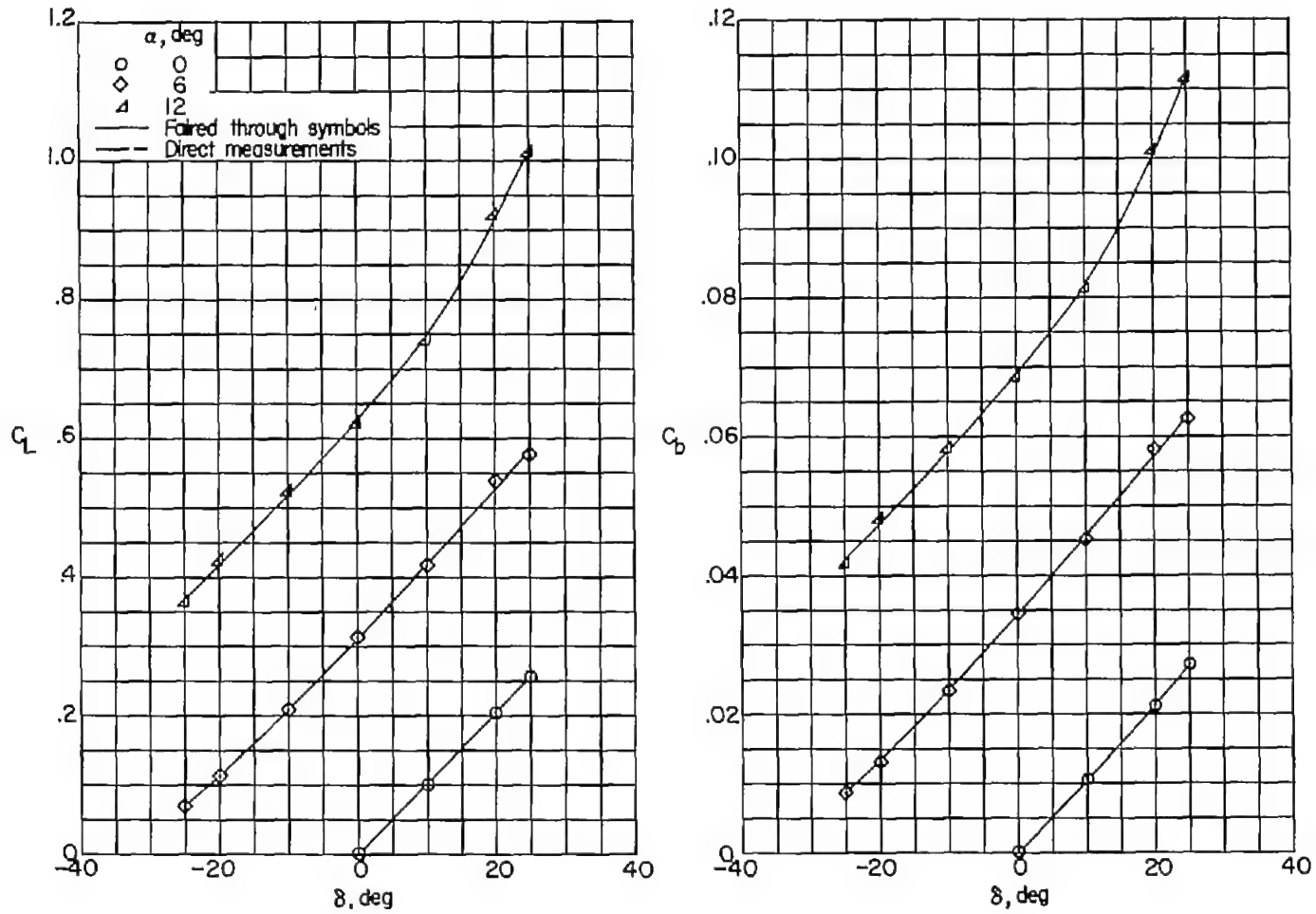

(a) C_L.

(b) C_b.

Figure 12.- Variation of basic coefficients with control deflection for configuration 4. M = 1.61; R = 1.7×10^6.

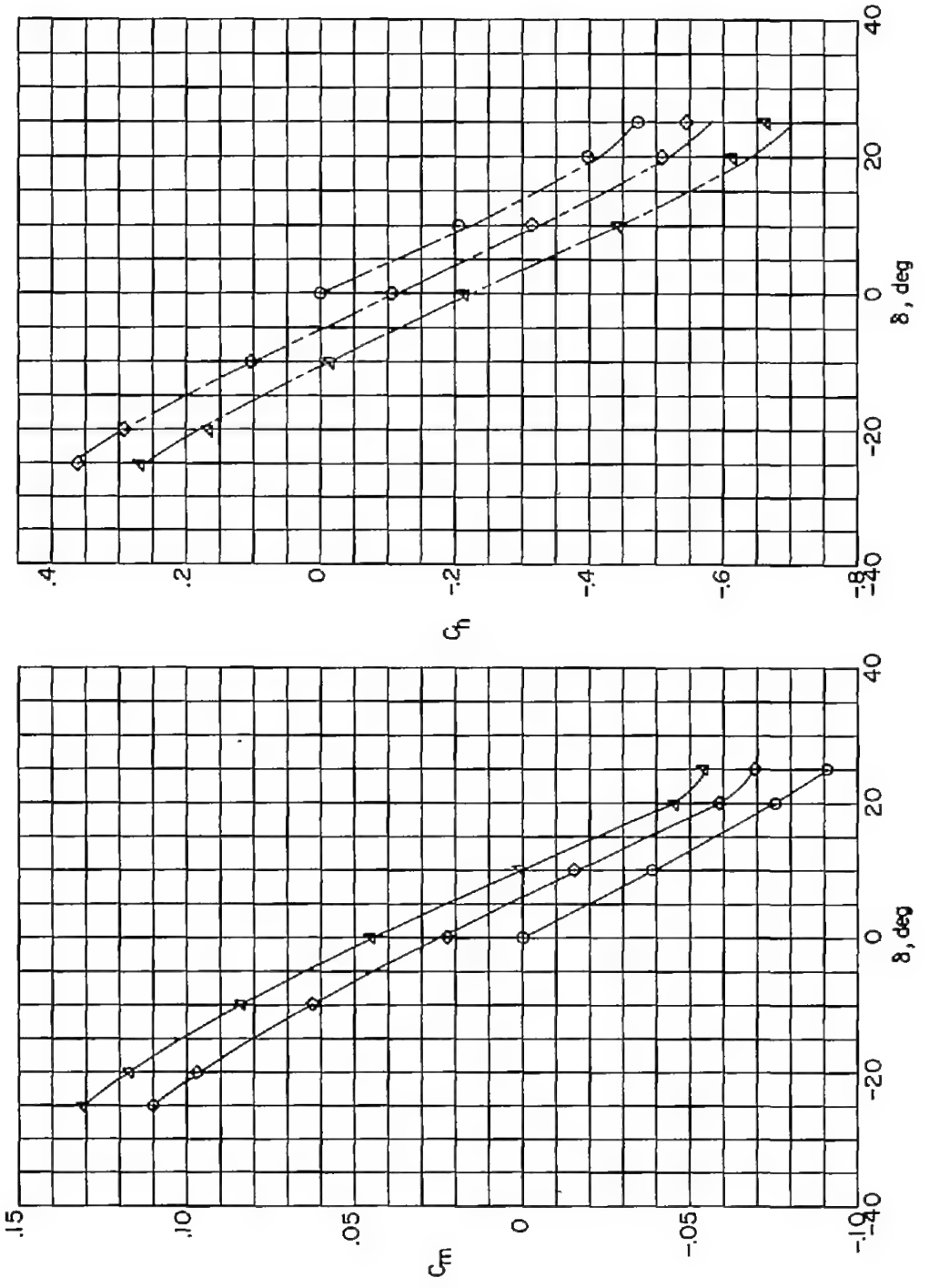

(c) C_m.

(d) C_n.

Figure 12.- Concluded.

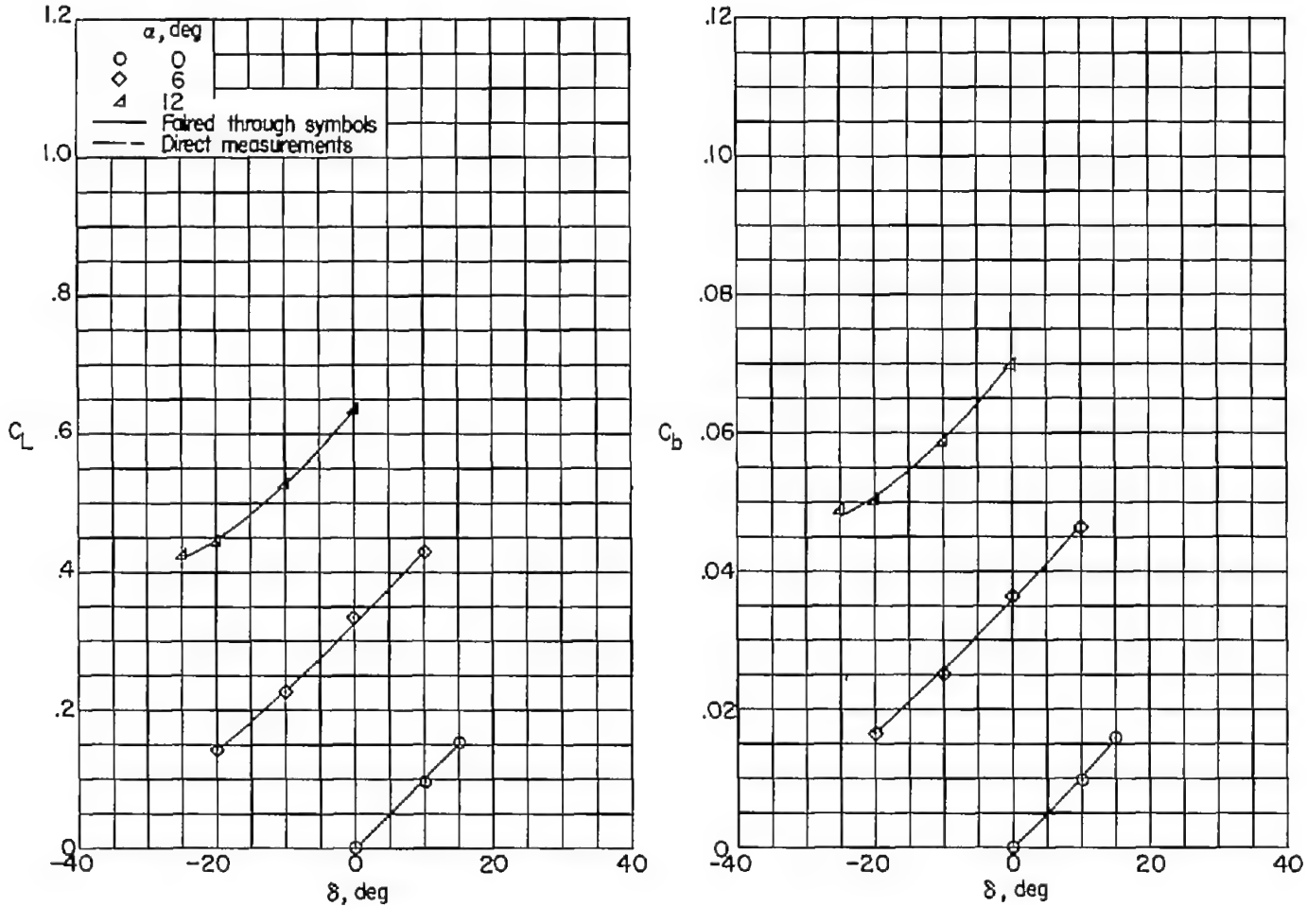

(a) C_L.

(b) C_b.

Figure 13.- Variation of basic coefficients with control deflection for configuration 4. M = 1.61; R = 5.6×10^6.

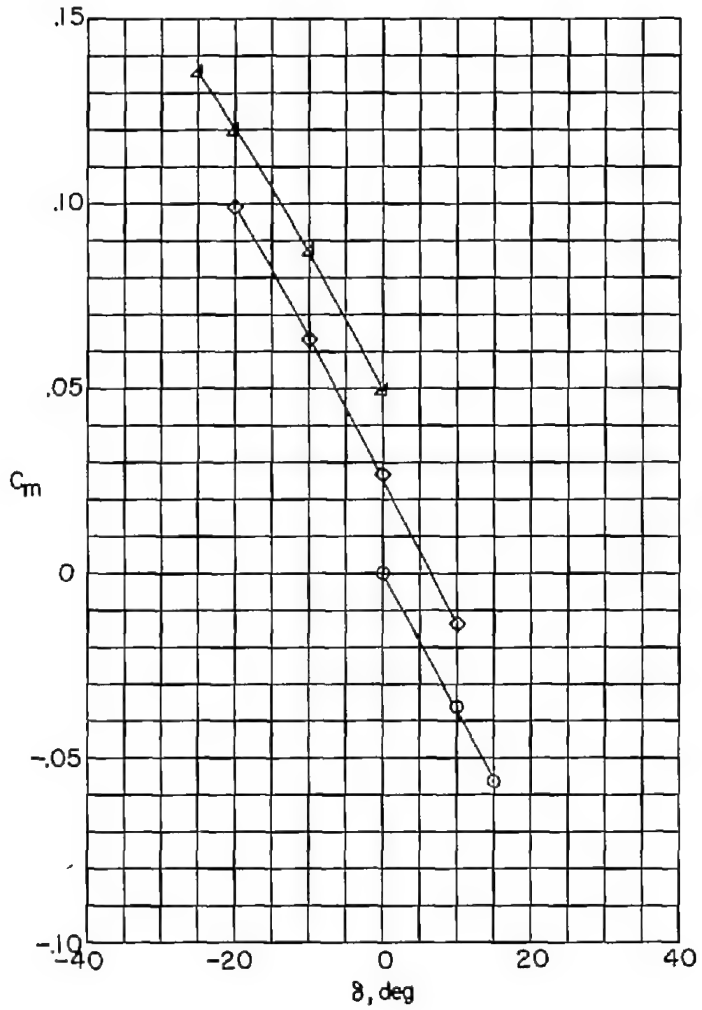

(c) C_m.

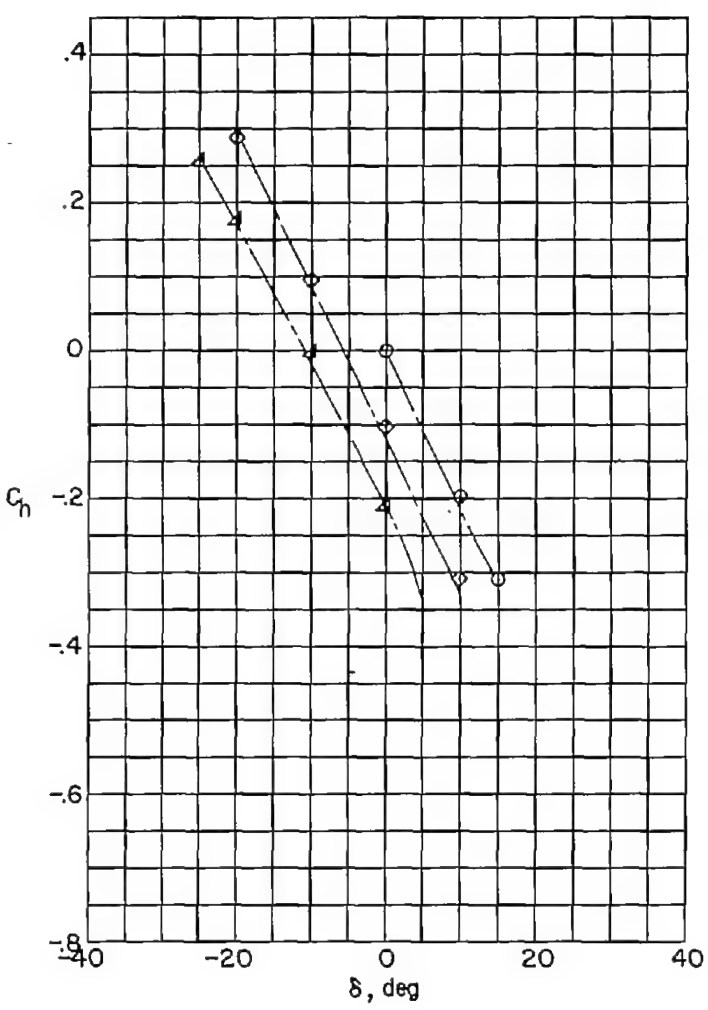

(d) C_h.

Figure 13.- Concluded.

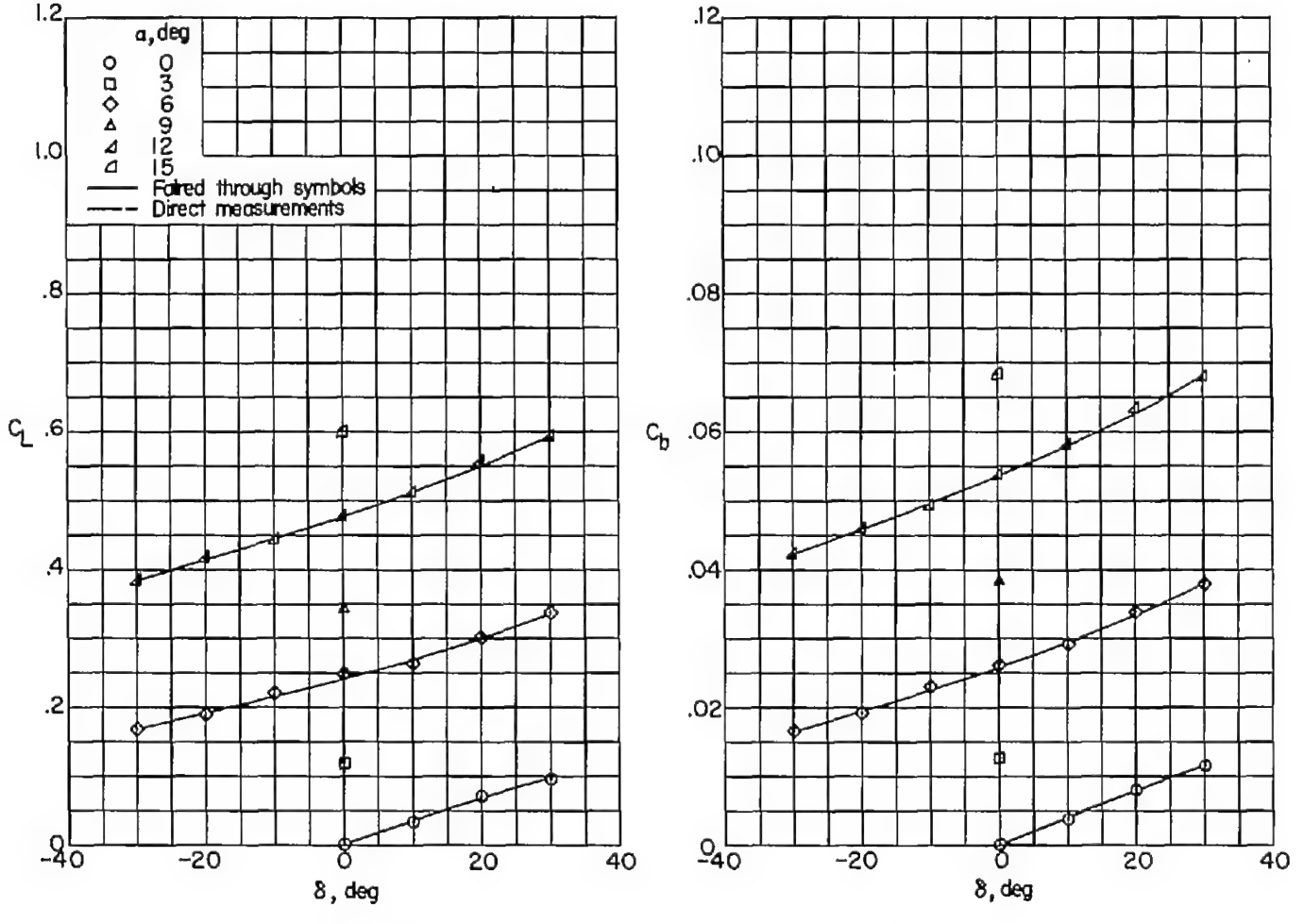

(a) C_L.

(b) C_b.

Figure 14.- Variation of basic coefficients with control deflection for configuration 2. M = 2.01; R = 3.6×10^6.

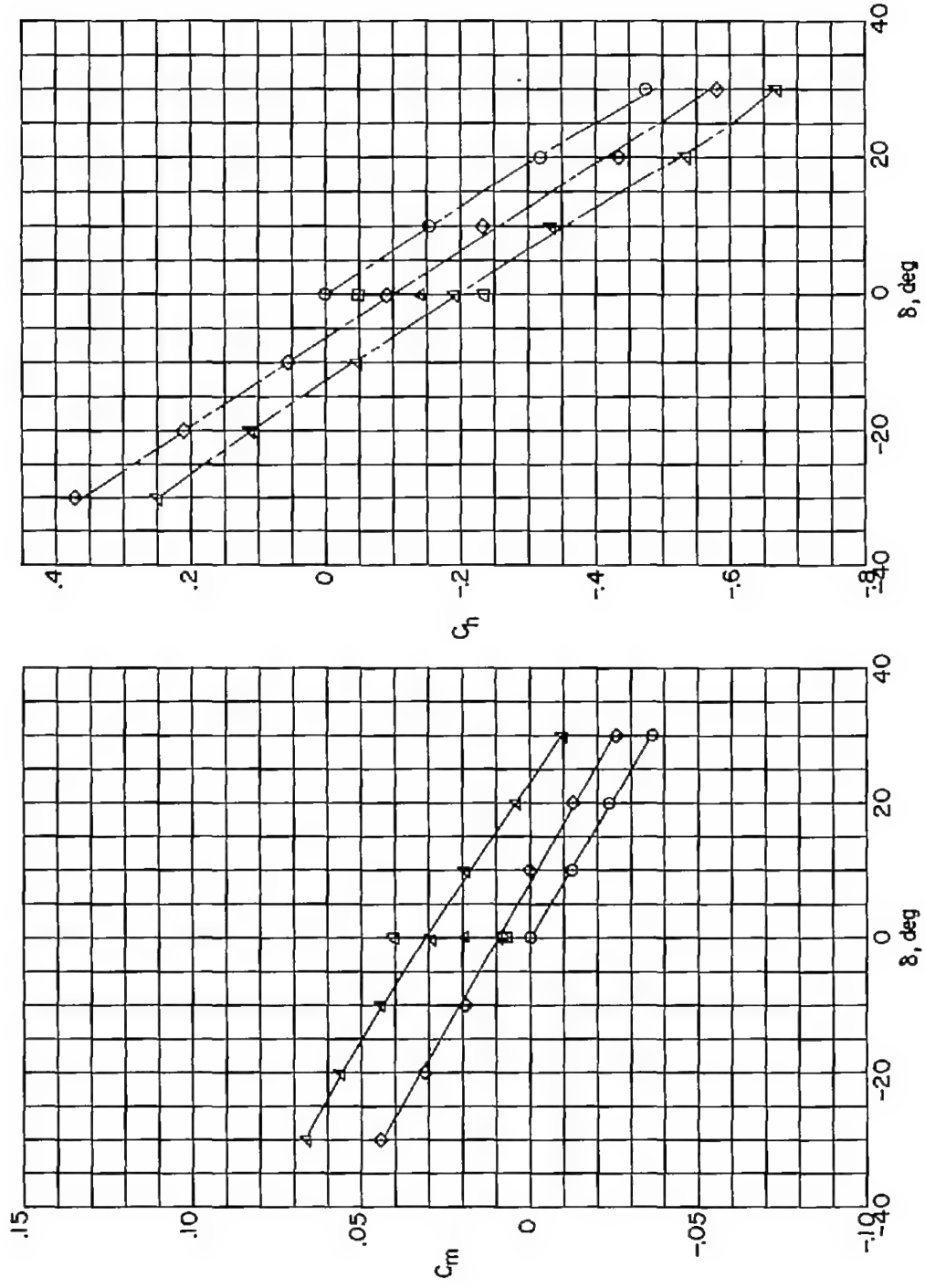

(d) C_h.

(e) C_m.

Figure 14.- Concluded.

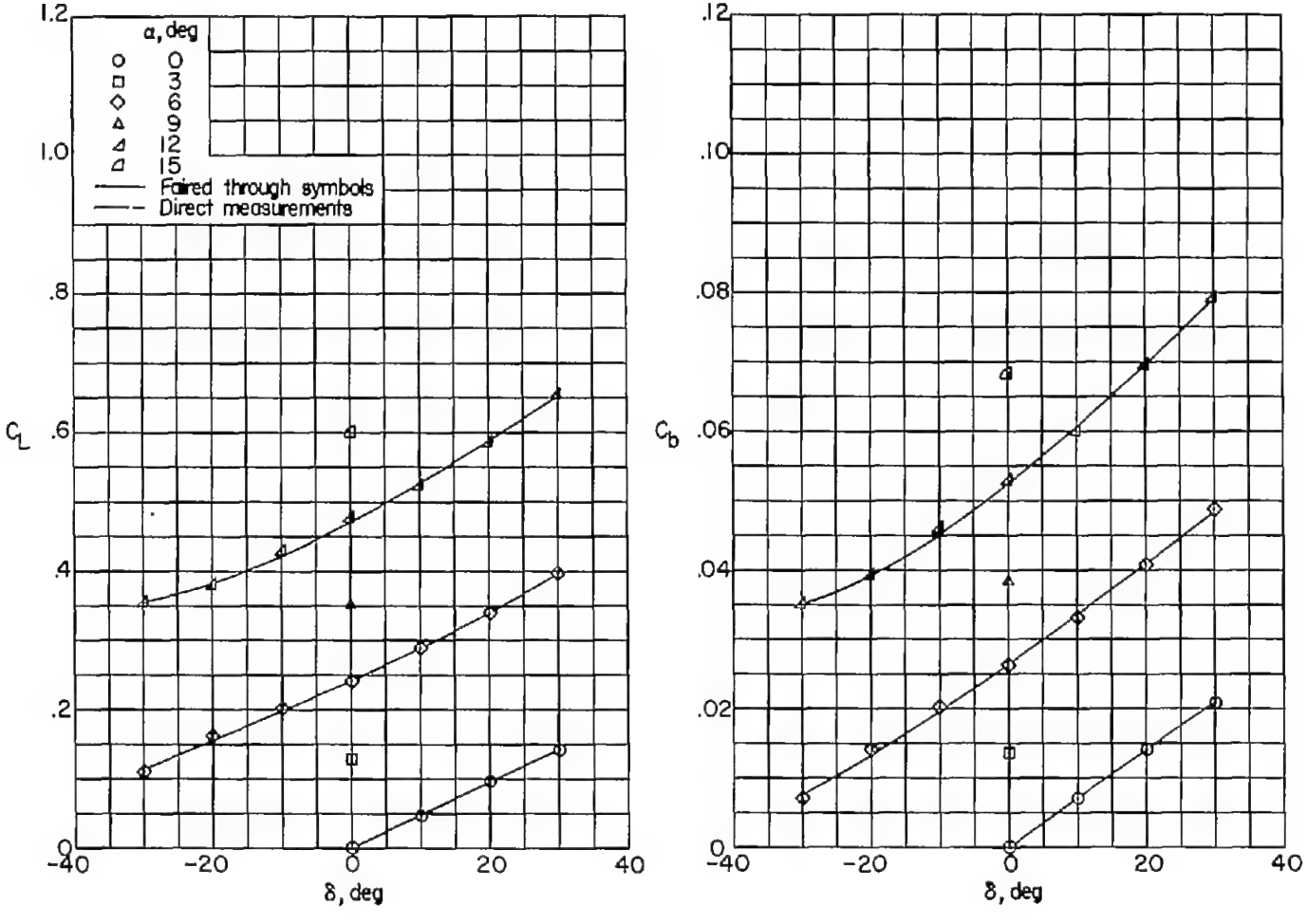

(a) C_L.

(b) C_b.

Figure 15.- Variation of basic coefficients with control deflection for configuration 3. M = 2.01; R = 3.6×10^6.

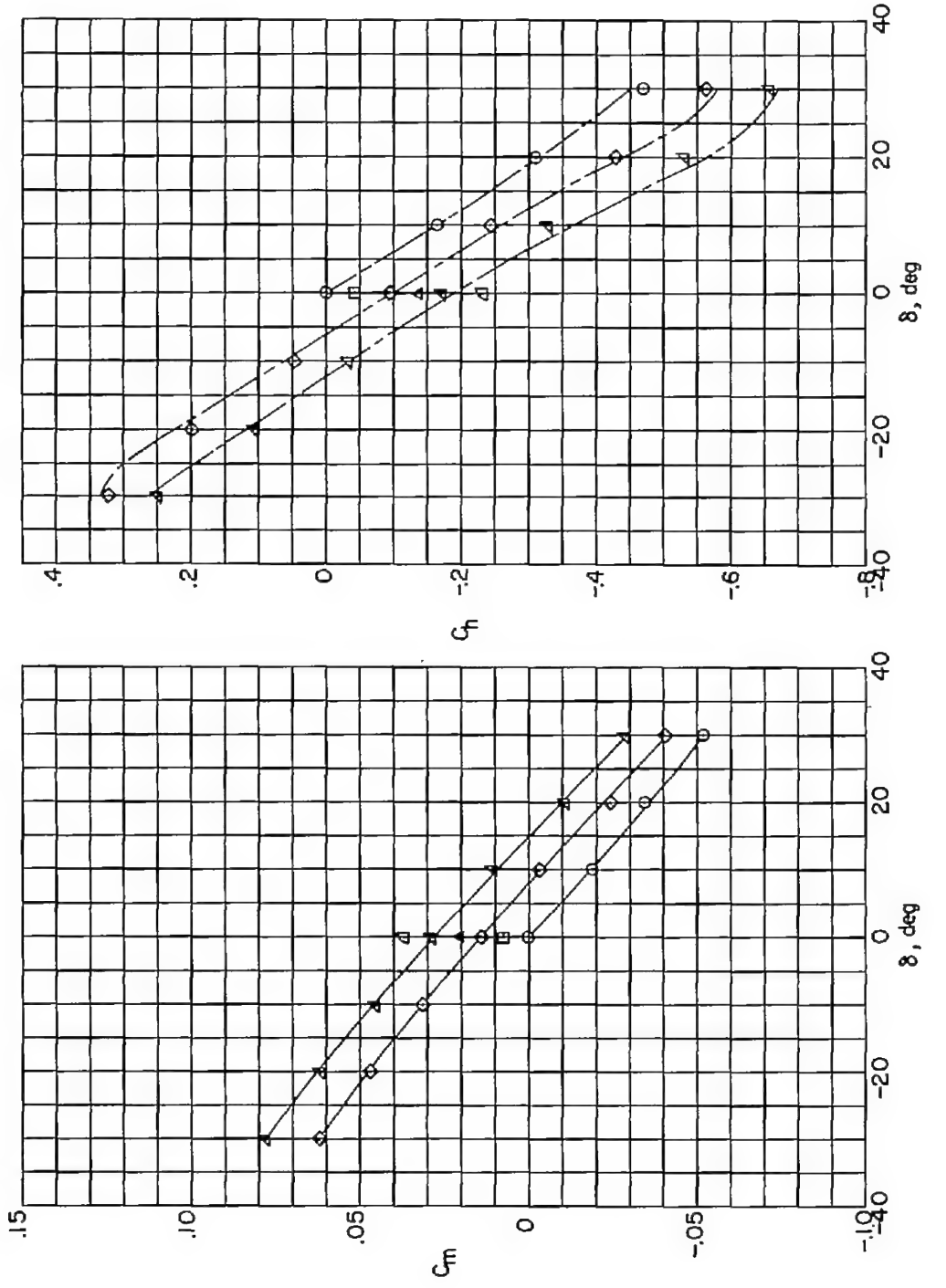

(a) C_n.

(c) C_m.

Figure 15.- Concluded.

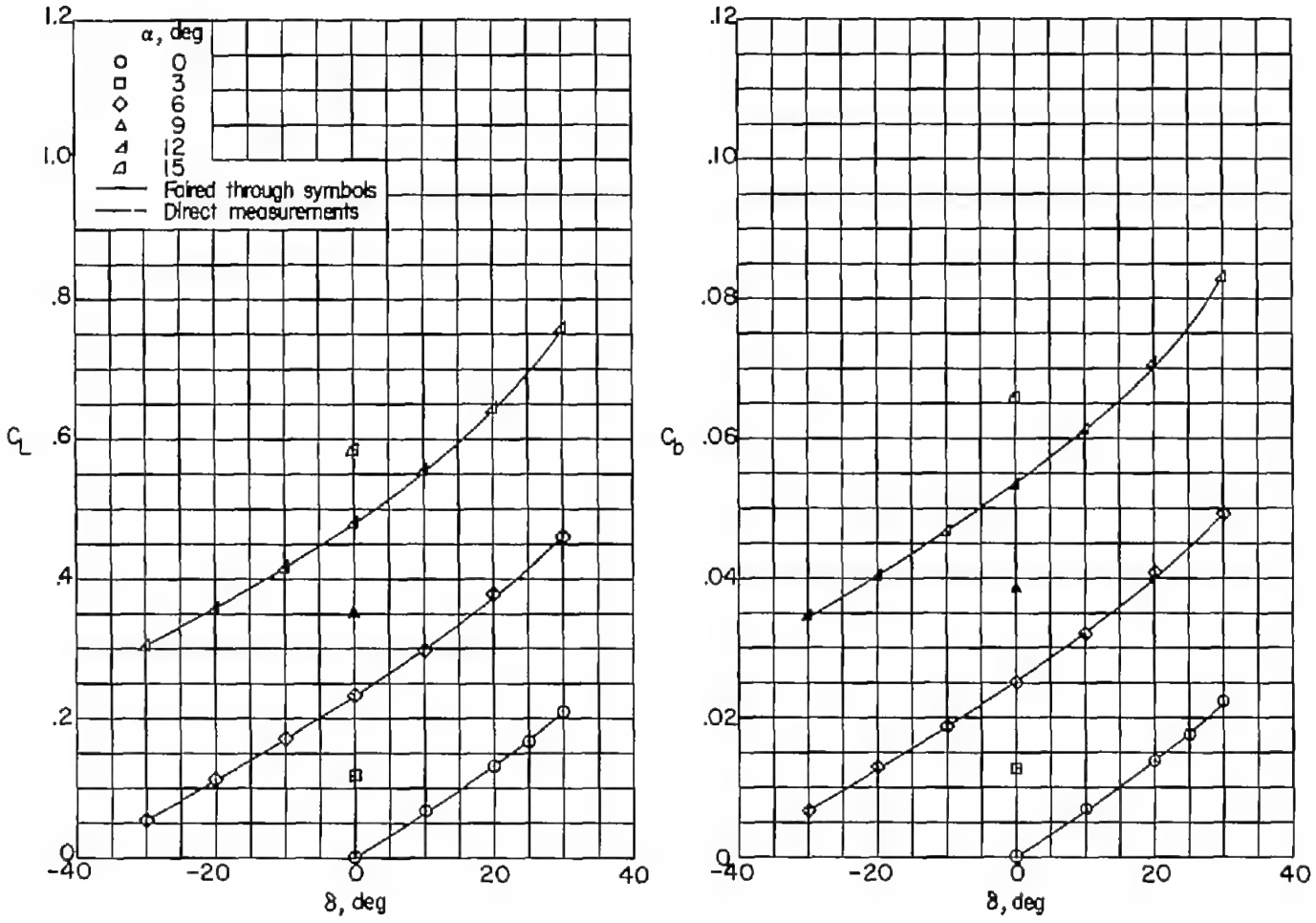

(a) C_L.

(b) C_D.

Figure 16.- Variation of basic coefficients with control deflection for configuration 4. M = 2.01; R = 3.6×10^6.

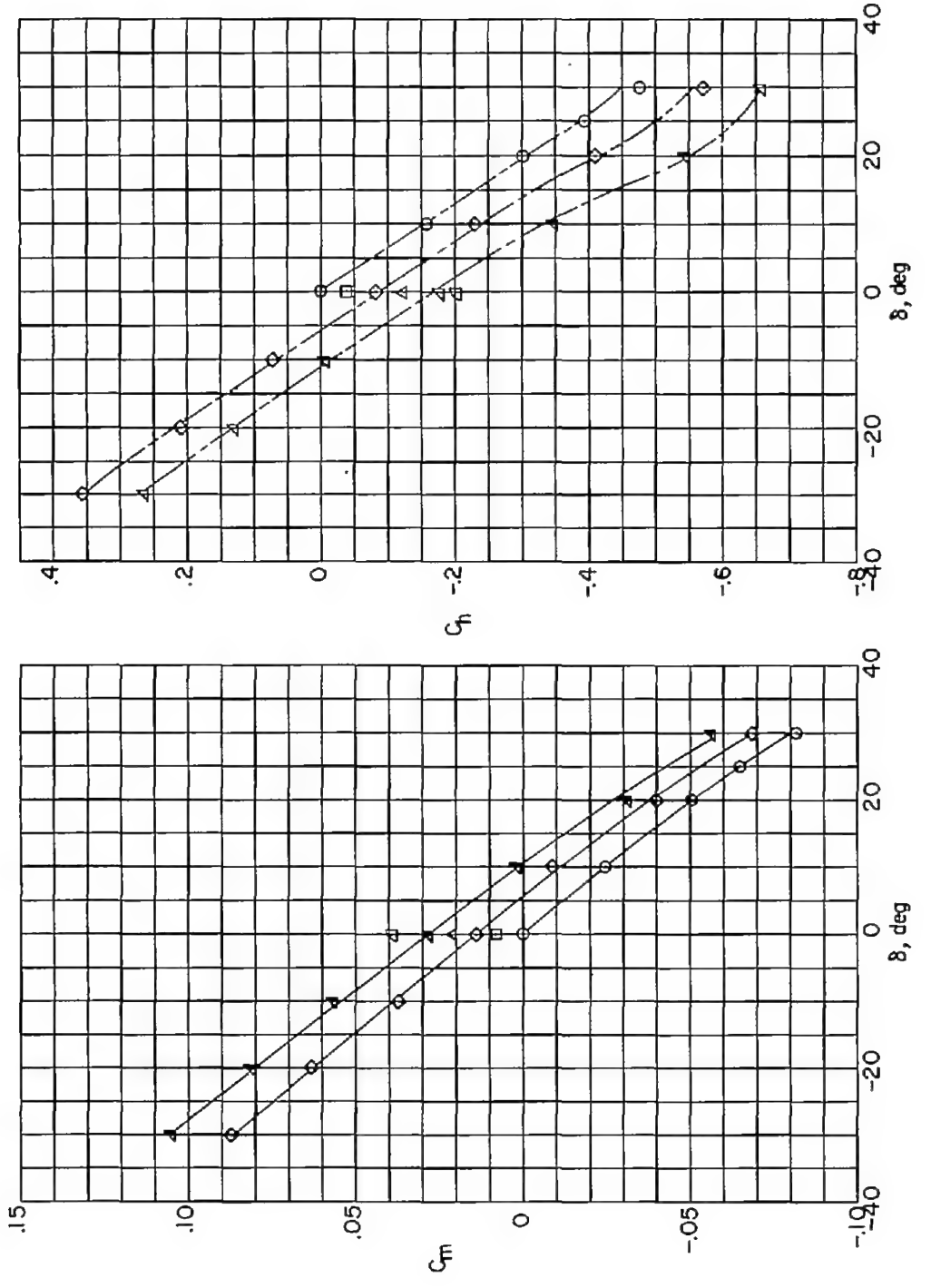

(a) C_h.

(c) C_m.

Figure 16.- Concluded.

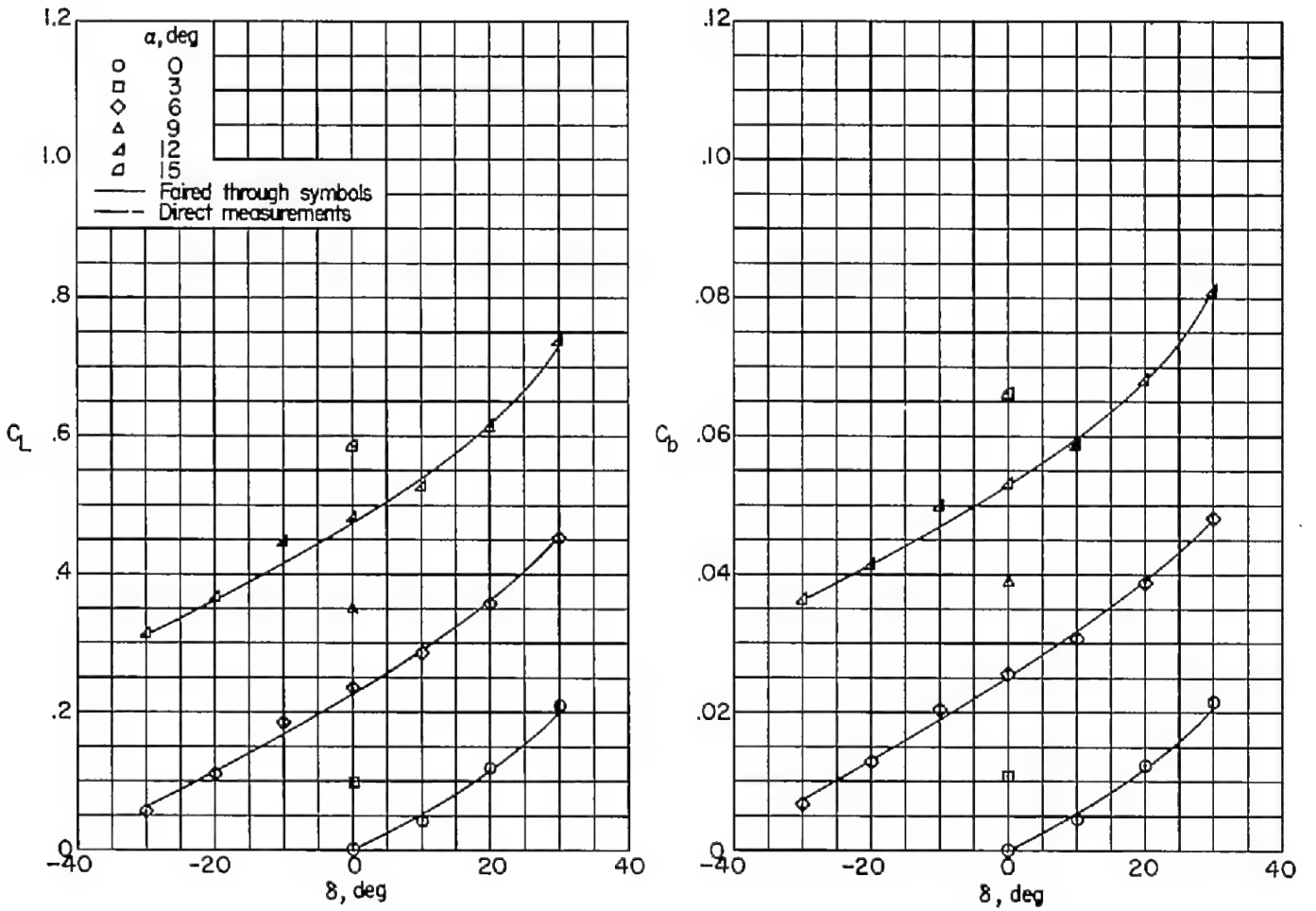

(a) C_L.

(b) C_b.

Figure 17.- Variation of basic coefficients with control deflection for configuration 4. M = 2.01; R = 1.7×10^6.

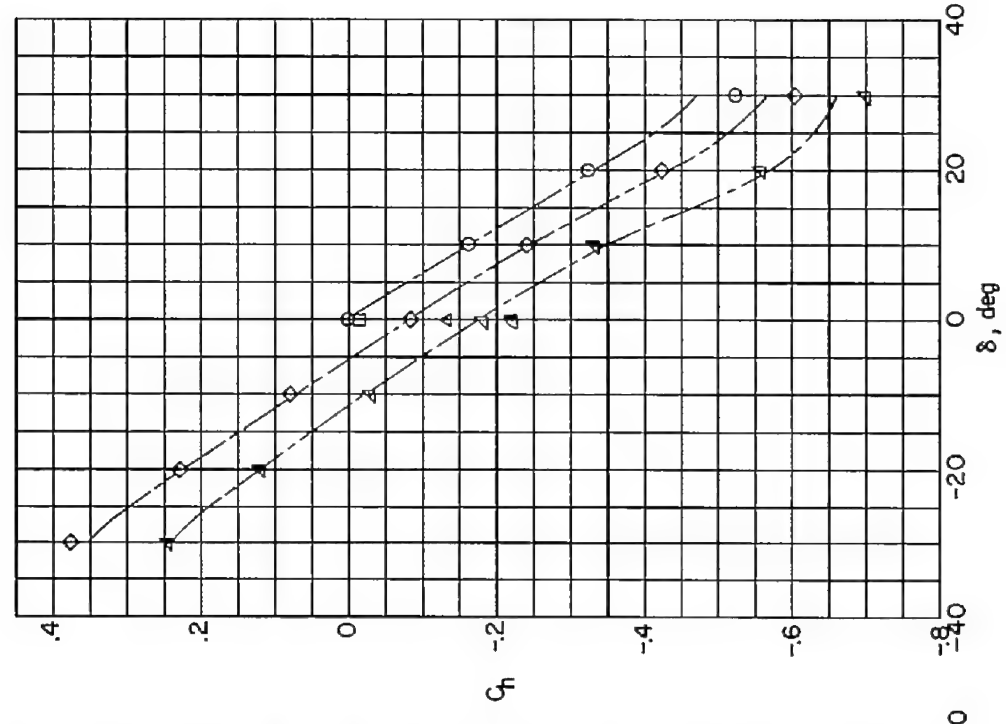

(a) C_n.

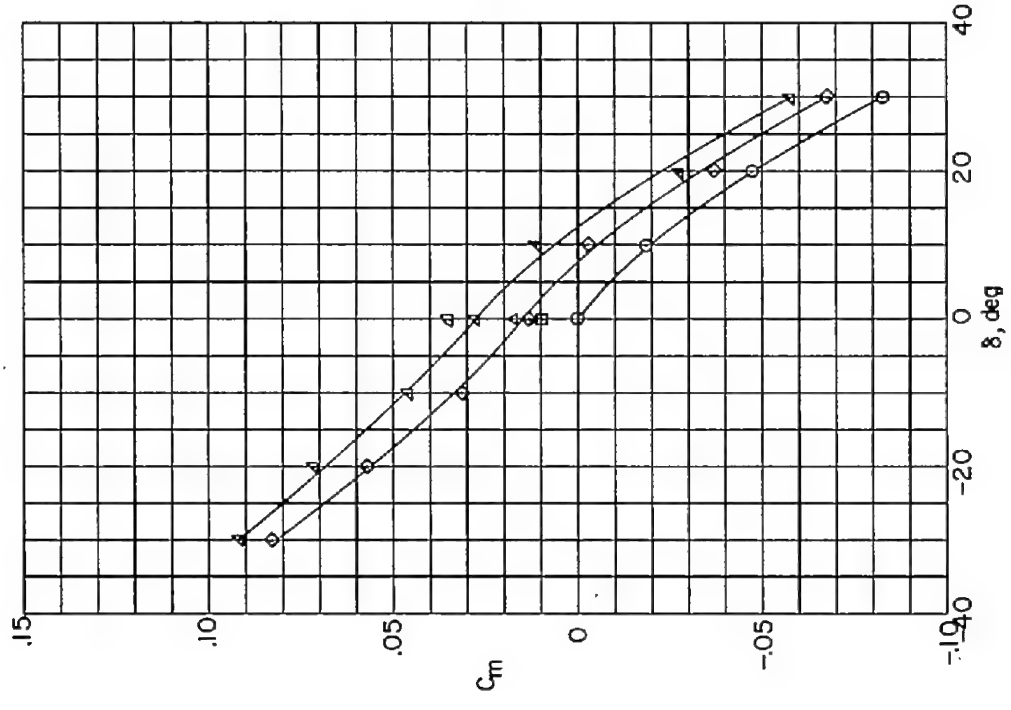

(c) C_m.

Figure 17.- Concluded.

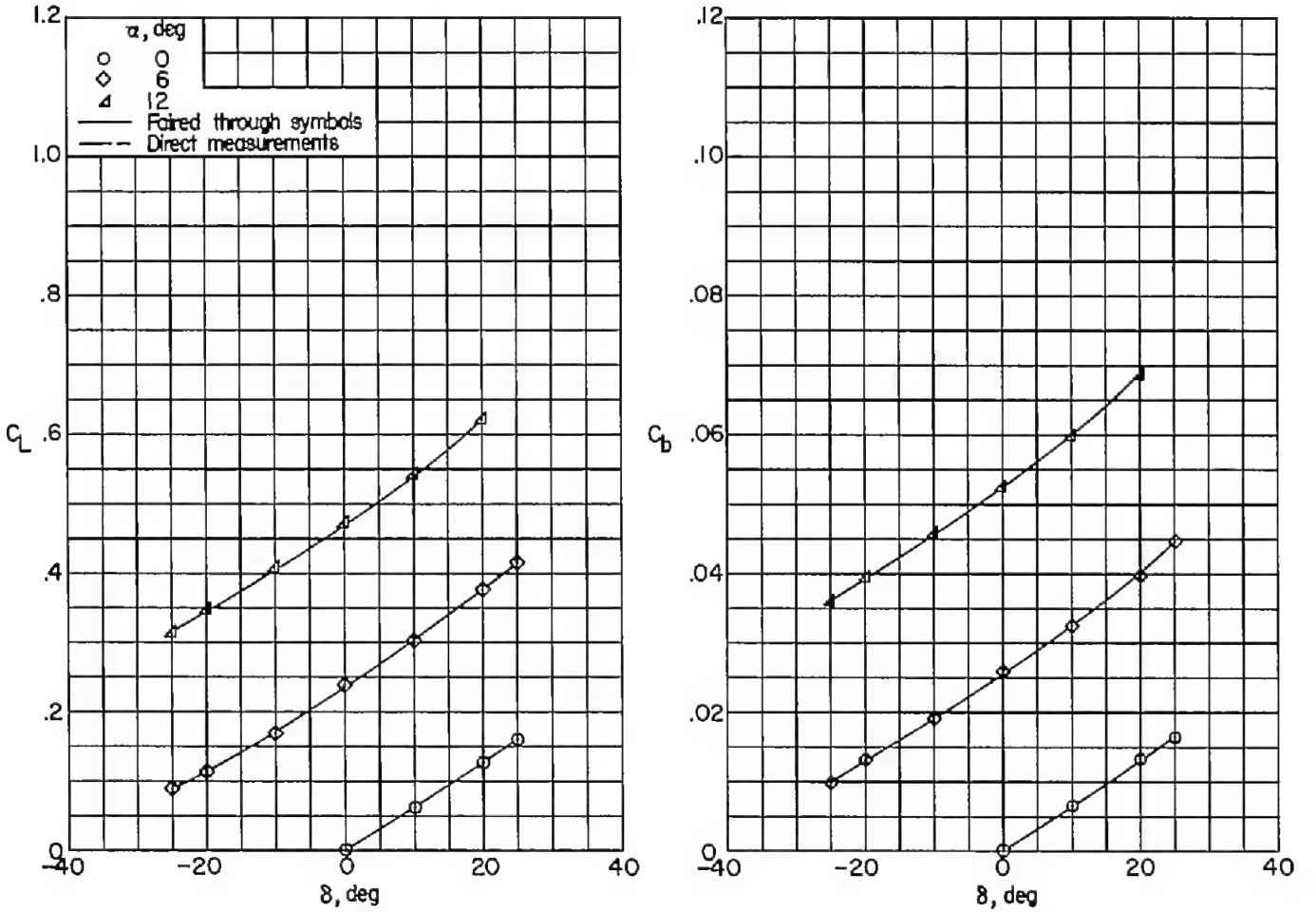

(a) C_L.

(b) C_b.

Figure 18.- Variation of basic coefficients with control deflection for configuration 4. M = 2.01; R = 4.5×10^6.

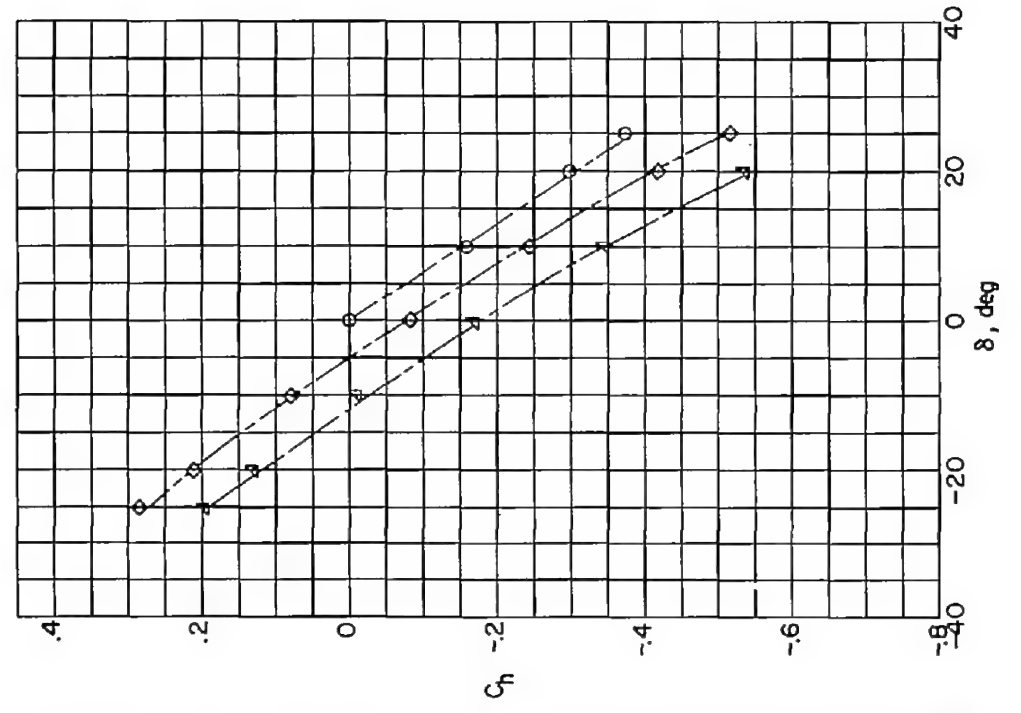

(d) C_h.

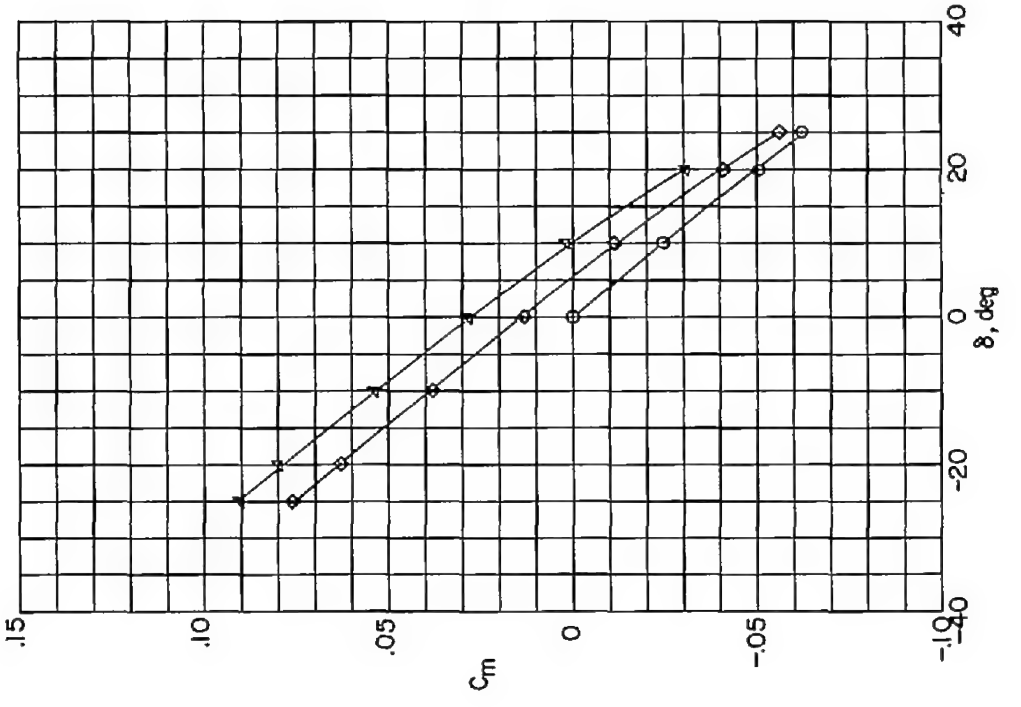

(c) C_m.

Figure 18.- Concluded.

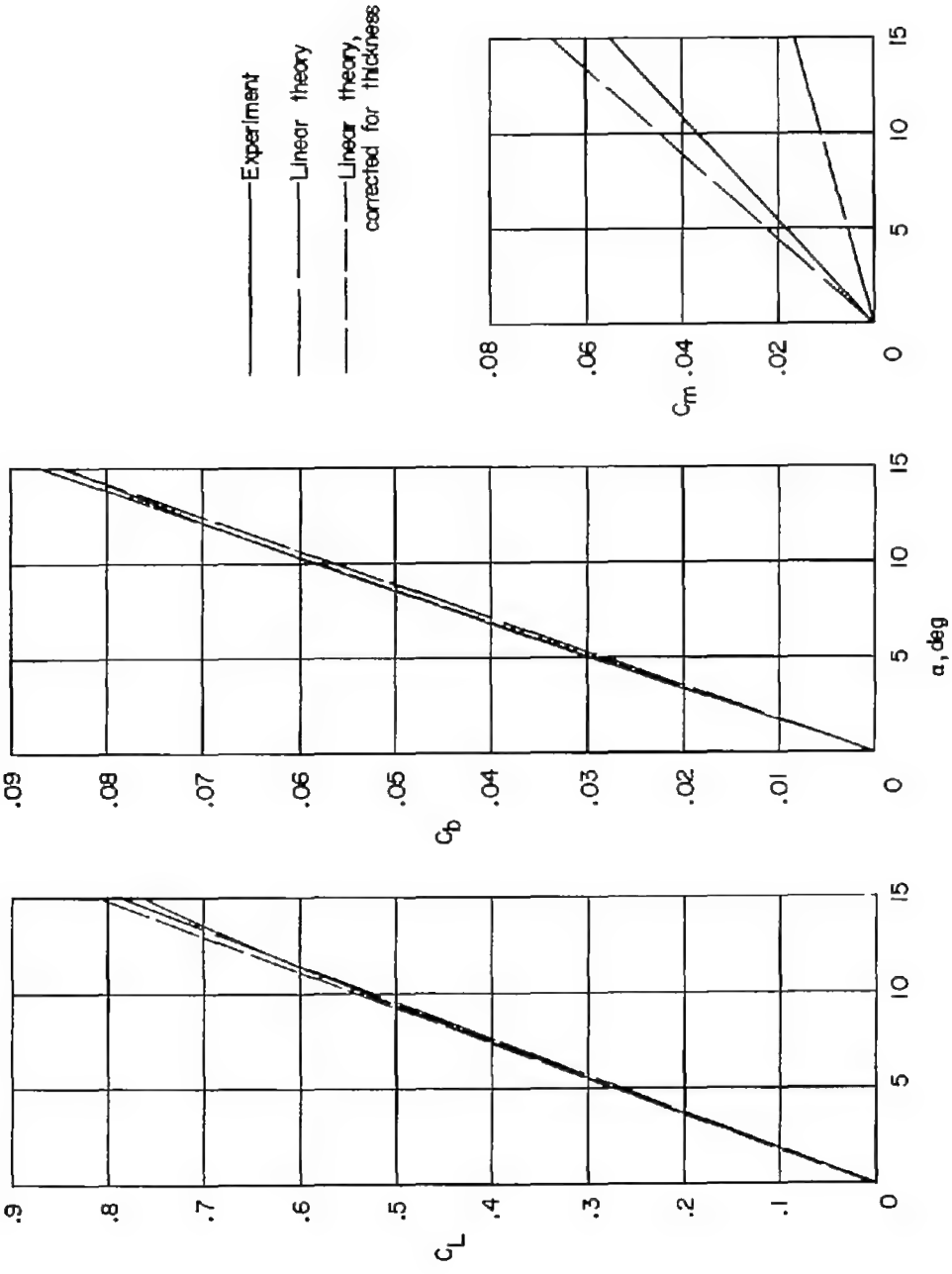

(a) M = 1.61; R = 3.6×10^6.

Figure 19.- Variations of wing lift, bending-moment, and pitching-moment coefficients with angle of attack for configurations 1, 2, 3, and 4. $\delta = 0^\circ$.

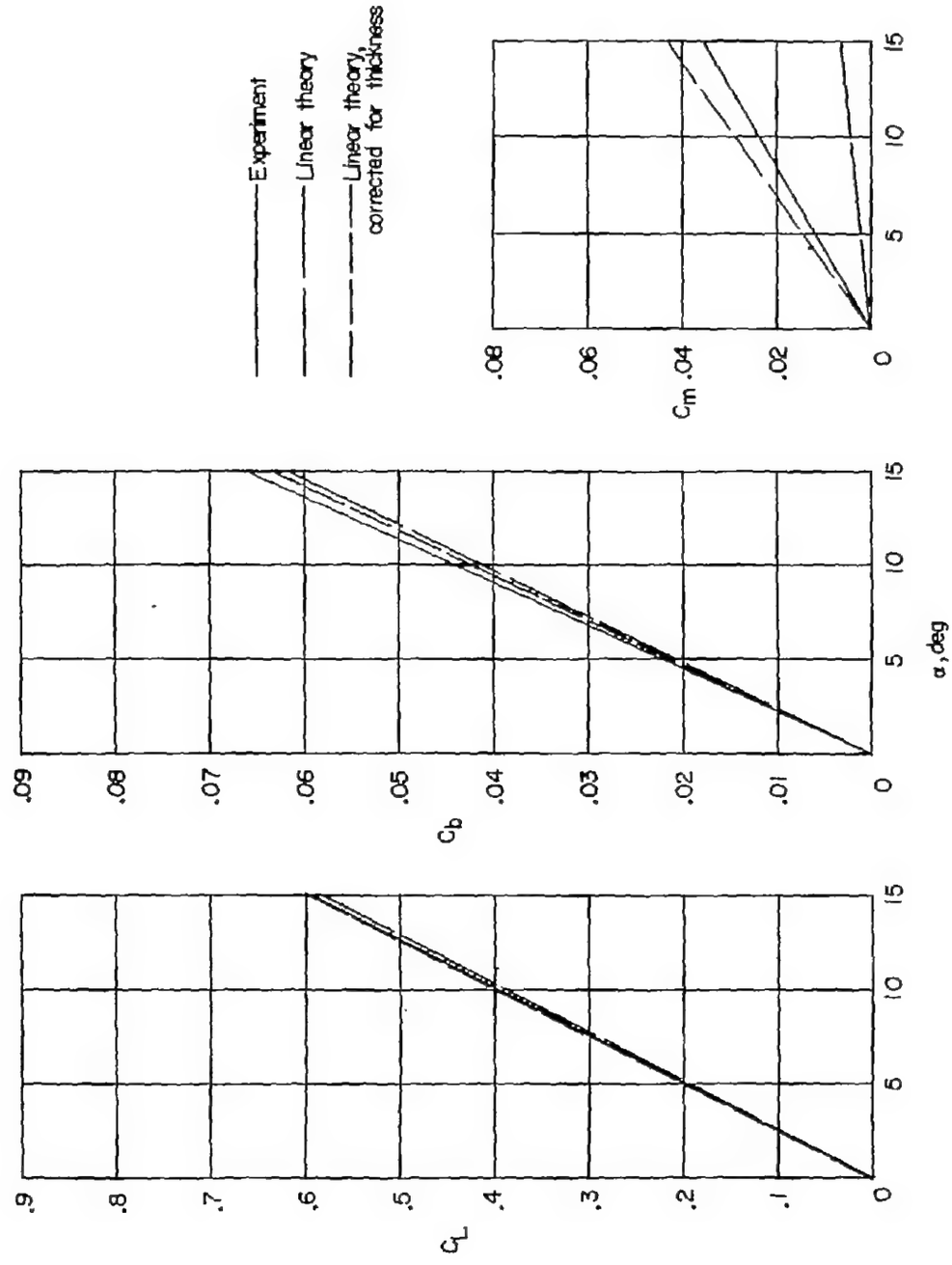

(b) M = 2.01; R = 3.6 × 10^6.

Figure 19.- Concluded.

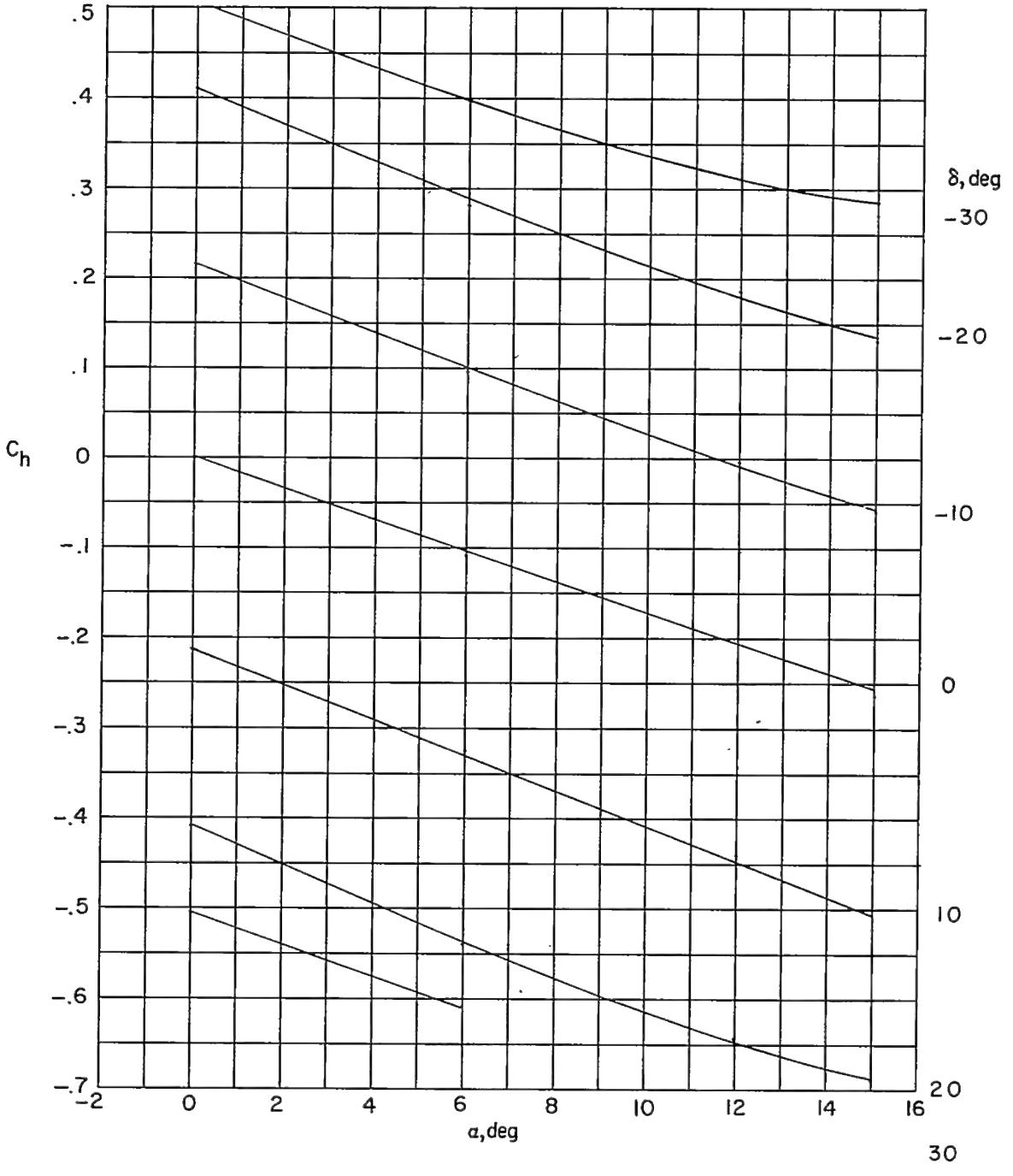

(a) M = 1.61; R = 3.6×10^6.

Figure 20.- Variations of control hinge-moment coefficients with angle of attack for configuration 4.

[redacted]

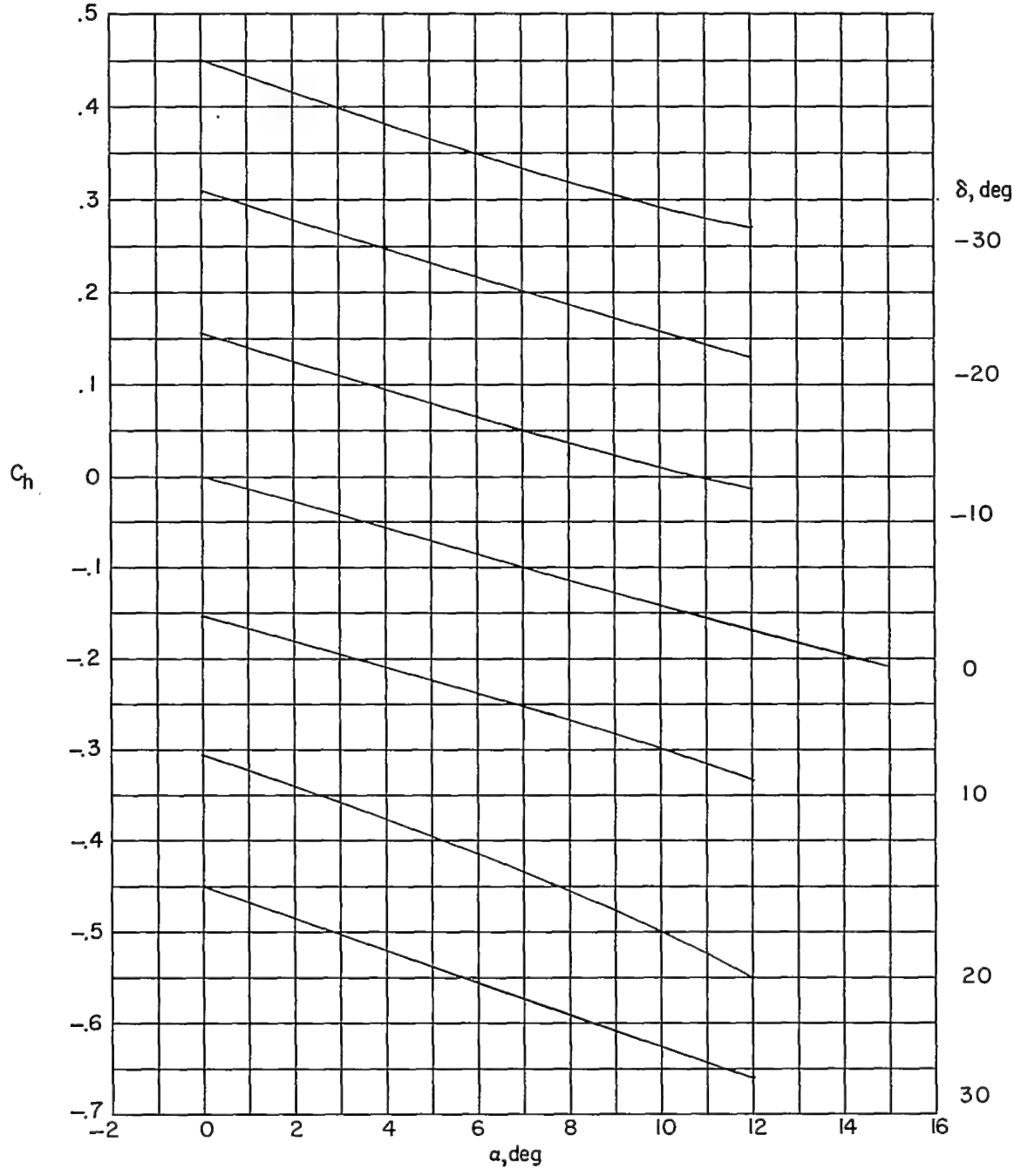

(b) M = 2.01; R = 3.6×10^6.

Figure 20.- Concluded.

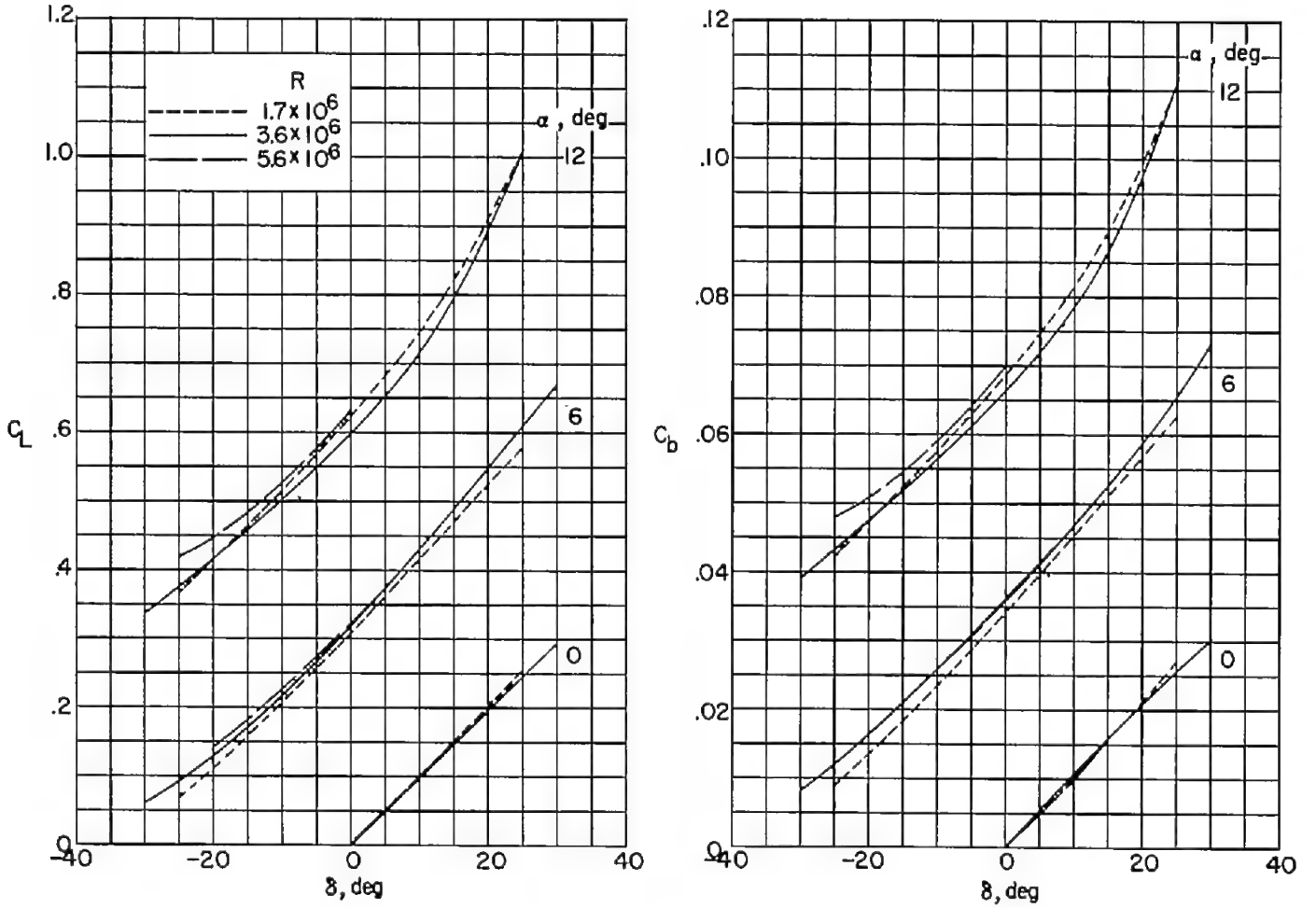

(a) C_L.

(b) C_b.

Figure 21.- Effect of Reynolds number on the variations of the basic coefficients with control deflection. M = 1.61.

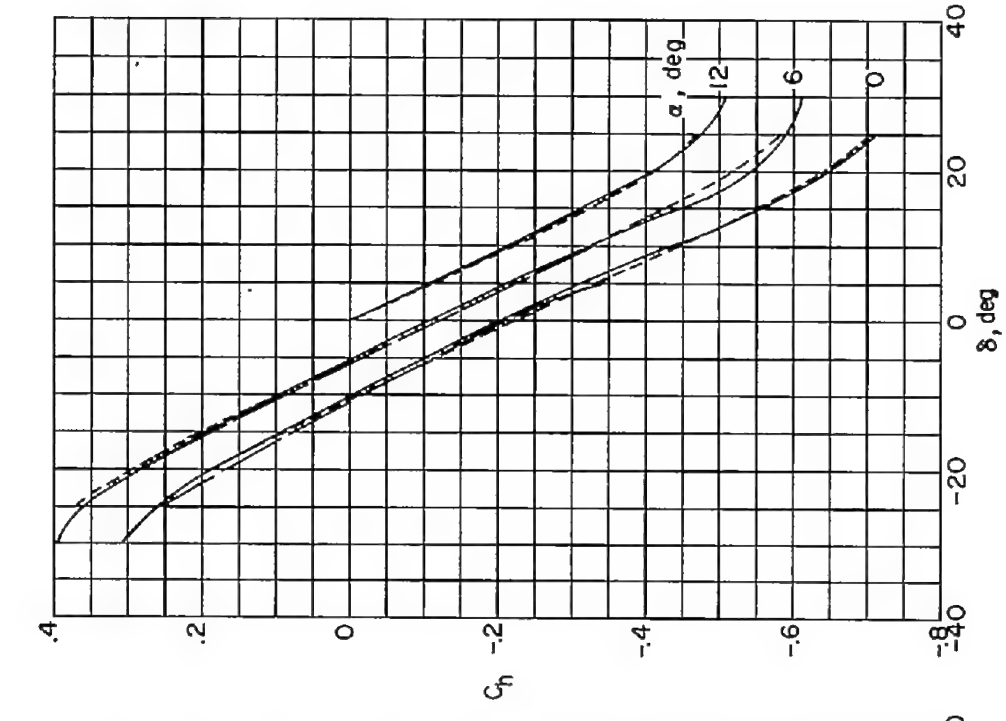

(d) C_n.

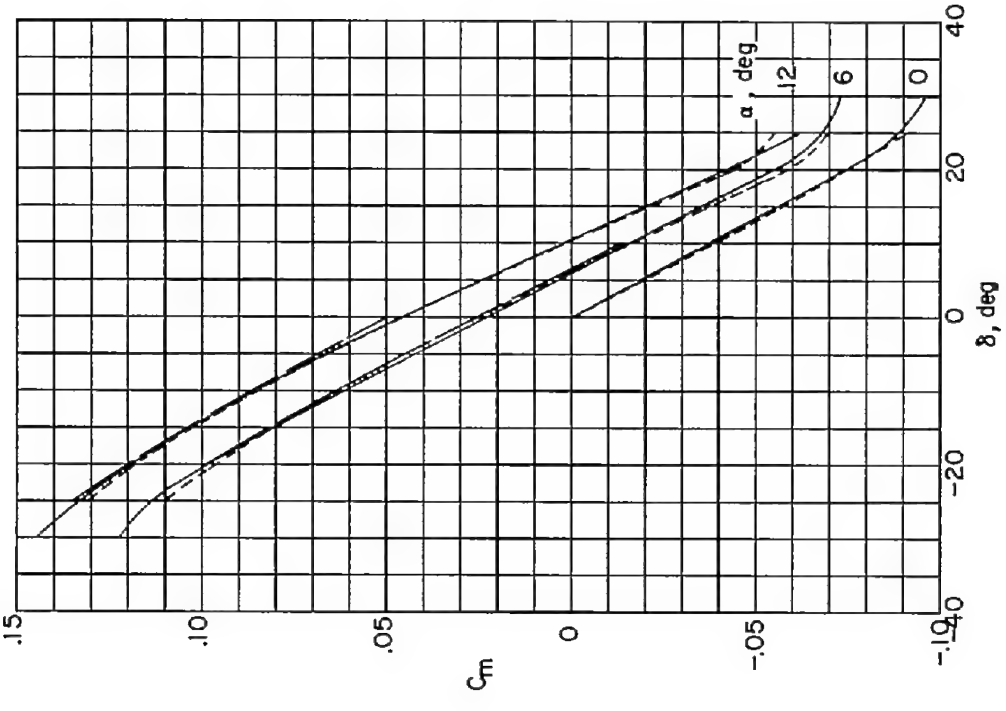

(c) C_m.

Figure 21.- Concluded.

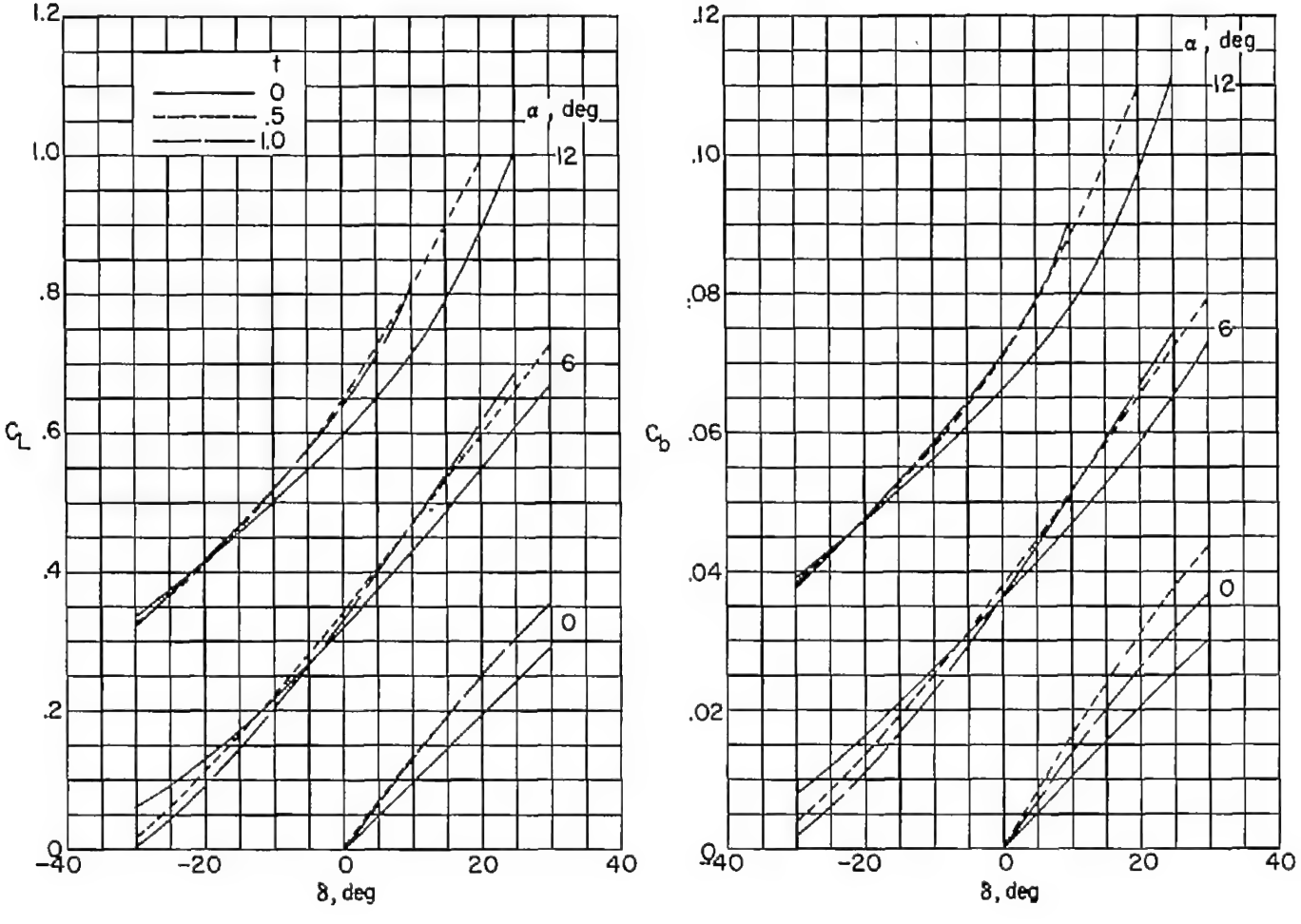

(a) C_L.

(b) C_b.

Figure 22.- Effect of trailing-edge thickness on the variations of the basic coefficients with control deflection. M = 1.61; R = 3.6×10^6.

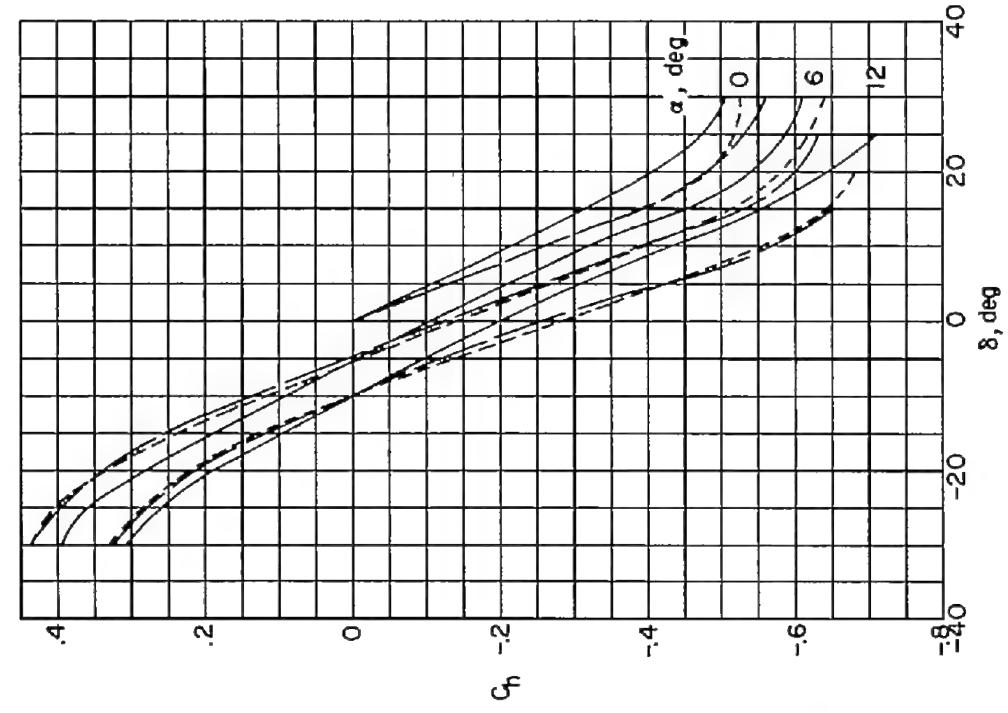

(a) C_n.

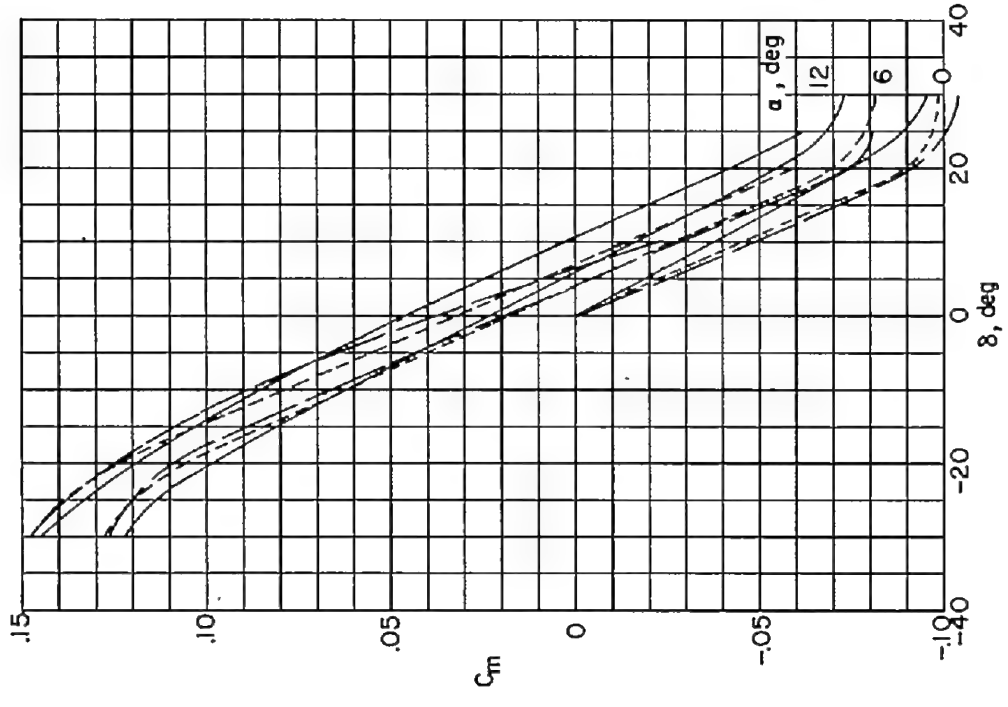

(c) C_m.

Figure 22.- Concluded.

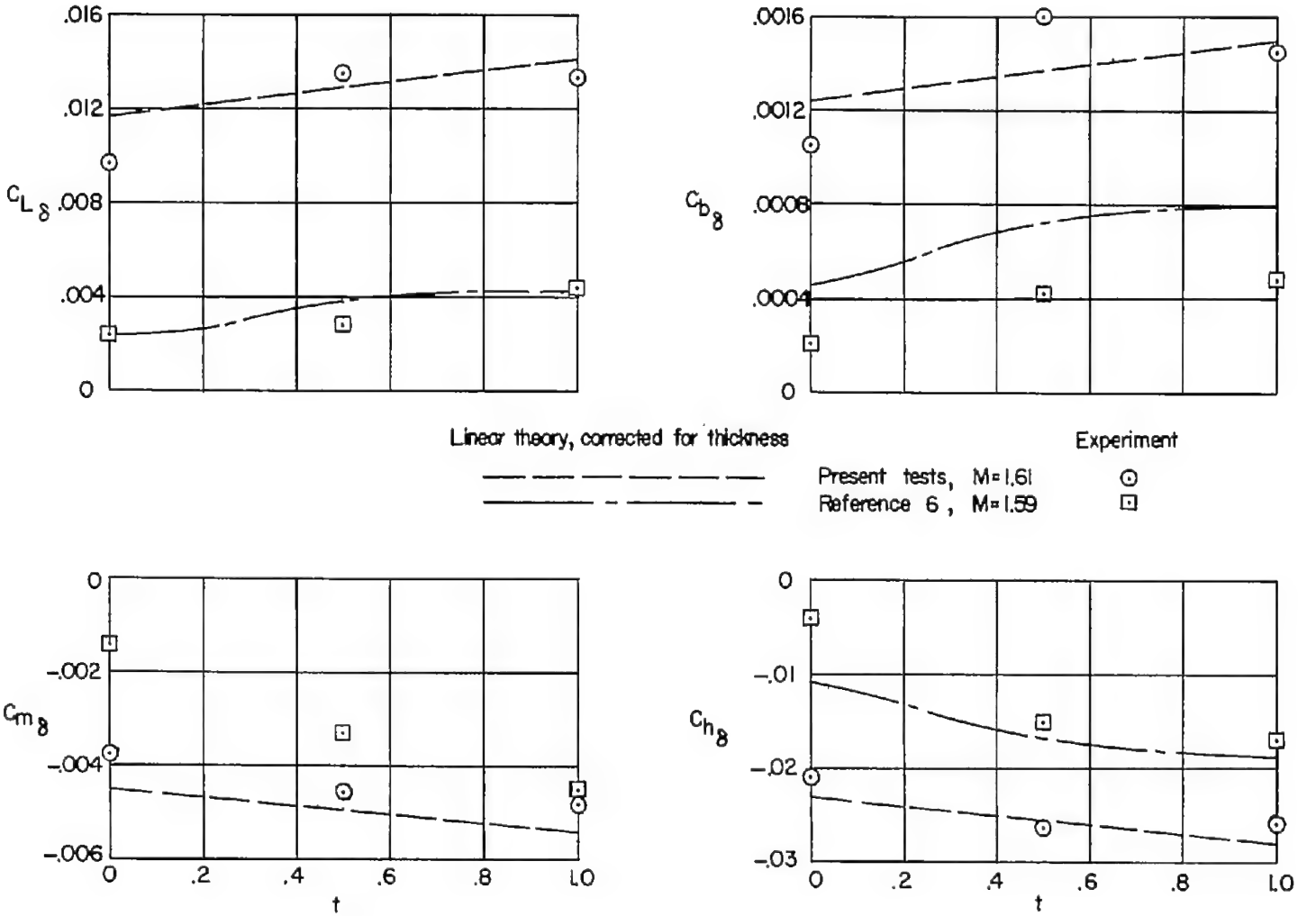

Figure 23.- Variation of control effectiveness and hinge-moment coefficient slopes with trailing-edge thickness. M = 1.61; R = 3.6×10^6.

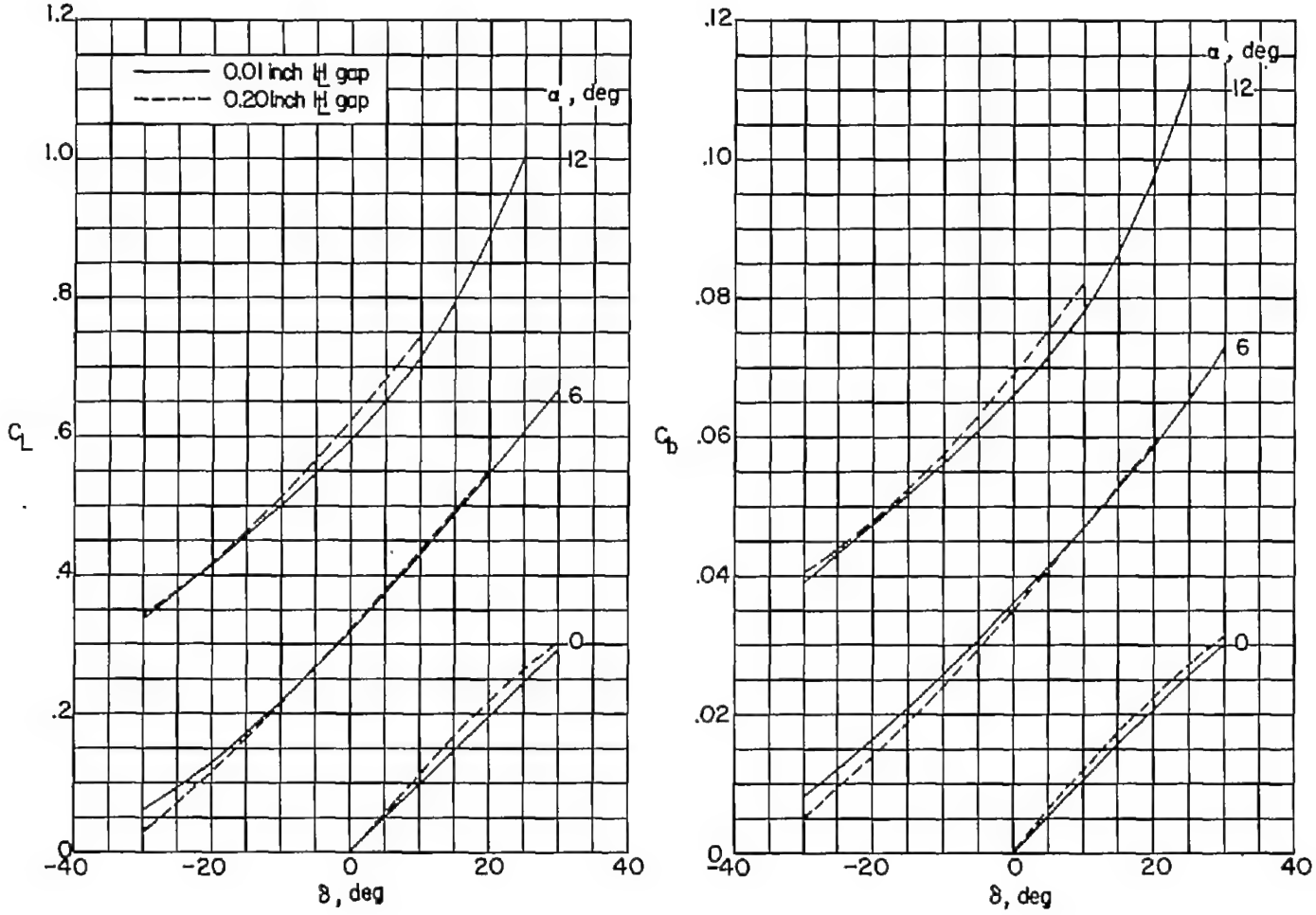

(a) C_L.

(b) C_b.

Figure 24.- Effect of hinge-line gap on the variations of the basic coefficient with control deflection. M = 1.61; R = 3.6×10^6.

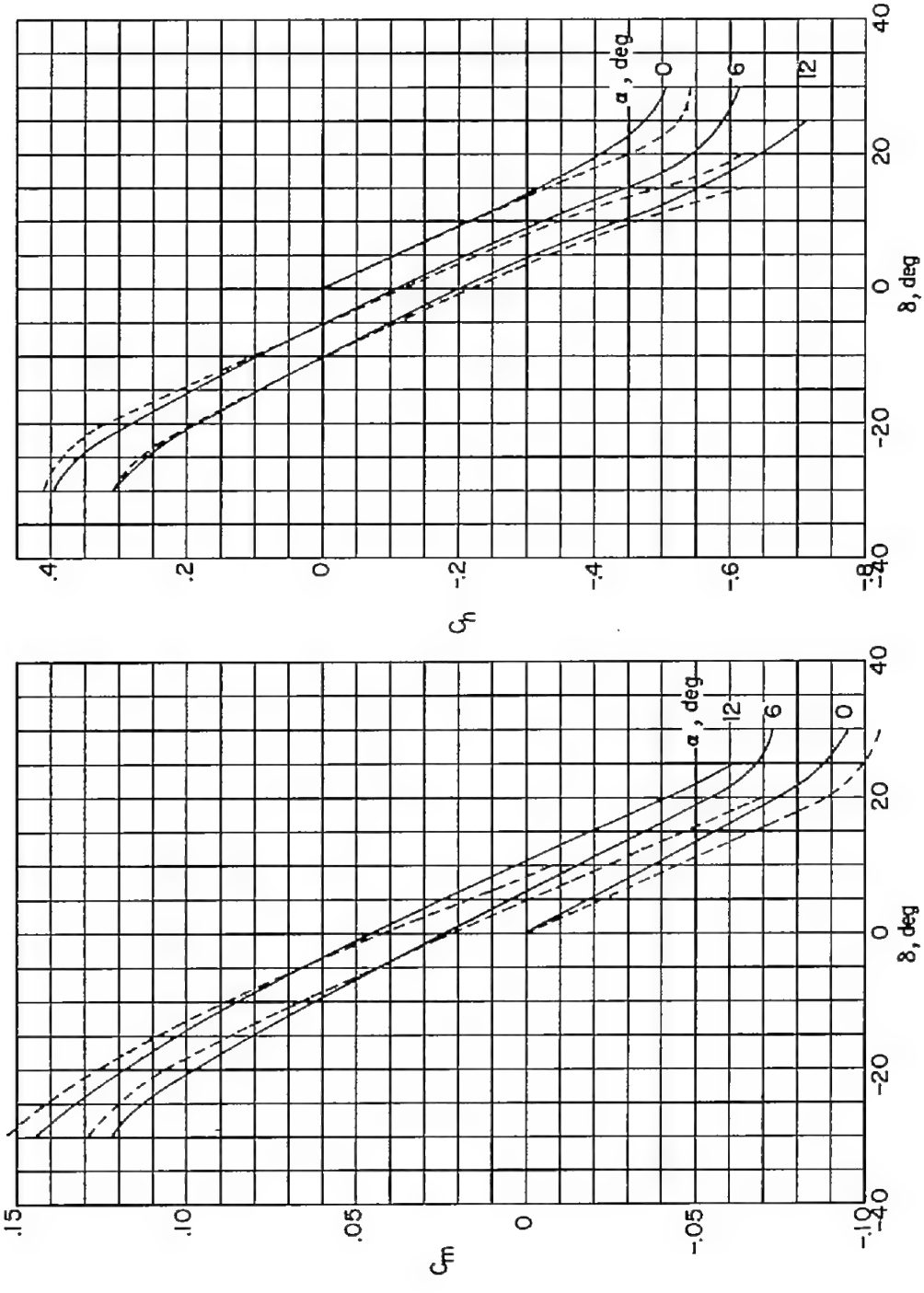

(d) C_n.

(c) C_m.

Figure 24.- Concluded.

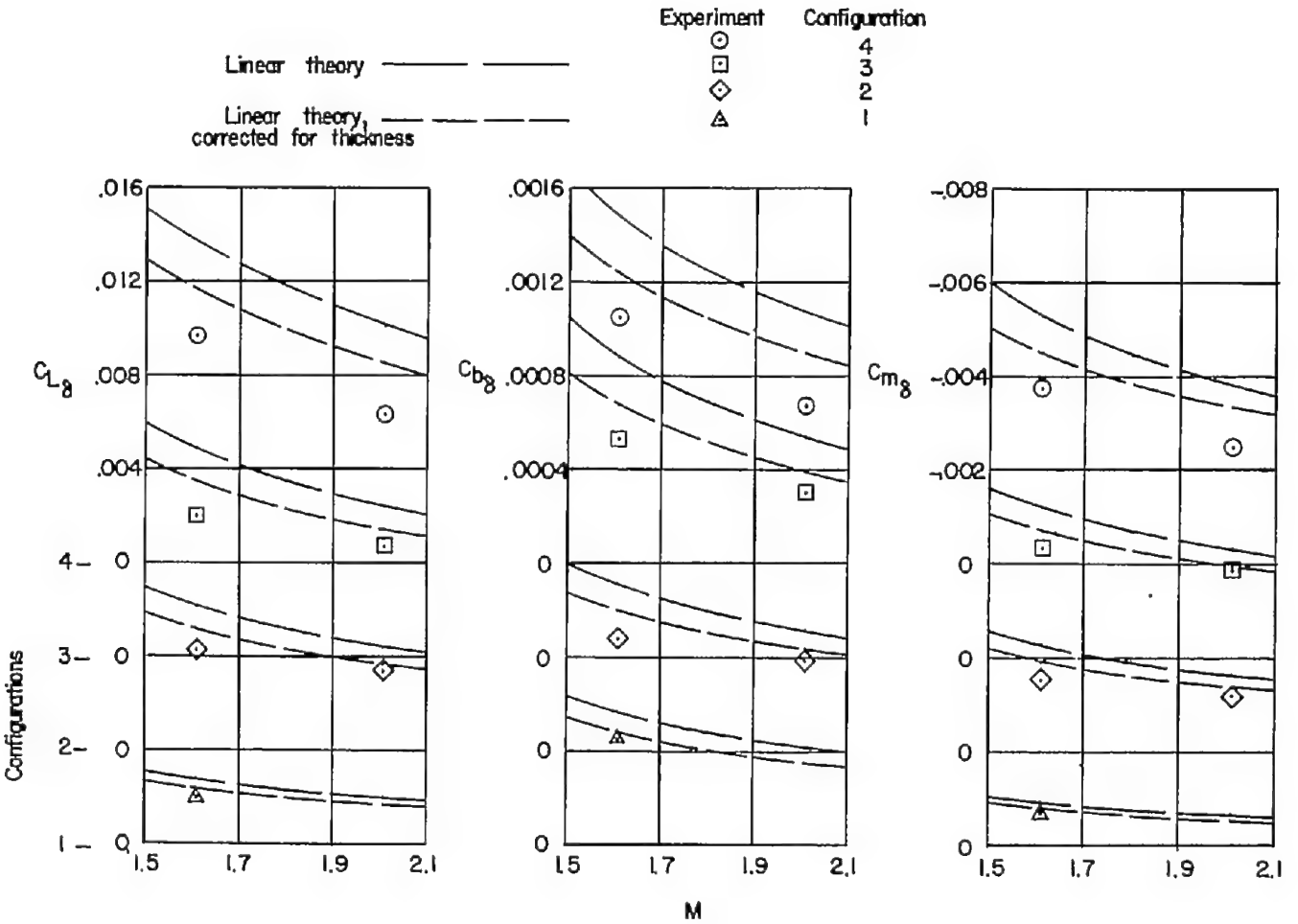

(a) Control effectiveness.

Figure 25.- Variation of control effectiveness and hinge-moment coefficient slopes with Mach number. $R = 3.6 \times 10^6$; $t = 0$.

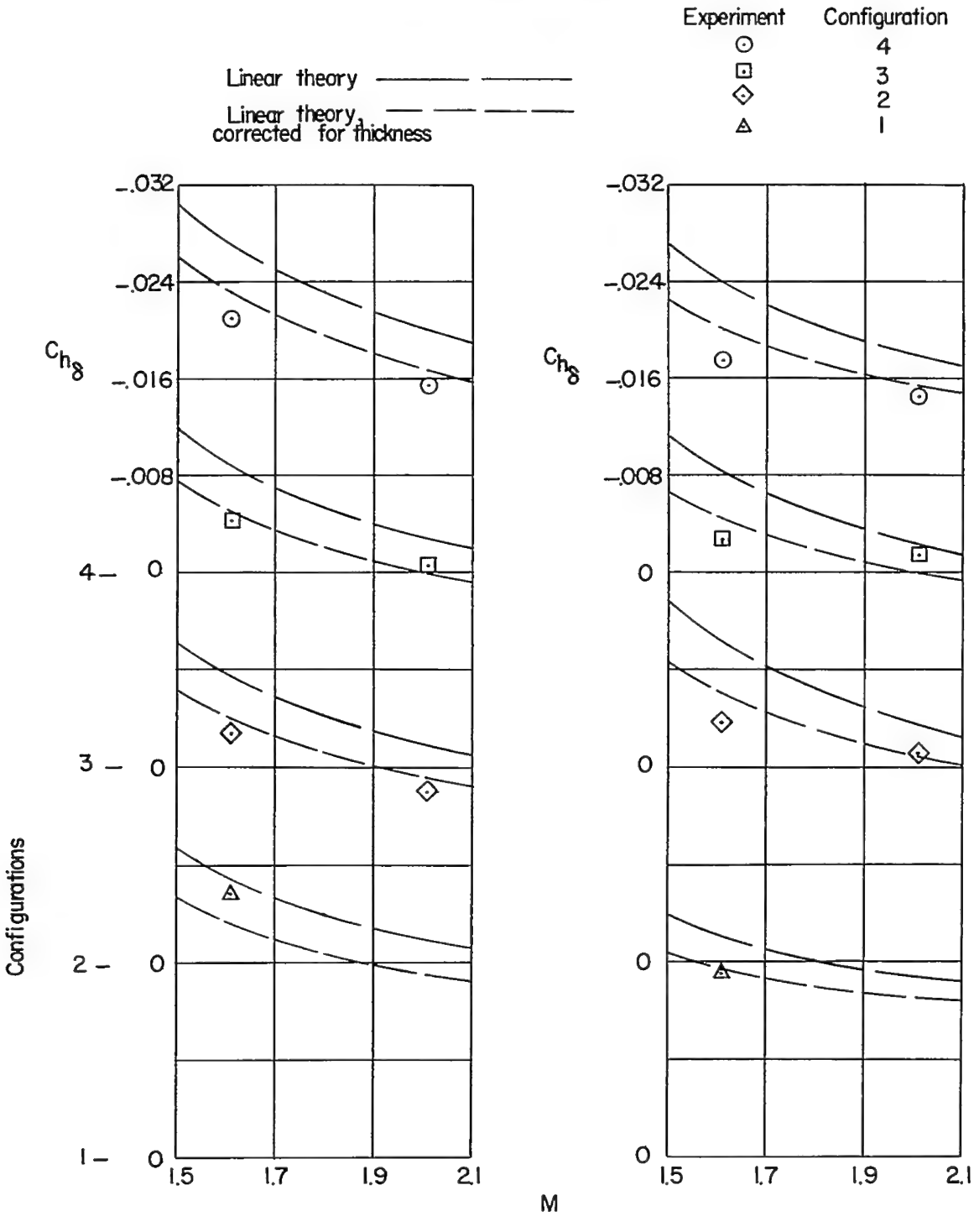

(b) Control hinge-moment coefficient slopes.

Figure 25.- Concluded.

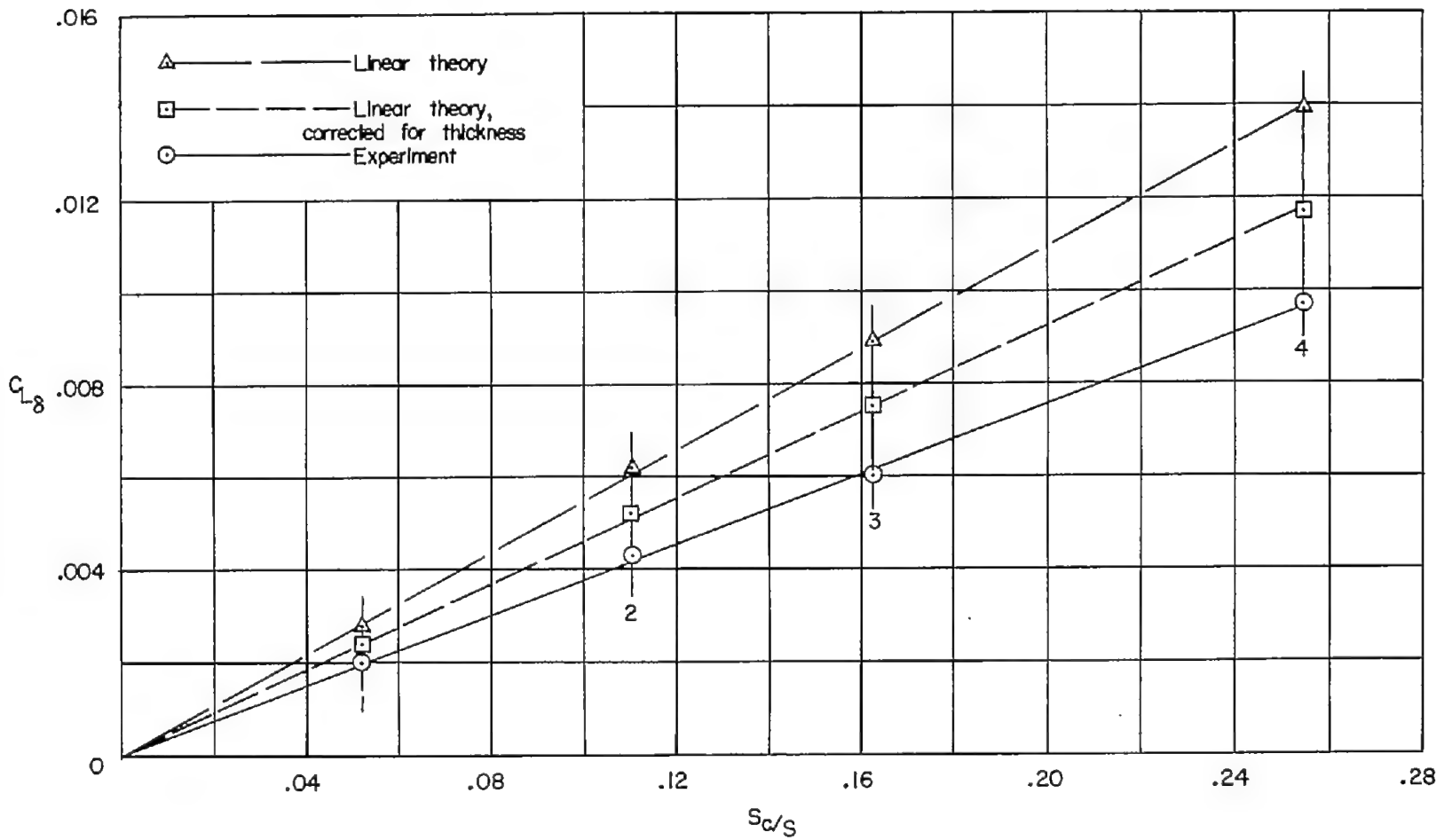

(a) C_{l_δ}; M = 1.61.

Figure 26.- Correlations of control effectiveness parameters with control-area and control-area-moment ratios. R = 3.6×10^6; t = 0.

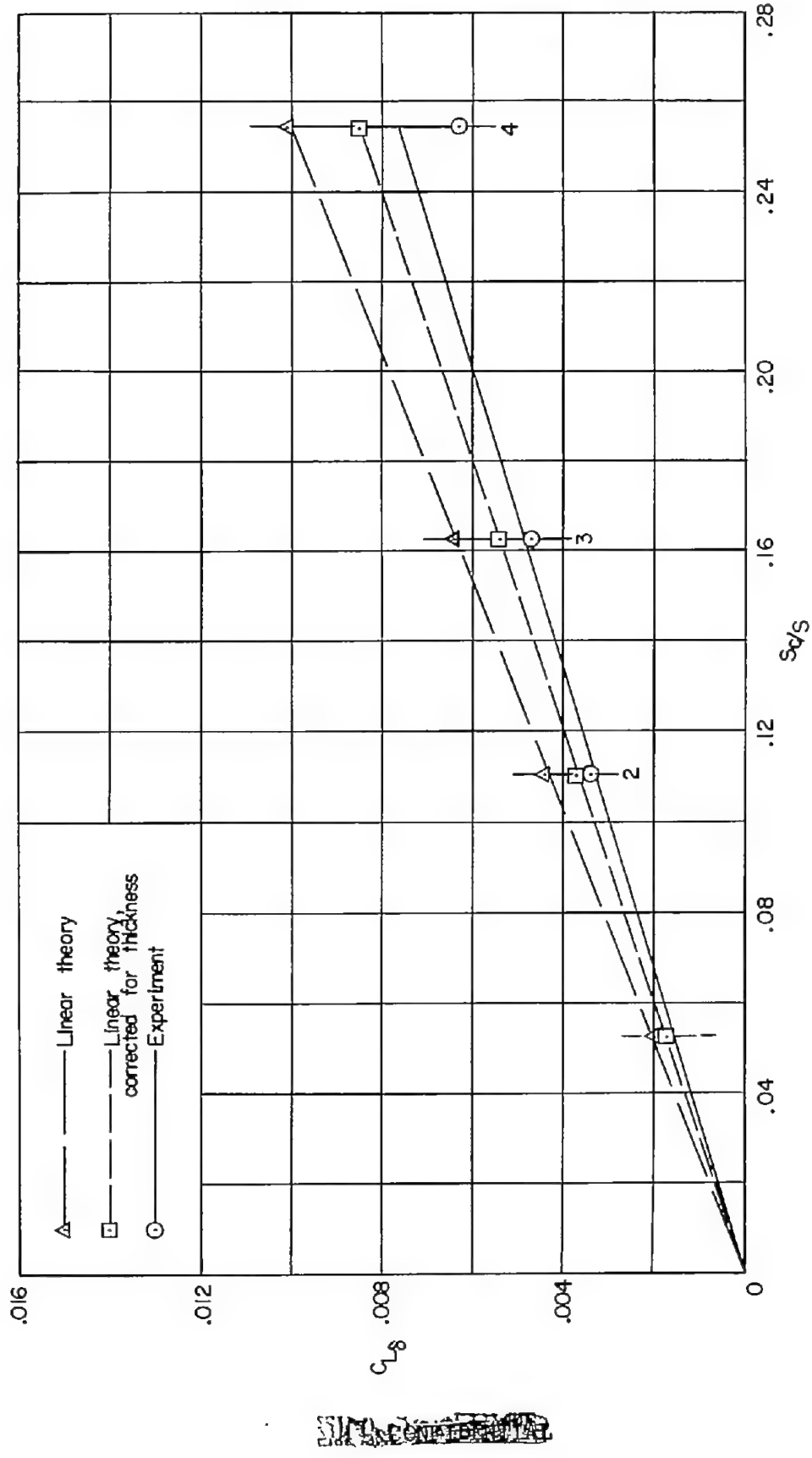

(b) C_{L_δ}; M = 2.01.

Figure 26.- Continued.

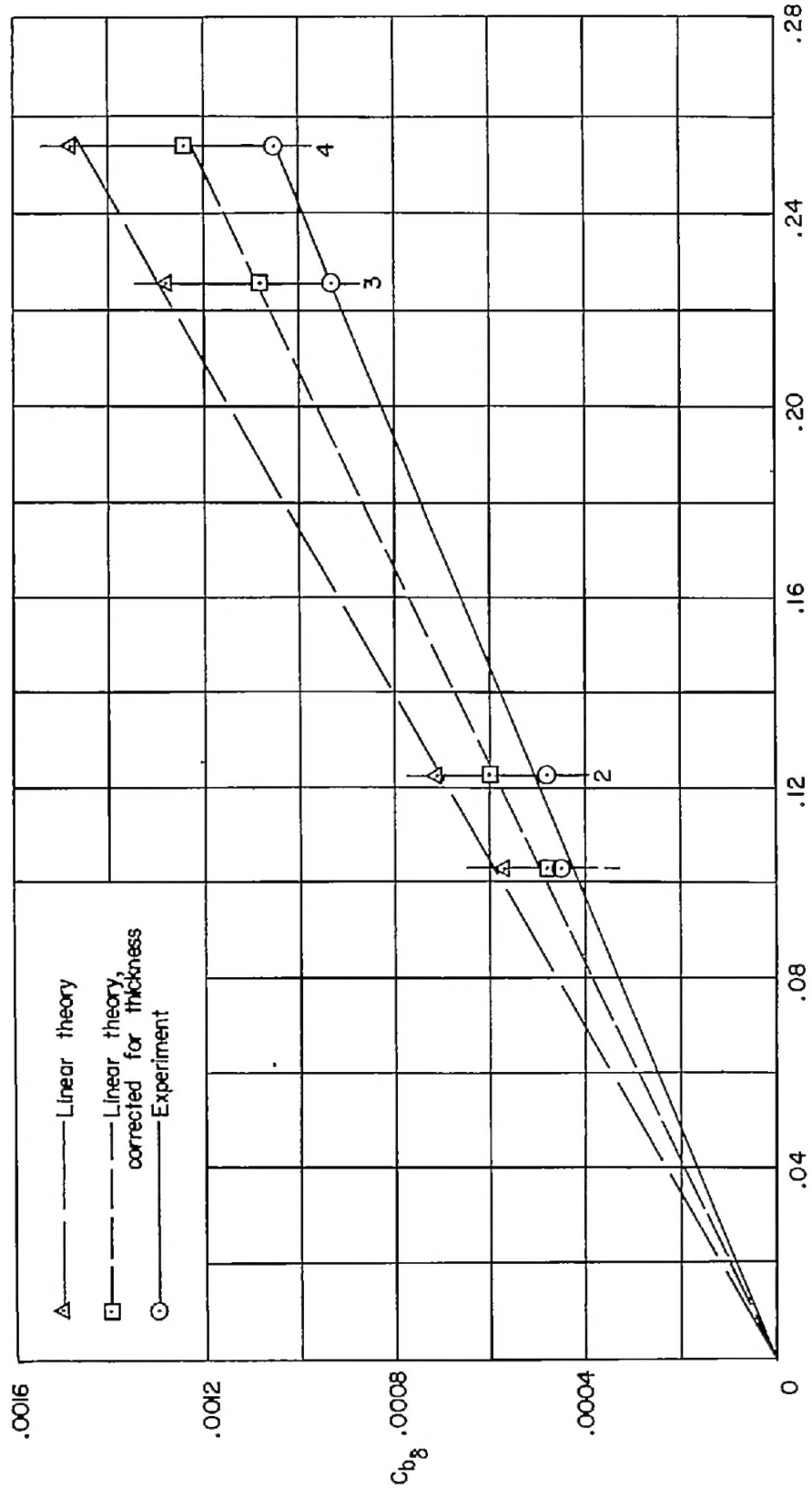

(c) C_{b_8}; M = 1.61.

Figure 26.- Continued.

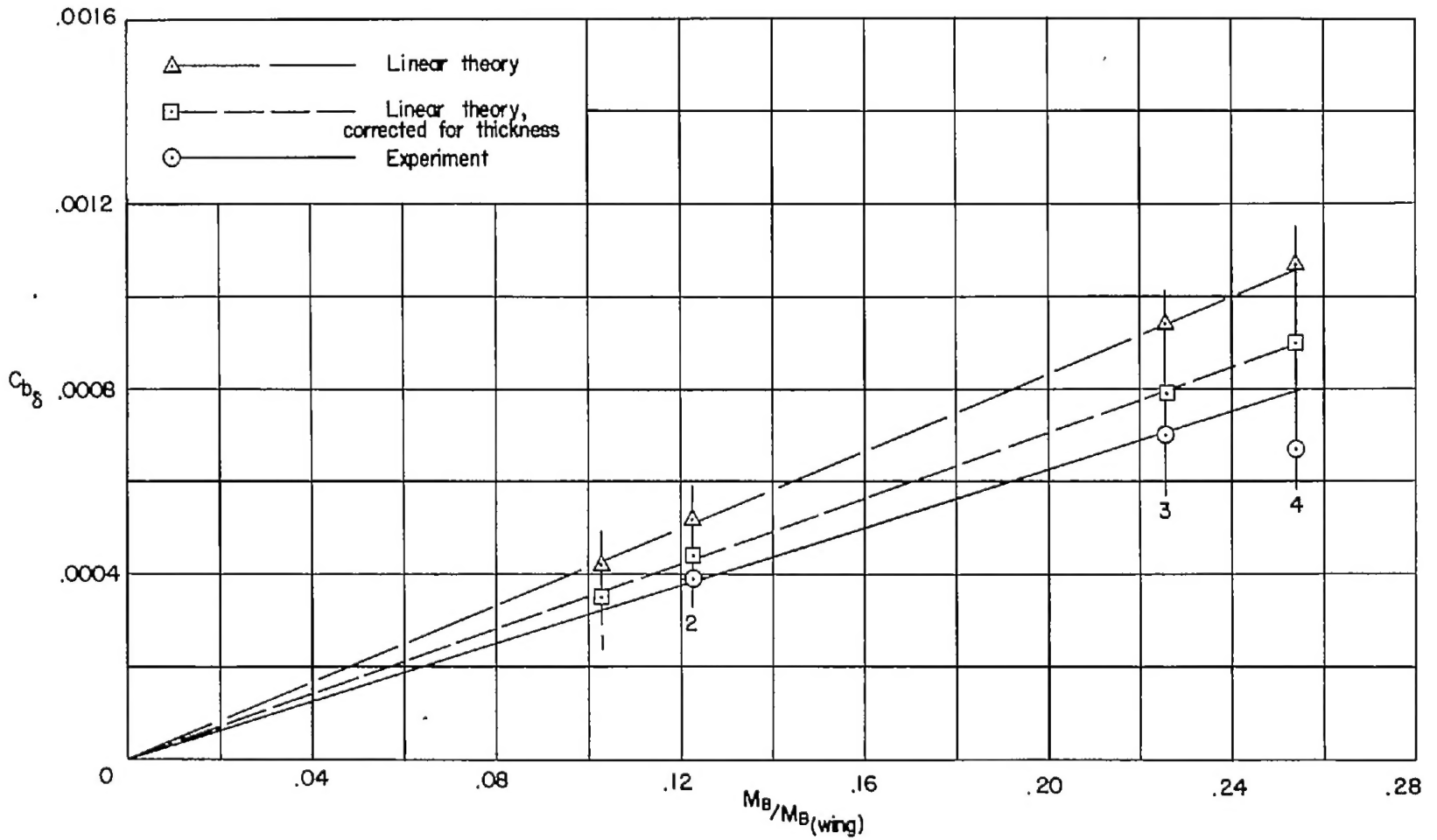

(d) C_{b_δ}; M = 2.01.

Figure 26.- Continued.

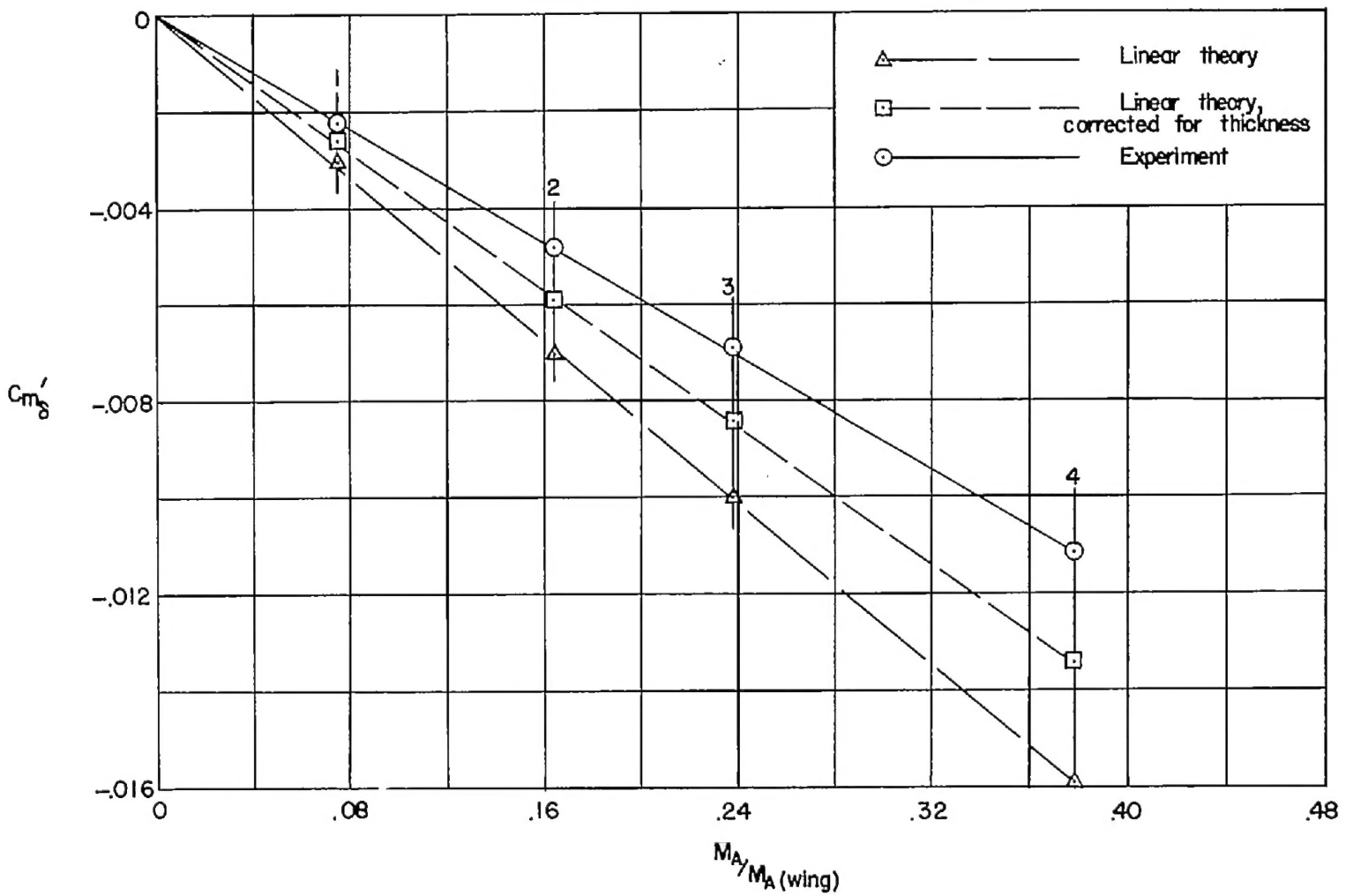

(e) $C_{m}'_{\delta}$; M = 1.61.

Figure 26.- Continued.

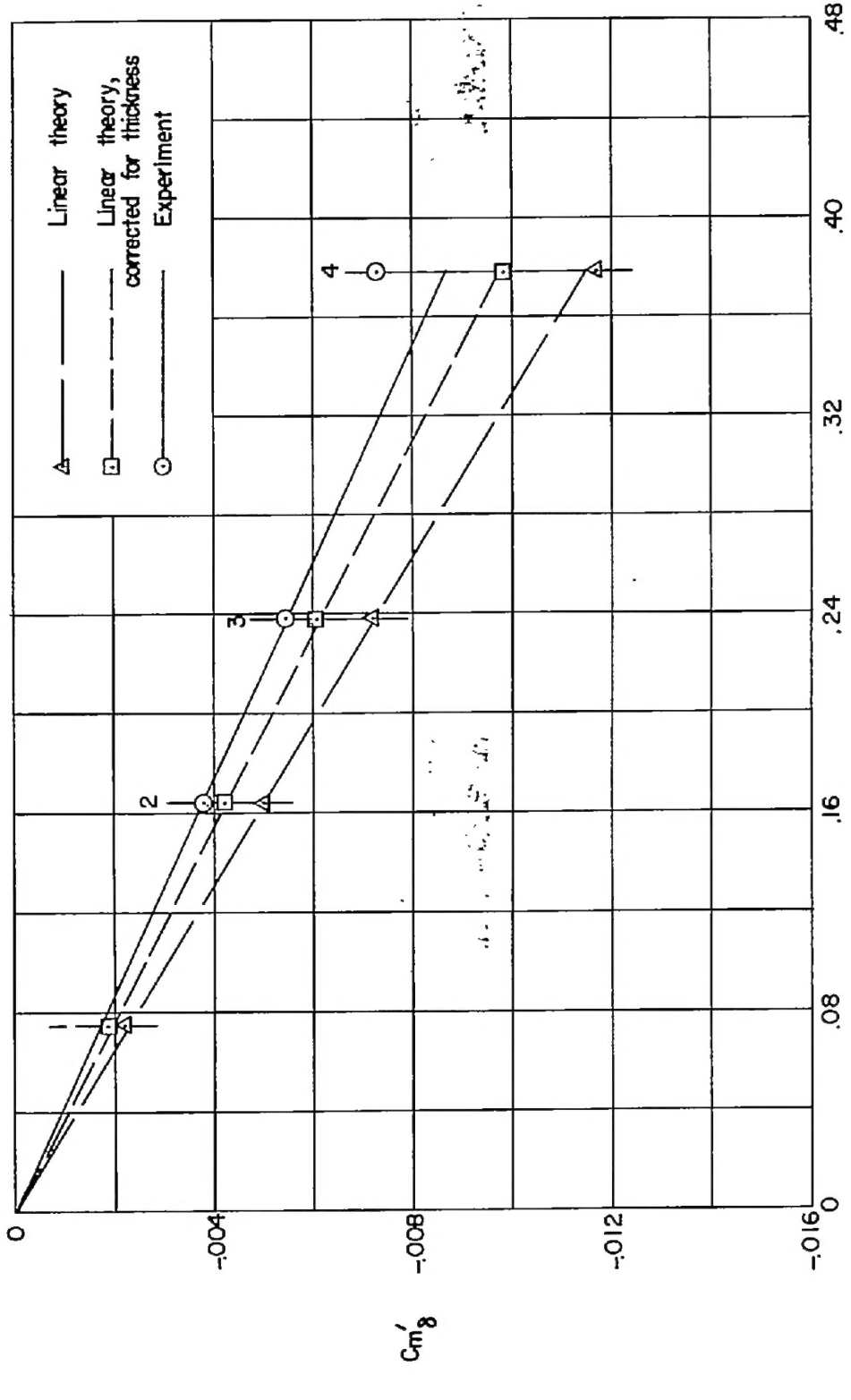

(f) $C_{m'_\delta}$; M = 2.01.

Figure 26.- Concluded.